SIMULATION OF STRONG GROUND MOTION USING SEMI EMPIRICAL MODELLING TECHNIQUE

A THESIS
Submitted in partial fulfilment of the
requirements for the award of the degree
of
DOCTOR OF PHILOSOPHY
in
EARTH SCIENCES

by

PUSHPA KUMARI

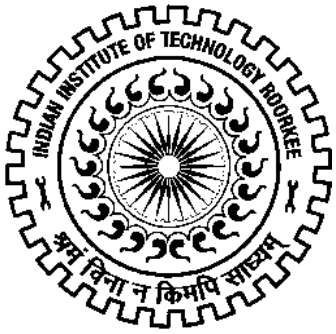

DEPARTMENT OF EARTH SCIENCES
INDIAN INSTITUTE OF TECHNOLOGY ROORKEE
ROORKEE-247 667 (INDIA)

SEPTEMBER, 2013

INDIAN INSTITUTE OF TECHNOLOGY ROORKEE
ROORKEE

CANDIDATE'S DECLARATION

I hereby certify that the work which is being presented in the thesis entitled "**SIMULATION OF STRONG GROUND MOTION USING SEMI EMPIRICAL MODELLING TECHNIQUE**" in partial fulfilment of the requirements for the award of the Degree of **Doctor of Philosophy** and submitted in the **Department of Earth Sciences** of the Indian Institute of Technology Roorkee is an authentic record of my own work carried out during a period from July, 2009 to September, 2013 under the supervision of **Dr. Anand Joshi**, Department of Earth Sciences and **Prof. M.L. Sharma**, Department of Earthquake Engineering, Indian Institute of Technology Roorkee, Roorkee.

The matter presented in the thesis has not been submitted by me for the award of any other degree of this or any other Institute.

(PUSHPA KUMARI)

This is to certify that the above statement made by the candidate is correct to the best of our knowledge.

(M.L. SHARMA)
Supervisor

(ANAND JOSHI)
Supervisor

Dated: September , 2013

The Ph.D. Viva-Voce Examination of **Ms. Pushpa Kumari**, Research Scholar has been held on . . . . . .

Signature of Supervisors **Signature of Chairman, SRC** **Signature of External Examiner**

Head of the Department/Chairman, ODC

ABSTRACT

Strong ground motion prediction is one of the indispensable prerequisites for earthquake resistant design of structures. Safe design of any structure in a seismically active environment require various engineering parameters which are obtained either directly from strong motion time histories or from simulated strong motion records. Strong motion data are not easily available at all construction sites therefore simulation techniques are required for generating useful strong motion data for such sites. Simulation techniques require several parameters of earthquake and other seismic information prior to the modeling of any earthquake ground motion in any tectonic setup. Estimation of such parameters is practically difficult task, especially in a region where we have limited information in hand. This has motivated a need for a technique of simulation of strong ground motion which should depend on the easily available parameters at any new site.

The semi-empirical method was used for strong motion simulation of major to large earthquake in a broad frequency range by Kumar et al. (1999), Joshi et al. (2001), Joshi and Midorikawa (2004) and Joshi and Mohan (2008). This technique has never been tested for simulating ground motions due to great earthquakes. Modifications in the semi-empirical method have been made in the present thesis to incorporate the effect of radiation pattern and seismic moment of the target earthquake. These modifications have removed the dependency of semi-empirical method on attenuation relation. The semi-empirical method has been also modified to resolve the obtained record into two horizontal components. The modified technique has been studied in detail to check the presence of various strong motion properties like directivity effect and variation of peak ground acceleration with respect to surface projection of rupture plane. Strong motion records have been simulated for the well recorded Niigata earthquake (M_w = 6.6) of October 23, 2004 to validate the modified technique. Iterative modeling suggests that rupture propagate bilaterally in northwestern direction at a depth of 13 km with rupture velocity 3.1 km/sec which is similar with the findings of Honda et al. (2005). Based on satisfactory results obtained from present simulation technique of this well recorded and well-studied earthquake, two earthquakes in Indian subcontinent viz., the Sikkim earthquake (M_w = 6.9) of September 18, 2011 and the Sumatra earthquake (M_w = 9.0) of December 26, 2004 have been studied to test the applicability of the modified technique. The technique is further applied to present a ground motion scenario due to a great hypothetical earthquake in the Andaman Island, India. The rupture

plane is placed in the Andaman region for this hypothetical great earthquake and records have been simulated using both the modified semi-empirical and empirical Green's function technique.

The rupture responsible for the Sikkim earthquake has been placed at a depth of 44 km between Tista and Gangtok lineaments. The length and width of the rupture plane for the Sikkim earthquake are assumed to be 51 and 13 km, respectively. The strike of the rupture plane is assumed to be parallel to the Tista lineament and is 328°N which is close to that obtained from fault plane solution of this earthquake given by Global CMT. Acceleration records have been simulated for near-field as well as far-field stations. Several simulations from different source models and its comparison with observed records in the frequency range of 0.01–20.0 Hz indicate that the Sikkim earthquake was generated by a rupture originating at a depth of 47 km and propagating in southward direction with rupture velocity of 2.9 km/sec.

The source of the Sumatra earthquake has been modeled using both modified semi-empirical and empirical Green's function techniques. The final rupture model of the Sumatra earthquake obtained after iterative modeling using modified semi-empirical and empirical Green's function techniques has further been used to simulate both horizontal component of ground motion at PSI and MDRS stations which lies at an epicentral distances of 355 and 2060 km, respectively. It has been further observed that due to dependency of empirical Green's function technique on aftershock record, simulations at a far-field station has been compared in the frequency range of 0.3 to 2.0 Hz; whereas modified semi-empirical technique simulations have been compared in the frequency range of 0.3 to 4.0 Hz for the great Sumatra earthquake. Iterative modeling of the source of the Sumatra earthquake with several possibilities of rupture parameters indicate that this earthquake was originated at 38 km depth and started propagating in northwestern direction with rupture velocity of 3.0 km/sec. The simulation technique developed in this work is further used to model a hypothetical earthquake of magnitude 8.5 (M_w) in the Andaman region of Indian subcontinent. This region lies close to the epicenter of the Sumatra earthquake. The causative rupture for this hypothetical earthquake is placed in the Source Zone 81 marked by Bhatia et al. (1999). This source zone has potential of generating 8.5 magnitude earthquake (Bhatia et al. 1999). The Andaman region itself has experienced earthquakes of both reverse and oblique strike-slip fault mechanism (Ortiz and Bilham 2003; Chatherine et al. 2009). Both NS and EW component of horizontal record has been simulated for reverse and oblique strike-slip type of earthquake source mechanism in this region. It has been observed that peak ground acceleration obtained from several

records using both methods with different possibility of nucleation point lies within a range of 0.3 to 2.0 g for reverse source mechanism at POR station. This range of peak ground acceleration from simulated records for oblique strike-slip source mechanism is between 0.1 to 2.0 g at POR station.

Several strong motion parameters are required for the estimation of seismic hazard in any region which is sometimes not easily available at all sites. This thesis presents modified semi-empirical method which has advantage of using easily available parameters. The technique can be applied to a region having scarcity of observed strong motion data and can be effectively used for estimating earthquake resistant design parameters.

ACKNOWLEDGEMENT

I would like to thank all the following people who have been helping me in one way or in many ways during my Ph.D. study at IIT Roorkee:

It gives me a great pleasure to express my deepest gratitude to my Ph.D. supervisor **Dr. Anand Joshi** from Department of Earth Sciences, for their guidance, encouragement and providing a professional environment in tenure of my research work. I highly appreciate all his contributions of time, ideas, persistence in high quality results, and make my Ph.D. experience productive and stimulating.

I equally grateful to my guide **Prof. M.L. Sharma** from Department of Earthquake Engineering for his wise pieces of advice in my Ph.D. work. I also thankful to **R.P. Gupta** (former Head), **P.K. Gupta** (former Head) and **A.K. Saraf**, Head of the Department of Earth Sciences, Indian Institute of Technology Roorkee, for providing departmental facilities for carrying out my research work.

I sincerely thank **Department of Atomic Energy** (DAE) for financial support of this research work under project Grant no: 2009/36/01-BRNS. I sincerely thank Indian Institute of Technology Roorkee and **Bhaba Atomic Research Center** (BARC) for supporting this work. The strong motion data of October 23, 2004 Niigata earthquake obtained from KiK-net network available at http://www.kyoshin.bosai.go.jp site has been used in thesis is thankfully acknowledged. I sincerely thank **Ministry of Earth Sciences** (MoES), Government of India supported project (Grant no: MoES/P.O.(Seismo)/1(42)/2009) for providing far-field strong motion data of September 18, 2011 Sikkim earthquake. The near-field strong motion data obtained from http://www.pesmos.in maintained by **Department of Earthquake Engineering**, IIT Roorkee are thankfully acknowledged. The broadband data of December 26, 2004 Sumatra earthquake recorded at PSI station has been obtained from http://ohpdmc.eri.u-tokyo.ac.jp and at MDRS station obtained from **India Meteorological Department** (IMD) are thankfully acknowledged.

I am thankful to my colleagues and friends who assisted me in different ways during stay at the department specially (Late) **Mr. Om Prakash Verma**, M.Tech. student whenever I needed their help.

I express love and gratitude to all my family and friends. I would particularly like to thank my parents for their constant love and moral support.

Last but not the least, I express my gratitude to the Almighty God for always keeping me in high spirit during all tenure of this work and providing me strength to perform this task successfully.

(Pushpa Kumari)

CONTENTS

LIST OF FIGURES

LIST OF TABLES

LIST OF SYMBOLS AND ABBREVIATIONS

$G_i^S(x,t)$	Green's function
$Ac^{NS}(t)$	North-south component of acceleration record
$Ac^{EW}(t)$	East-west component of acceleration record
$A(f)$	Acceleration spectra of target earthquake
$A(t)$	Ground motion time history for target earthquake
$a(t)$	Ground motion time history for small earthquake
$Ac(t)$	Resultant acceleration record at the observation point
$ac_{ij}(t)$	Acceleration record released from *ij*th sub-fault
$a_f(i)$	Observed record
$a_{ij}(t)$	Filtered acceleration record
$A_{ij}(t)$	Acceleration record after convolution
A_o	Long term flat level of acceleration spectra of target earthquake
A_o'	Long term flat level of acceleration spectra of small earthquake
$a_s(i)$	Simulated record
C	Constant scaling factor
C'	Ratio of stress drop of the target and small earthquake
d	Slip of the small earthquake
D	Slip of the target earthquake
$D_S(f)$	Filter represent near site attenuation of high-frequencies
$e_{ij}(t)$	Envelope function
f	Frequency
$F(t)$	Correction function
f_c	Corner frequency of small earthquake
F_c	Corner frequency of target earthquake
f_m	High frequency cutoff range in high-cut filter
$F_R(f, R)$	Filter representing effect of anelastic attenuation
FS	Amplification due to the free surface

i_ξ	Takeoff angle
i_a	Angle of incidence
L	Length of the rupture plane of the target earthquake
L_e	Length of the rupture plane of the small earthquake
M	Richter magnitude of an earthquake
m_b	Short-period body-wave magnitude
M_{JMA}	Magnitude scale used by Japan Meteorological Agency
M_o	Seismic moment of the target earthquake
M_o'	Seismic moment of the small earthquake
M_s	Surface-wave magnitude
M_w	Moment magnitude of target earthquake
M_w'	Moment magnitude of small earthquake
N	Number of sub-faults along length or width of the rupture plane
p	Ray parameter
$PRTITN$	Reduction factor that accounts for the partitioning of total shear-wave energy into two horizontal components
$Q_\beta(f)$	Shear wave Quality factor
R	Hypocentral distance of the target earthquake
r	Hypocentral distance of the small earthquake
r_{ij}	Distance from the observation point to the ijth sub-fault
r_s	Radius of circular crack
$R_{\theta\varphi}$	Radiation pattern coefficient
$S(f)$	Source acceleration spectrum
t	Time
T	Slip duration of the target earthquake
T_d	Duration parameter
t_{ij}	Arrival time
T_R	Rise time of the target earthquake
T_{ss}	Transmission coefficient of incident shear waves
U_o	Long term flat level of displacement spectra of target earthquake
U_o'	Long term flat level of displacement spectra of small earthquake

V	Velocity of propagation
V_r	Rupture velocity
W	Width of the rupture plane of the target earthquake
W_e	Width of the rupture plane of the small earthquake
β_i	Shear wave velocity in the *i*th layer
δ	Dip of rupture plane
$\delta(t)$	Delta function
$\Delta\Sigma$	Area of small earthquake
λ	Rake
μ_i	Modulus of rigidity in the *i*th layer
ξ_{ij}	Distance travelled by the rupture from nucleation point to *ij*th sub-fault
ρ	Density of medium
Σ	Area of rupture plane
τ	Slip duration of the small earthquake
φ	Source-receiver Azimuth
φ_s	Strike of rupture plane
ϕ	Strike of the modelled rupture plane with respect to geographic north
EGFT	Empirical Green's Function Technique
MSET	Modified Semi-Empirical Technique
MSETCS	Modified Semi-Empirical Technique for Component-wise Simulation
RMSE	Root Mean Square Error

Chapter – 1

INTRODUCTION

1.1 Synthetic Strong Ground Motion- Introduction

Strong ground motion prediction is one of the indispensable prerequisites for earthquake resistant design of structures. Many sites of construction seldom contain any past strong motion records that pose a major constraint in earthquake resistant designs. Several engineering parameters are required for safe design of any structure in a seismically active environment. These parameters are obtained either directly from strong motion time histories or from simulated strong motion records. In addition to some of the empirically predicted ground motion procedures, simulation is the only options left for evaluation of safe engineering design parameters in a region of limited, or no strong motion data. Simulation techniques require several parameters of target earthquake and other seismic information prior to simulation. Estimation of these parameters is a difficult task especially in a region where there is limited information in hand.

Prediction of strong ground motion parameter using attenuation relationship is one of the simplest ways for estimation of strong motion parameters required for safe engineering design. It is a regression relation between design parameter and parameters related to earthquake size, distance of observation point from earthquake source and other tectonic and site specific information. Several such ground motion prediction equations are available for different regions worldwide (McGuire 1977; Boore et al. 1980; Campbell 1981, 1985, 2001; Hanks and McGuire 1981; Joyner and Boore 1981; Abrahamson and Litehiser 1989; Sharma 1998; Sharma et al. 2009; Arroyo et al. 2010). The comprehensive list of such relations is given by Campbell (1997) and Douglas (2011). Major advantages of using such relations are that these relations are based on a real database, are easy to use, however, it has been observed that these equations are largely data dependent and work only for a specific environment (Joshi 2001). The ray path of seismic energy from source reaching the observation point is assumed as a straight line in the attenuation relation (McGuire 1977; Campbell 1981; Abrahamson and Litehiser 1989). This assumption is valid only for

homogeneous earth model. However this assumption fails to explain propagation of seismic energy in the layered earth model. The earthquake source is treated as a point source in the development of attenuation relation. This assumption also fails to explain finite nature of earthquake source in the near-source region. It has been observed that as long as the data set is similar to that used for generating ground motion prediction equation, the normality and model adequacies are broadly satisfied in the attenuation relation, however, clear deviation from normality is observed when using ground motion prediction equations for predicting different data sets (Joshi et al. 2012a). Failure of attenuation relation for predicting important engineering parameters for finite earthquake source in the layered earth model has motivated both engineers and seismologist a strong need for development of techniques of simulation of strong ground motion.

1.2 Generation of Ground Motion- Review

Simulation techniques can be classified into four broad categories. These are (i) Stochastic simulation technique, (ii) Empirical Green's function technique, (iii) Composite source modeling technique and (iv) Semi-empirical technique. This section describes these techniques in detail and possible identified gaps in the research.

1.2.1 Stochastic Simulation Technique

Stochastic nature of high-frequency strong ground motion was recognized by both seismologists and engineers in late seventies. Simulation of strong ground motion by engineers (Housner and Jennings 1964; Iyengar and Iyengar 1969; Nau et al. 1982) using stochastic simulation technique is based on purely empirical approach. Strong ground motion is simulated by engineers in such a way that it agree with existing data in all essential ways in terms of frequency content, amplitude and duration of real data (Iyengar and Iyengar 1969; Nau et al. 1982). The actual methods for simulation of high-frequency ground motion make use of filtering and windowing of Gaussian noise and adding together to suitably scaled recorded accelerograms (Boore 1983). The stochastic simulation technique is one of the earliest techniques that are used to simulate strong ground motion. Housner and Jennings (1964) simulated strong motion records having pertinent properties of recorded strong motion earthquakes. The model accelerogram in this case is a stationary, Gaussian, random process with a power spectral density found from the average of undamped velocity spectra of recorded ground acceleration. Eight pseudo earthquake

records of thirty seconds durations were simulated by Housner and Jennings (1964) which concluded that synthetic earthquake records are satisfactory models of strong ground motion records for the purpose of structural analysis and it can be used for design of structures. The major limitation of this technique of modeling is that it does not include conceptual model of earthquake source and the passage of the energy released by the source through the medium.

The simulation techniques developed by seismologists make use of the physical model of earthquake sources. The stochastic simulation technique developed by seismologist borrowed the idea of stochastic nature of high-frequency ground motion from engineers and combined it with physical model of earthquake source defined by seismologists. In stochastic simulation technique a band limited random white Gaussian noise is passed through number of filters representing earthquake process to get a synthetic ground motion (Hanks and McGuire 1981; Boore 1983; McGuire et al. 1984; Boore and Joyner 1991; Shinozuka and Sato 1967; Lai 1982). The stochastic model is a widely used tool to simulate acceleration time series and to develop ground motion prediction equations (Hanks and McGuire 1981; Boore 1983; Atkinson and Boore 1995, 1997; Atkinson and Silva 2000; Boore 2003; Motazedian and Atkinson 2005). Stochastic method begins with the specification of the Fourier spectrum of a ground motion as a function of magnitude and hypocentral distance. The source acceleration spectrum is typically modeled by a spectrum with a ω^{-2} shape (Aki 1967; Brune1970, 1971; Boore 1983, 2003). Hanks and McGuire (1981) have studied approximately 300 horizontal components of ground motion and suggested that these acceleration records are in band limited white Gaussian noise in form within the S-wave arrival window. These band limited records are defined by the spectral corner frequencies and estimated root mean square acceleration in terms of stress drop, hypocentral distance, shear-wave velocity and the spectral frequencies. It has been concluded by Hanks and McGuire (1981) that acceleration time histories of finite duration can be obtained by assuming reference root mean square acceleration at a site. Stochastic model does not take into account the finite-fault effects and the directivity effects and is based on a point source assumption (Boore 1983). In case of large earthquake, finite-fault effects are an important effect to be considered (Boore 1983).

Peak ground acceleration and response spectra for the Taipai area was calculated by Sokolov et al. (2001) using stochastic simulation technique on the basis of obtained empirical model that was given by Boore (1983). Large collection of ground motion recording obtained since 1991 in the Taiwan area was used to characterize source, path and site effects (Sokolov et al.

2001). It was observed that ω^{-2} point source model compared with regional anelastic attenuation and duration model provide a satisfactory estimation of ground motion parameter for rock site.

Atkinson and Boore (2006) have developed ground motion prediction equations for rock and soil sites in Eastern North America (ENA) using stochastic simulation technique. Atkinson and Boore (2006) have suggested that ground motion prediction equations using stochastic simulation technique provide a basis for estimating peak ground motions and response spectra for earthquakes of magnitudes (M_w) ranging from 4 to 8, at hypocentral distances between 1 to 200 km for the frequency range of 0.2–20 Hz. Boore et al. (2010) determined the stress parameter for eight earthquakes studied by Atkinson and Boore (2006) using a revised point-source stochastic model.

Beresnev and Atkinson (1997) proposed finite-fault source model, in which the fault planes are discretized into equal rectangular elements and each of them are treated as a point source. The rupture propagates radially from the hypocenter with the specified rupture velocity. This stochastic finite-fault modeling was used by Beresnev and Atkinson (1997, 1998) for the 1994 Northridge, California earthquake of magnitude 6.7 (M_w). A large uncertainty was associated with the relation given by Beresnev and Atkinson (2001) due to paucity of large earthquake recordings. To overcome this limitation, Motazedian and Atkinson (2005) enhanced the algorithm by introducing dynamic corner frequencies and the method was tested on California earthquake.

Ghasemi et al. (2010) simulated strong ground motions recorded during the 2008 Wenchuan, China earthquake (M_w = 7.9) using the stochastic simulation technique proposed by Beresnev and Atkinson (1997). Simulations were made for two source models. Both models were based on the fault geometry that was proposed by Koketsu et al. (2008) through inversion of teleseismic body wave data. The slip distribution obtained by this inversion was used for the first type of source model, while a random slip distribution was used for the second type of source model. The performance of each source model was quantified by Ghasemi et al. (2010) by calculating the bias and standard deviation of response spectra predicted by each model. Although strong motion simulations using stochastic simulation technique gives reliable estimation of strong ground motion, it fails to model earthquake having finite-fault appearance and complex rupture geometry.

1.2.2 Empirical Green's Function Technique

The finite-fault nature of earthquake source has been modeled by the simulation technique known as Empirical Green's Function (EGF) technique. This technique was initially started by Hartzell (1978) and in this technique the records of the aftershocks of the main event were used as empirical Green's function to simulate ground motion of the target earthquake at an observation point (Hartzell 1978, 1982; Kanamori 1979; Hadley and Helmberger 1980; Mikumo et al. 1981; Irikura and Muramatu 1982; Hadley et al. 1982; Coats et al. 1984; Houston and Kanamori 1984; Imagawa et al. 1984; Munguia and Brune 1984; Hutchings 1985; Irikura 1986; Heaton and Hartzell 1989). This technique simulates strong ground motion due to finite earthquake source in a layered earth model. It was observed that simulation of synthetic records using earth model involve two major problems. The first one was associated with the description of source and second one with the estimation of earth response (Hartzell 1978). Summation of point sources was in media ranging from full space (Aki 1968) to layered half space (Heaton and Helmberger 1977). A method was presented by Hartzell (1978) for modeling strong ground motion which uses aftershocks associated with large earthquake as Green's function. A major earthquake with large surface area is modeled by a collection of point sources distributed over a fault plane (Hartzell 1978). The method was used to model the El Centro displacement record for the 1940 Imperial Valley earthquake (Hartzell 1978).

Irikura (1986) proposed the method of EGF technique which is consistent with spectral scaling at high-frequencies. The total number of small events used by Irikura (1986) in the EGF technique is consistent with the scaling laws given by Kanamori and Anderson (1975). The method of EGF technique used by Irikura (1986) uses records of both the target and small events having spectral characteristics that can be predicted by ω^{-2} model (Irikura 1986). Irikura (1986) have modeled the strong motion records of the 1983 Japan Sea earthquake (M_{JMA} = 7.7) using records of the aftershock of magnitude 6.1 (M_{JMA}) as EGF. The original idea of EGF technique makes use of small earthquake as an empirical Green's function to simulate large earthquake. The distribution of small earthquake within the fault plane of large earthquake is based on the scaling laws of source parameters studied by Kanamori and Anderson (1975). The fault area of large earthquake is divided into large number of small event fault area to simulate strong motion records of very large earthquake using the records of small earthquake (Irikura and Kamae 1994). It is observed that some deficiencies of synthetic spectra are inevitably produced even if small event records are

accurate enough in broad frequency range (Irikura and Kamae 1994). To avoid such spectral deficiencies, Irikura and Kamae (1994) introduced a fractal distribution of a set of sub-faults with different sizes in fault area for simulating large earthquake motion. Irikura and Kamae (1994) modeled 1983 Akita-Oki earthquake using records of smaller aftershocks (M_{JMA} = 3.9 and 5.0) as an empirical Green's function. The records of earthquake (M_{JMA} = 5.1) occurred in the near source region of the 1946 Nankai earthquake (M_{JMA} = 8.2) were used as an empirical Green's function to model the Nankai, Japan earthquake by Irikura and Kamae (1994).

A technique of simulating strong ground motion was developed by Somerville et al. (1991) by summing contributions from sub-faults to simulate the propagating rupture over the fault surface. The radiation from the fault elements are represented by empirical source functions derived from near-source strong motion records of magnitude 7.0 (M_w) aftershock (Somerville et al. 1991). The aspects of wave propagation were modeled by calculating Green's functions (Somerville et al. 1991). The method was used to simulate strong motion records of 1985 Michoacán, Mexico earthquake (M_w = 8.0) and Valparaiso, Chile earthquake (M_w = 8.0). The comparison of simulated and actual records for the model of heterogeneous slip explain the high-frequency recorded strong ground motion. The strong motion parameters like peak ground acceleration, duration and shape of envelope of the time histories were in good agreement with time series (Somerville et al. 1991). The comparison also showed that uncertainty associated with misfit between response spectra of the recorded and simulated shows dependency on period and site condition.

Kamae and Irikura (1998) estimated strong ground motion of the 1995 Hyogo-ken Nanbu, Japan earthquake using EGF technique by considering an initial source model with the asperities based on the rupture process by inversion of strong ground motion records. These asperities were considered as subevents with uniform stress drop. The assumed initial model was improved by Kamae and Irikura (1998) by matching the synthetic and observed ground motions using a trial and error procedure. A method for simulating strong ground motion for a large earthquake based on synthetic Green's function was presented by Pitarka et al. (1998). Pitarka et al. (1998) used the synthetic motions of a small event as Green's functions instead of observed records of small events. Both deterministic and stochastic methods were used for simulation of ground motions from small events by Pitarka et al. (1998). The long-period motions from the small events were deterministically calculated using the 3D finite-difference method, whereas the high-frequency

motions were simulated using Boore's (1983) stochastic simulation method. This method was termed as hybrid Green's function method by Pitarka et al. (1998). The small event motions are synthesized by summing the long-period and short-period motions after passing them through a pair of matched filters to follow the omega-squared source model. Ground motions from a large earthquake were simulated by using EGF technique given by Irikura (1986). This method was applied to simulate the ground motion from the 1995 Hyogo-ken Nanbu, Japan earthquake (M_w = 6.9). The hybrid Green's function method as well as the EGF method performed a very good agreement between the synthetics and observed records in regions where there was enough information about the deep and shallow geological structure. The only constrained in this method was the detail requirement of the geophysical and geological information of the region.

Strong motion records in near-source area from March 2011 Tohoku earthquake (M_w = 9.0) showed several isolated wave-packets arriving from different origins on the source fault (Irikura and Kurahashi 2012). The source model was estimated by Irikura and Kurahashi (2012) from the forward modeling by simulating high-frequency ground motions using EGF technique. The forward modeling showed that the final model has five strong motion generation areas located west of the hypocenter and along the down-dip edge of the source fault (Irikura and Kurahashi 2012).

Singh et al. (2002) have simulated strong ground motion in Delhi, India for a scenario great earthquake with the possibility of earthquake occurring in the central seismic gap region of the Himalayan arc. Two methods were used to synthesize the expected ground motions. In first method, recordings in Delhi (three on soft sites and one on a hard site) of the 1999 Chamoli earthquake (M_w 6.5; epicentral distance, ~300 km) were used as empirical Green's functions (Singh et al. 2002). Ground motion during the target earthquake was synthesized by random summation of the empirical Green's functions. In second method, ground motions were estimated from the expected Fourier spectrum of the ground motion in Delhi through the application of Parseval's theorem and results from random vibration theory (Singh et al. 2002). The largest ground motions were predicted in Delhi for rupture occurring between the Main Boundary Thrust (MBT) and Main Central Thrust (MCT) and the hypocenter located at the edge of the fault.

It has been observed that simulations from EGF technique are considered as one of the most reliable one; however the most difficult requirement in this technique is the availability of aftershock record at the site of simulation. This is rarely attained for new construction sites where limited information is available.

1.2.3 Composite Source Model

Simulation of strong ground motion for a site having limited or no prior strong motion data require a technique which should be based purely on theoretical assumptions. The technique of composite source modeling is based on the principle that an earthquake is made up of numerous subevents that are arranged at the passage of the rupture front (Ruiz et al. 2011). Each of the subevent is defined by size, seismic moment, stress drop, slip and source-time function. Boatwright (1982) was one of the first to propose a source composite model with a fractal distribution, inspired by the pioneer self-similar concepts of earthquake model suggested by Hanks (1979) and Andrews (1980). Boatwright (1982) made the assumption that the total surface of the subevents should be equal to the surface of the target event and that the subevents must not overlap. Boatwright (1982) was able to model the high-frequency characteristics of the spectral acceleration in the far-field region using this model.

Several composite source models are proposed in literature to model the heterogeneities of the seismic rupture such as the specific barrier model (Papageorgiou and Aki 1983), the fractal composite model (Boatwright 1982, 1988; Frankel 1991; Zeng et al. 1994) and the empirical Green's functions models (Hartzell 1978; Irikura and Kamae 1994; Frankel 1995). The main differences between these models arise from the hypothesis made on the subevent size distribution, either assuming an equal-size distribution (Hartzell 1978; Papageorgiou and Aki 1983; Frankel 1995; Beresnev and Atkinson 1997), or a heterogeneous-size distribution (Frankel 1991; Zeng et al. 1994) and on the overlapping (Zeng et al. 1994) or non-overlapping (Frankel 1991) character of the subevents. Most commonly used technique to correct the mismatch between target and modeled spectrum is to apply appropriate filtering technique. Frankel (1991) proposed a more general composite source model in which the size of the subevents was described by a fractal distribution. Frankel (1991) showed that the resulting high-frequency falloff of the displacement spectrum follows the spectral source model given by Aki (1967), provided that a fractal dimension of 2 and a constant stress drop are used in simulations.

Zeng et al. (1994) presented a composite source model for convolution with synthetic Green’s function to simulate strong ground motion due to a complex rupture process of an earthquake. Subevents with power law distribution located within the rupture plane radiates a displacement pulse with a shape of Brune’s pulse in the far-field at a time determined by a constant rupture velocity propagating from hypocenter (Zeng et al. 1994). The simulations using this

technique were made for event-station pairs recorded by Guerrero accelerograph network, Mexico. The study showed that the simulated records bear realistic amplitude, duration and Fourier spectra. It has been observed that the composite source model given by Zeng et al. (1994) failed to demonstrate that a single model can give accelerograms consistent with a large number of observations (Yu et al. 1995). Yu et al. (1995) have simulated 1991 Uttarkashi earthquake of 7.0 magnitude (M_s) by using composite source model defined by Zeng et al. (1994). In this approach, Yu et al. (1995) have used two velocity models for near and far-field stations rather than using single velocity model as Zeng et al. (1994) had used. These two velocity model were further used to predict strong ground motions at the same stations from a potential earthquake of magnitude 8.5 in the seismic gap region along the Himalayan frontal faults. The stress drop was assumed to be constant in the composite source models whereas it was seen that this parameter can fluctuate very strongly on the fault plane due to heterogeneous slip (Ruiz et al. 2011).

The composite source model was used by Ruiz et al. (2011) to simulate broad-band accelerograms with spectral amplitudes proportional to a fraction of the directivity coefficient. This approach was based on a composite source description. Each elementary source was described as a crack-type slip model growing circularly from a nucleation point when the rupture front reaches it. In order to control the directivity effect, the location of the nucleation point for an elementary source was assumed to be scale-dependent (Ruiz et al. 2011). The nucleation point was located near the intercept of the crack for the large sources, whereas for smaller sources it is randomly chosen within the crack (Ruiz et al. 2011). Rupture front propagates at constant rupture velocity from the hypocenter location (Ruiz et al. 2011). Each subevent was arranged with scale-dependent rise-time, assuming a boxcar source-time function; hence filtering out its own high-frequency radiation from rupture front propagating at constant rupture velocity from the hypocenter location (Ruiz et al. 2011). Ground motion synthetics were computed by convolving the slip-velocity functions with the Green's functions.

Kumar et al. (2011) presented a hybrid method for simulation of strong ground motion. This procedure is the combination of the techniques of envelope function (Midorikawa 1993) and composite source model (Zeng et al. 1994). This technique is based on the construction of the envelope function of the large earthquake by superposition of envelope functions of smaller earthquakes. The smaller earthquakes (subevents) of varying sizes are distributed randomly, instead of uniform distribution of same size on the fault plane (Kumar et al. 2011). The

accelerogram of target earthquake is obtained by combining the envelope function with a band-limited white noise. This technique requires parameters like fault area, orientation of the fault, hypocenter, size of the subevents, stress drop, rupture velocity, duration, source-site distance and attenuation parameter (Kumar et al. 2011). The applicability of this technique was demonstrated by modeling of the 1991 Uttarkashi, Himalaya earthquake (M_s = 7.0) by Kumar et al. (2011). Although the method of composite source modeling technique give realistic records it require detail velocity and *Q* structure of the region as well as the fault plane solution and the stress drop parameter of the target earthquake (Kumar et al. 1999). It is further seen that the calculation of the complete Green's functions is quite time-intensive (Kumar et al. 1999).

1.2.4 Semi-Empirical Technique

Midorikawa (1993) proposed a simplified method for simulating strong ground motion from a target earthquake for engineering use. This method was based on semi-empirical method of Irikura (1986) in which the rupture plane of the target earthquake is divided into small elements. Midorikawa (1993) has determined the resultant acceleration envelope waveforms, instead of the time histories using this method. The envelope waveforms from the elements are summed to synthesize the resultant envelope waveform of the target earthquake. This method is applied to simulate peak ground accelerations of the Central Chile earthquake (M_s = 7.8) of 1985 (Midorikawa 1993).

Joshi and Patel (1997) have modeled rupture along identified active lineaments in the Doon valley using semi-empirical method given by Midorikawa (1993). Efficacy of this modeling technique for its applicability in modeling earthquakes in the Himalayan region was established after simulating peak ground accelerations of the Uttarkashi earthquake of October 20, 1991 and comparing it with observed values. It is observed that the semi-empirical method is dependent on the attenuation relation and the relation given by Abrahamson and Litehiser (1989) are used in this technique by Joshi and Patel (1997), Kumar et al. (1999), Joshi (2001), Joshi et al. (2001), Joshi and Midorikawa (2004). Kumar et al. (1999) have used semi-empirical method for calculating synthetic accelerograms for a wide range of earthquake magnitudes based on semi-empirical method of Midorikawa (1993). The fidelity of this method was demonstrated by modeling the strong motion records of the 1986 Dharmsala (M_s = 5.3) and the 1991 Uttarkashi (M_s = 7.0) earthquakes.

The final output of the semi-empirical technique (Midorikawa1993; Joshi and Patel 1997) was the envelope of accelerogram which only gives the idea about peak ground acceleration at a particular site and the total duration of the record. The realistic earthquake time series using semi-empirical method was simulated from the rupture plane buried in a layered earth model by Joshi et al. (1999). In this technique filtered white noise was multiplied with the resultant envelope of accelerogram obtained at an observation point. Several filters were used to include the effect of geometrical spreading, anelastic attenuation and near site attenuation of high-frequencies. The method was applied to simulate the records of the Uttarkashi earthquake and comparison is made with the observed records (Joshi et al.1999). The semi-empirical technique was modified by Joshi et al. (2001) to include the effect of layered earth model. In this approach the resultant envelope of acceleration record take into account the transmission of energy and travel time taken by energy at various boundaries within the layered earth model. The simulated resultant envelope is used as window function to simulate accelerograms by multiplying filtered white noise at a particular site. The applicability of this technique was tested to simulate the strong motion records of the Uttarkashi earthquake of October 20, 1991.

Joshi and Midorikawa (2004) presented a simplified method to simulate strong ground motion for a realistic representation of a finite earthquake source buried in a layered earth medium. Joshi and Midorikawa (2004) have simulated ground motion data of the Geiyo, Japan earthquake (M_w = 6.8) of March 24, 2001 using stochastic method of Boore (1983) with the help of shaping window based on the kinetic source model of the rupture plane. This shaping window is depended on the geometry of the earthquake source and the propagation characteristics of the energy released by various sub-faults. The shaping window was modified by Joshi and Midorikawa (2004) to take into account the effect of the transmission of energy released from the finite fault at various boundaries of the layered earth model above the source. Strong motion records have simulated at eight near-field stations and compared with the observed data and the record simulated by using empirical Green's function method of Irikura (1986). The comparison establishes the efficacy of this method.

Joshi and Mohan (2008) have modified semi-empirical technique initially started by Midorikawa (1993) for simulation of strong ground motion due to a rupture buried in earth medium consisting of several layers of different velocities and thicknesses. Simulations in the semi-empirical technique was made by considering, transmission of energy at each layer,

frequency filtering properties of medium, earthquake source, correction factor for slip of large and small magnitude earthquakes and site amplifications at various stations (Joshi and Mohan 2008). Calculation of site amplification is based on H/V spectral ratio method of Nakamura (1989). Several workers have used H/V spectral ratio method for estimation of site characterization (Rosa-Cintas et al. 2011; Parolai and Galiana-Merino 2006; Field and Jacob 1993; Lermo and Chavez-Garcia 1994; Mucciarelli 1998; Bard 1999; Parolia et al. 2001). Strong motion records were simulated by Joshi and Mohan (2008) at different stations that had recorded the 2004 Niigata-ken Chuetsu, Japan earthquake (M_w = 6.6) using H/V spectral ratio in the semi-empirical technique. The comparison of synthetic with the observed records over wide range of frequencies showed that this technique is an effective tool to predict various strong motion parameters from simple deterministic model which is based on simple regression relations and modeling parameters (Joshi and Mohan 2008). Simulation from this technique is based on estimate of H/V spectral ratio which requires sufficient data at the site of simulation, which is an additional constrain in this study. Also an open debate exists within the seismological community about practical and theoretical aspect of the H/V spectral ratio method (Bard 1998, Bonnefoy-Claudet et al. 2006, Lachet and Bard 1994, Parolai et al. 2001).

1.3 Research Gaps

The literature review of various techniques for simulation of strong ground motion gives an extensive idea about the advantages and disadvantages of those techniques. The method of stochastic simulation lacks complete representation of finite rupture plane (Joshi and Mohan 2010). The method of EGF technique has an advantage that there is no need to remove propagation effects (Fukuyama and Irikura 1986) and this technique is suitable to model finite rupture source. However, the small earthquakes needed in this method are required to be located ideally near the source and recorded at a site at which simulation is desired (Joyner and Boore 1988). This is the most difficult condition to be met when applying this method in practice and hence it is of limited use. In the composite fault modeling technique (Zeng et al. 1994; Yu 1994; Yu et al. 1995) fault plane solution, detailed velocity and Q structure is required for successful prediction. This is among the most difficult part of this method for those regions, which have very few earthquake records and limited seismic data. Recently a semi-empirical method has used for simulating earthquake ground motion due to rupture process (Midorikawa 1993; Joshi 1997, 2000, 2001,

2003, 2004; Joshi and Midorikawa 2004, 2005; Kumar et al. 1999; Joshi and Patel 1997). This method has an advantage of both empirical Green's function technique and stochastic simulation technique and is dependent on simple attenuation laws applicable in the study area. However, these simple laws are always not available at the site of investigation and the users are compelled to use worldwide attenuation laws like that used by Joshi and Patel (1997), Kumar et al. (1999), Joshi and Mohan (2008). Although recent studies by Joshi and Patel (1997), Kumar et al. (1999), Joshi and Mohan (2008) have shown that worldwide laws are useful for computation of parameters of strong ground motion simulated using semi-empirical approach, however their applicability in new region is still questionable. Direct dependency of semi-empirical method on simple parameter like energy released during an earthquake has not been considered in all previous simulations using semi-empirical methods given by Joshi and Patel (1997), Kumar et al. (1999), Joshi and Mohan (2008). Based on extensive literature survey following research gaps have been identified in the semi-empirical simulation technique:

- The size of earthquake is an important parameter in the simulation technique. Various workers starting from Midorikawa (1993), Joshi and Patel (1997), Kumar et al. (1999), Joshi (2001), Joshi et al. (2001), Joshi and Midorikawa (2004), Joshi and Mohan (2008) have simulated strong ground motion and compared it with observed ground motion due to earthquakes of magnitude ranging from 6.6 to 7.8. The applicability of this method for modeling of the great earthquake is still questionable.
- The faulting mechanism of an earthquake controls the shape of simulated strong motion records. Theoretically, source mechanism of an earthquake is defined by the radiation pattern which depends on fault plane solution. So far, no modification in the semi-empirical technique has been made to incorporate the use of the radiation pattern in the modeling of finite rupture sources.
- The semi-empirical method of simulation gives only single record which can be compared either with maximum of two horizontal components or resultant record and is dependent on the use of attenuation relation. The method of semi-empirical modeling still requires modifications for component-wise simulations of strong ground motion and removing its dependency on empirical relations.

1.4 Research Objectives

Literature survey reveals that the Empirical Green's Function and Semi-empirical simulation techniques are two methods of simulation of strong ground motion which are based on deterministic modeling of the rupture plane of an earthquake source with limited and easily available parameters. Both the methods have their own advantages. It is observed that though empirical Green's function technique gives reliable results, its requirement of aftershocks at the site of simulation is a condition which is rarely satisfied for simulation of strong ground motion at a new site. This condition is not a hurdle in the semi-empirical technique where the envelope of accelerogram is basic input for strong motion simulation. It has been observed from literature survey, regarding the semi-empirical simulation technique that further refinements in this technique may add our confidence in this method and reliability on simulated records. A strong need has been felt to add concept of earthquake source mechanism and component-wise division of energy in the semi-empirical simulation technique which can simulate components of strong motion records with a confidence shown by the empirical Green's function technique. Following objectives have been identified for this Ph.D. work on the basis of literature survey and identified research gaps in this area:

1. Component-wise simulation of strong ground motion using semi-empirical modeling technique in a broad frequency range.
2. Use of simple and easily accessible parameters in the semi-empirical technique of simulation of strong ground motion from earthquakes of wide ranging magnitude.
3. Validation of developed technique with case studies of known earthquakes and with well-established technique of simulation of strong ground motion.
4. Generation of scenario earthquake for various techno economically important locations in Indian subcontinent using modified technique and comparing its obtained results with well-established simulation technique.

1.5 Thesis Layout

This thesis comprises of six chapters. Chapter 1 presents a brief review of literature regarding different simulation techniques used for generation of synthetic ground motion. Various aspects related to ground motion synthesis adopted by different researchers, different procedures to

obtained source parameters are described in this chapter. In this chapter research gaps are identified on the basis of literature review. Based on these identified gaps in this field, objectives of this thesis have been defined in this chapter.

In Chapter 2 the methodologies for generating synthetic ground motion using semi-empirical technique and empirical Green's function technique are briefly explained. The chapter also explains the numerical tests applied for checking the suitability of modified semi-empirical method in defining various strong motion properties.

Synthetic ground motions have been generated for the Niigata-ken Chuetsu, Japan earthquake (M_w = 6.6) in Chapter 3 using both modified semi-empirical and empirical Green's function technique described in Chapter 2. The simulations obtained for same rupture model using two different techniques are compared with the observed records in terms of root mean square error for several strong motion parameters. This well recorded and well-studied earthquake has been used to confirm the efficacy of modified technique.

Applicability of the modified technique for simulation of strong ground motion due to earthquakes in the Indian subcontinent has been considered in the present thesis. Chapter 4 presents the simulation of strong ground motions of the Sikkim earthquake (M_w = 6.9) of September 18, 2011. The rupture plane of this earthquake has been identified in this chapter on the basis of seismicity and seismotectonics of region and the parameters of the modeled rupture plane have been calculated using various available information and relations. The source spectra of the mainshock and aftershock have been calculated in this chapter to compute various source parameters such as seismic moment, corner frequency and stress drop. The ratio of stress drop of the mainshock and aftershock and other parameters are used for computation of the parameters of sub-faults modeled within the rupture plane of the target event. Records of the Sikkim earthquake have been simulated at near-field as well as far-field stations and compared with the observed records to check the efficacy of the proposed method for component-wise simulation of ground motion.

Chapter 5 describes the ground motion simulation of the Sumatra earthquake using the simulation techniques described in Chapter 2. Various parameters of the rupture model of this earthquake have been finalized using iterative forward modeling. The chapter includes simulation of time histories and response spectra at several recording stations that have recorded this earthquake and its comparison with the observed records. This chapter also presents the seismic

hazard potential of the Andaman region due to a scenario earthquake of magnitude 8.5 (M_w) in this region.

Chapter 6 summarizes all the research done in the present study. Chapter also highlighted the important conclusions drawn from the present study.

Chapter – 2

TECHNIQUES USED FOR SIMULATION OF STRONG GROUND MOTION

Strong ground motion is an essential part of any engineering study of structure. Various techniques of simulation of strong ground motion and their limitations have been discussed in Chapter 1. In the present work empirical Green's function and semi-empirical technique have been used for simulation of strong ground motion. This chapter discusses mathematical formulation and numerical experiments regarding these techniques.

2.1 Empirical Green's Function (EGF) Technique

Empirical Green's function approach suggested by Hartzell (1978) is one of the popular and widely used methods of simulating acceleration time histories. According to this method the fault is divided into segments which are assumed to represent small earthquakes (subevents). The source time function of each subevent has its spectral shape, corner frequency and seismic moment. Contributions of subevents are summed in a specific way to get proper seismic moment and spectral shape of the source function corresponding to the whole fault. In this approach an aftershock is considered as the record of the small earthquake. Within the scope of linear system theory, Green's function or impulse response function is used for forward modeling of earth model. This function is the surface level response of the region under consideration to a buried impulsive double couple applied at an arbitrary point. The small magnitude earthquakes with point like sources provide an important clue to the regional Green's function.

In the elastodynamic wave theory, Green's function means the displacement at an observation point due to a point force. In EGF simulation method the records of small earthquake that share the source area and observation station with the main shock are called as empirical Green's function. Empirical Green's function shares the path and the local amplification effects with the mainshock but has significant difference in the source effect (Hartzell 1978). This difference has defined by the relation of small and target earthquakes. The spectral scaling laws

(Aki 1967) and the scaling law of the fault parameters (Kanamori and Anderson 1975) gives the way to estimate this relation for earthquakes up to intermediate-size (Yokoi and Irikura 1991).

2.1.1 Self-Similarity

In the EGF technique the earthquake source is considered as a rectangular plane. This plane is divided into several small rectangles known as sub-faults, elements or elementary earthquakes. Division of rupture plane into sub-faults is based on self-similarity laws between the target and elementary earthquake. The record of earthquake representing each sub-fault is called as empirical Green's function. Figure 2.1 shows the division of the rectangular rupture plane of size $L \times W$ into several sub-faults of size $L_e \times W_e$.

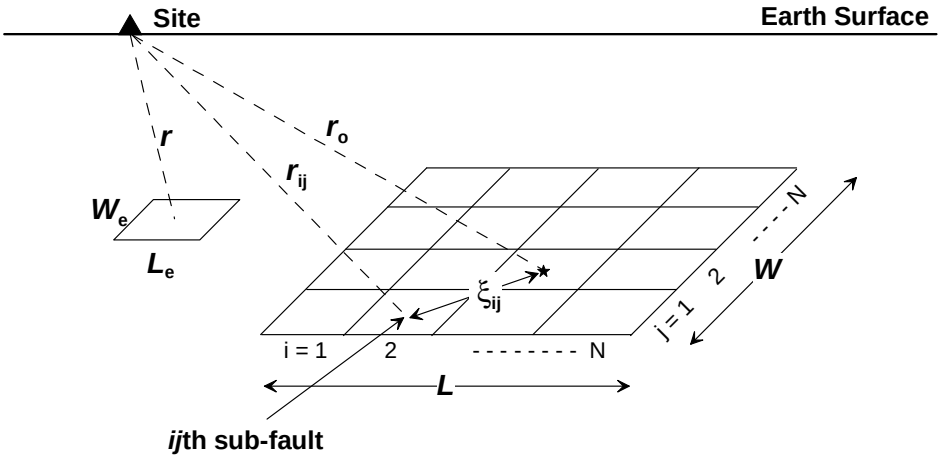

Figure 2.1 Schematic illustrations of fault areas of target and small earthquakes are defined to be $L \times W$ and $L_e \times W_e$, respectively. Star indicates the rupture initiating point at distance r_o km from site and at ξ_{ij} km distance from the *ij*th sub-fault. The parameter r_{ij} denotes the distance of *ij*th sub-fault from site (Figure modified after Irikura 1986)

Division of rupture plane of target earthquake into sub-faults is based on the self-similarity law of the source parameter given by Kanamori and Anderson (1975) and the self-similarity law of source spectra given by Aki (1967). Scaling relationship for source parameters such as rupture length, rupture width, slip, slip duration and magnitude are defined by the self-similarity laws given by Kanamori and Anderson (1975) as follows:

$$L/L_e = W/W_e = T/\tau = D/d = \left(M_o \big/ M_o'\right)^{1/3} = N \tag{2.1}$$

where,

L and L_e = length of the rupture plane of the target and small earthquakes or sub-faults, respectively;

W and W_e = width of the rupture plane of the target and small earthquakes, respectively;

T and τ = slip duration of the target and small earthquakes, respectively;

D and d = slip of the target and small earthquakes, respectively;

M_o and M_o' = seismic moment of the target and small earthquakes, respectively and

N = total number of sub-faults along the length or the width of the modeled rupture plane.

Above relation has modified by using the following empirical relationship between seismic moment and the earthquake magnitude by Kanamori (1977):

$$\log_{10} M_o = 1.5M_w + 16.1 \tag{2.2}$$

where, M_o and M_w are the seismic moment and moment magnitude of an earthquake, respectively. Following relation of self-similarity is obtained by using equation (2.1) and (2.2) as:

$$N = 10^{0.5\left(M_w - M_w'\right)} \tag{2.3}$$

where, M_w and M_w' are the moment magnitude of the target and small earthquakes, respectively. The scaling laws mentioned above are required for defining the parameter of rupture plane responsible for causing target earthquake. The other scaling relation which is used in the simulation technique is the spectral scaling model given by Aki (1967) and Brune (1970) and is called as Omega square (ω^{-2}) spectral scaling model. The ω^{-2} source model is considered as a reference model even for study of great earthquakes (Houston and Kanamori 1986) as well as of intermediate-sized earthquakes (Hanks and McGuire 1981). According to ω^{-2} model (Aki 1967; Brune 1970) the theoretical shapes of source spectrum is given as:

$$U(f) = \frac{M_o}{\left[1+(f/f_c)^2\right]} \tag{2.4}$$

The source displacements spectra of both the target and small earthquakes can be defined as follows:

$$U_o(f) = \frac{M_o}{\left[1+(f/F_c)^2\right]} \tag{2.5}$$

$$U_o'(f) = \frac{M_o'}{\left[1+(f/f_c)^2\right]} \tag{2.6}$$

where, F_c and f_c are corner frequency of the target and small earthquakes, respectively.

According to ω^{-2} model, Irikura (1986) proposed following approximation:

$$U(f \to 0) \approx \omega^o, U(f \to \infty) \approx \omega^{-2} \tag{2.7}$$

The self-similarity law for spectral properties between the target and small earthquakes is formulated as follows:

$$\frac{U_o}{U_o'} = \frac{M_o}{M_o'} = N^3 \tag{2.8}$$

where, U_o and U_o' are the constant levels of the displacement spectra of the target and small earthquakes, respectively. This scaling relation is called as ω^{-2} spectral scaling model (Aki 1967; Brune, 1970). If the average stress drop is independent of M_o, self-similarity exists among these earthquakes (Aki 1967). Under such cases high-frequency acceleration flat level A_o is proportional to $M_o^{1/3}$, which gives the following form of the spectral relationship between the target and small earthquakes (Irikura 1986):

$$\left(A_o / A_o'\right) = \left(M_o / M_o'\right)^{1/3} = N \tag{2.9}$$

where, A_o and A_o' are the high-frequency flat level of the acceleration spectra of the target and small earthquakes, respectively. The constant stress drop model gives following scaling relation between the corner frequency of the target and small earthquakes (Boore 1983):

$$F_c / f_c = \left(M_o' / M_o \right)^{1/3} = 1/N \tag{2.10}$$

where, F_c and f_c are the corner frequency of the target and small earthquakes, respectively. The condition of constant stress drop does not always hold in wide magnitude range (Joshi and Midorikawa 2004). Therefore, Irikura (1986) has introduced a flexible condition for ω^{-2} model, having shape of ω^{-2} source spectrum but not constant stress. In such cases the self-similarity law of source spectra for including stress drop ratio C' of the target and small earthquakes is given as (Irikura 1986):

$$\frac{U_o}{U_o'} = \frac{M_o}{M_o'} = C'N^3 \tag{2.11}$$

$$\left(A_o / A_o' \right) = \left(M_o / M_o' \right)^{1/3} = C'N \tag{2.12}$$

where, C' is the stress drop ratio between the target and small earthquake, N and C' can be derived from constant levels of the source displacement and acceleration amplitude spectra of the target and small earthquakes with equations (2.10) and (2.11), respectively. In this case other scaling paramentes are given as:

$$L/L_e = W/W_e = T/\tau = D/d = \left(M_o / C'M_o' \right)^{1/3} = N \tag{2.13}$$

$$D/d = \left(A_o / A_o' \right) = C'N \tag{2.14}$$

where, C' is the ratio of stress drop of the target and the small earthquake.

2.1.2 Method of Simulation

The strong ground motion due to finite rupture can be modeled by using the records of small earthquake recorded at a hypocentral distance *r*, using the formulation of EGF method described by Irikura (1986). Mathematical development of this method is based on double couple dislocation theory given by Aki and Richards (1980). According to double couple dislocation theory, the displacement at an observation point at the surface of earth is given as (Joshi et al. 2012b):

$$U_i^{SH}(x,t) = \iint \frac{R_{ij}(\varphi_S, \delta, \lambda, i_\xi, \varphi)}{r_{ij}} G_i^S(x,t) * \Delta\dot{u}(\xi,t)\, d\Sigma \tag{2.15}$$

where, each function described above is defined as (Joshi et al. 2012b):

$U_i^{SH}(x,t)$ = displacement at the observation point at the surface of earth due to target earthquake;

$R_{ij}(\varphi_S, \delta, \lambda, i_\xi, \varphi)$ = radiation pattern of the target earthquake, with strike (φ_s), dip (δ), rake (λ), takeoff angle (i_ξ) and azimuth (φ);

$G_i^S(x,t)$ = Green's function which control the medium properties;

$\Delta\dot{u}(\xi,t)$ = time derivative of source displacement pulse of the target earthquake;

r_{ij} = distance of *ij*th sub-fault from the observation point;

Σ = area of rupture plane.

The displacement at the same observation point due to a small earthquake occurring nearby the target earthquake can also be defined according to double couple dislocation theory (Aki and Richards 1980). This modifies the equation (2.15) for small earthqauke as:

$$u_i^{SH}(x,t) = \iint \frac{R^S(\varphi_S, \delta, \lambda, i_\xi, \varphi)}{r} G_i^S(x,t) * \Delta\dot{u}_S(x,t)\, d(\Delta\Sigma) \tag{2.16}$$

where,

$u_i^{SH}(x,t)$ = displacement at the observation point at the surface of earth due to small earthquake;

$R^S\left(\varphi_S,\delta,\lambda,i_\xi,\varphi\right)$ = radiation pattern of the small earthquake, with strike (φ_S), dip (δ), rake (λ), takeoff angle (i_ξ) and azimuth (φ);

$\Delta\dot{u}_S\left(x,t\right)$ = time derivative of source displacement pulse of the small earthquake;

r = hypocentral distance of the small earthquake at recording site;

$\Delta\Sigma$ = area of small earthquake.

Amplitude of source pulse of target earthquake can be buildup by adding all small earthquakes, but if all small earthquakes occur at the same time, we get high amplitude with same duration. The records at the observation point cannot be directly added, due to appropriate difference of the slip function of the target and small earthquakes. In order to compensate the slip duration of target and small earthquake, a function $F(t)$ is convolved with each record of small earthquake before addition. This function $F(t)$ is called as correction function and is used to adjust the difference in the slip time function between small and target earthquake. The function $F(t)$ has asymptotic spectral level of unity at high-frequencies (Joshi and Midorikawa 2004). The spectral amplitude of the small earthquake in low-frequency limit being amplified N^3 times while the high-frequency spectral level of the subevent, being amplified N times (Irikura and Kamae 1994), respectively, where N denotes the number of sub-faults along length or downward extension of the rupture plane. Direct summation of synthetic records without considering correction factor $F(t)$ can give match in high-frequencies, however it will underestimate low-frequency simulation in the synthetic record (Joshi and Midorikawa 2004). Therefore, the correction factor has been used to get the synthetic record having basic spectral shape of ω^{-2} source model in the broad frequency range (Joshi and Midorikawa 2004). This function is defined as (Irikura et al. 1997; Irikura and Kamae 1994):

$$F\left(t\right)=\delta\left(t\right)+\left[\left(N-1\right)/T_R\left(1-\exp\left(-1\right)\right)\right]\cdot\exp\left(-t/T_R\right) \tag{2.17}$$

where, $\delta(t)$ is the delta function, N is the total number of sub-faults along the length or the width of the rupture plane, and T_R is the rise time of the target earthquake. The relation between source time function of small earthquake ($\Delta\dot{u}_S$) and target earthquake ($\Delta\dot{u}$) is calculated by using correction function $F(t)$ and is given as:

$$\Delta\dot{u}(\xi,t)=\sum_{N^2}\int_0^{\infty}F(\tau)\cdot\Delta\dot{u}_S(\xi,t-\tau)\,d\tau \tag{2.18}$$

$$\Delta\dot{u}(\xi,t)=\sum_{N^2}\int_0^{\infty}F(t-\tau)\cdot\Delta\dot{u}_S(\xi,\tau)\,d\tau \tag{2.19}$$

$$\Delta\dot{u}(\xi,t)=\sum_{N^2}F(t)*\Delta\dot{u}_S(\xi,t) \tag{2.20}$$

The displacement record at an observation point due to target earthquake is given as:

$$U_i^{SH}(x,t)=\iint\frac{R_{ij}(\varphi_S,\delta,\lambda,i_\xi,\varphi)}{r_{ij}}G_i^S(x,t)*\Delta\dot{u}(\xi,t)\,d\Sigma \tag{2.21}$$

Substituting the relation (2.19) between source time function of target $\Delta\dot{u}(\xi,t)$ and small earthquake $\Delta\dot{u}_S(\xi,t)$, the following modified form of expression for the displacement record due to target earthquake is obtained:

$$U_i^{SH}(x,t)=\iint\frac{R_{ij}(\varphi_S,\delta,\lambda,i_\xi,\varphi)}{r_{ij}}G_i^S(x,t)*\left[\sum_{N^2}F(t)*\Delta\dot{u}_S(\xi,t)\right]d\Sigma \tag{2.22}$$

$$U_i^{SH}(x,t)=\sum_{N^2}\left[\iint\frac{R_{ij}(\varphi_S,\delta,\lambda,i_\xi,\varphi)}{r_{ij}}G_i^S(x,t)*\Delta\dot{u}_S(\xi,t)\,d\Sigma\right]*F(t) \tag{2.23}$$

By introducing the radiation pattern $R^S(\varphi_S,\delta,\lambda,i_\xi,\varphi)$ and hypocentral distance *r* of small earthquake in above equation (2.23), following modified form of equation is obtained:

$$U_i^{SH}(x,t)=\sum_{N^2}\left[\iint\frac{R_{ij}(\varphi_S,\delta,\lambda,i_\xi,\varphi)}{r_{ij}}\cdot\frac{r}{R^S(\varphi_S,\delta,\lambda,i_\xi,\varphi)}\left\{\frac{R^S(\varphi_S,\delta,\lambda,i_\xi,\varphi)}{r}\right\}G_i^S(x,t)*\Delta\dot{u}_S(\xi,t)\,d\Sigma\right]*F(t) \tag{2.24}$$

$$U_i^{SH}(x,t)=\sum_{N^2}\left\{\frac{R_{ij}(\varphi_S,\delta,\lambda,i_\xi,\varphi)}{r_{ij}}\cdot\frac{r}{R^S(\varphi_S,\delta,\lambda,i_\xi,\varphi)}\right\}\left[\iint\frac{R^S(\varphi_S,\delta,\lambda,i_\xi,\varphi)}{r}G_i^S(x,t)*\Delta\dot{u}_S(\xi,t)\,d\Sigma\right]*F(t) \tag{2.25}$$

Substituting the expression of displacement at the surface of earth due to small earthquake given in equation (2.16), the following modified form of equation (2.25) is obtained:

$$U_i^{SH}(x,t) = \sum_{N^2} \left\{ \frac{R_{ij}(\varphi_S, \delta, \lambda, i_\xi, \varphi)}{r_{ij}} \cdot \frac{r}{R^S(\varphi_S, \delta, \lambda, i_\xi, \varphi)} u_i^{SH}(x,t) * F(t) \right\} \tag{2.26}$$

This equation serves as a basis for EGF technique. This expression does not require either source time function or the theoretical Green's function. Equation (2.26) can be modified into following form as:

$$A(t) = \sum_{i=1}^{N} \sum_{j=1}^{N} \left(\frac{r}{r_{ij}} \right) F(t - t_{ij}) * a(t) \tag{2.27}$$

where,

r, r_{ij} = the distances from the hypocenter of small earthquake and from the ijth sub-fault to the site, respectively;

t_{ij} = the sum of time delay from the rupture staring point via ijth sub-faults to the site;

$F(t)$ = the filtering function (correction function) to adjust the difference in the slip-time function between the target and small earthquakes;

$a(t)$ = the ground motion time history of the small earthquake;

$A(t)$ = the ground motion time history of the target earthquake.

Following form of equation using self-similarity laws given by Irikura (1986) has been used for the case when the stress drop ratio of the target and small earthquakes are not equal:

$$A(t) = C' \sum_{i=1}^{N} \sum_{j=1}^{N} \left(\frac{r}{r_{ij}} \right) \cdot \frac{R_{ij}(\varphi_S, \delta, \lambda, i_\xi, \varphi)}{R^s(\varphi_S, \delta, \lambda, i_\xi, \varphi)} F(t) * a(t - t_{ij}) \tag{2.28}$$

where, C' is the stress drop ratio of the target and small earthquake. The entire process of simulation using EGF technique is shown in Figure 2.2.

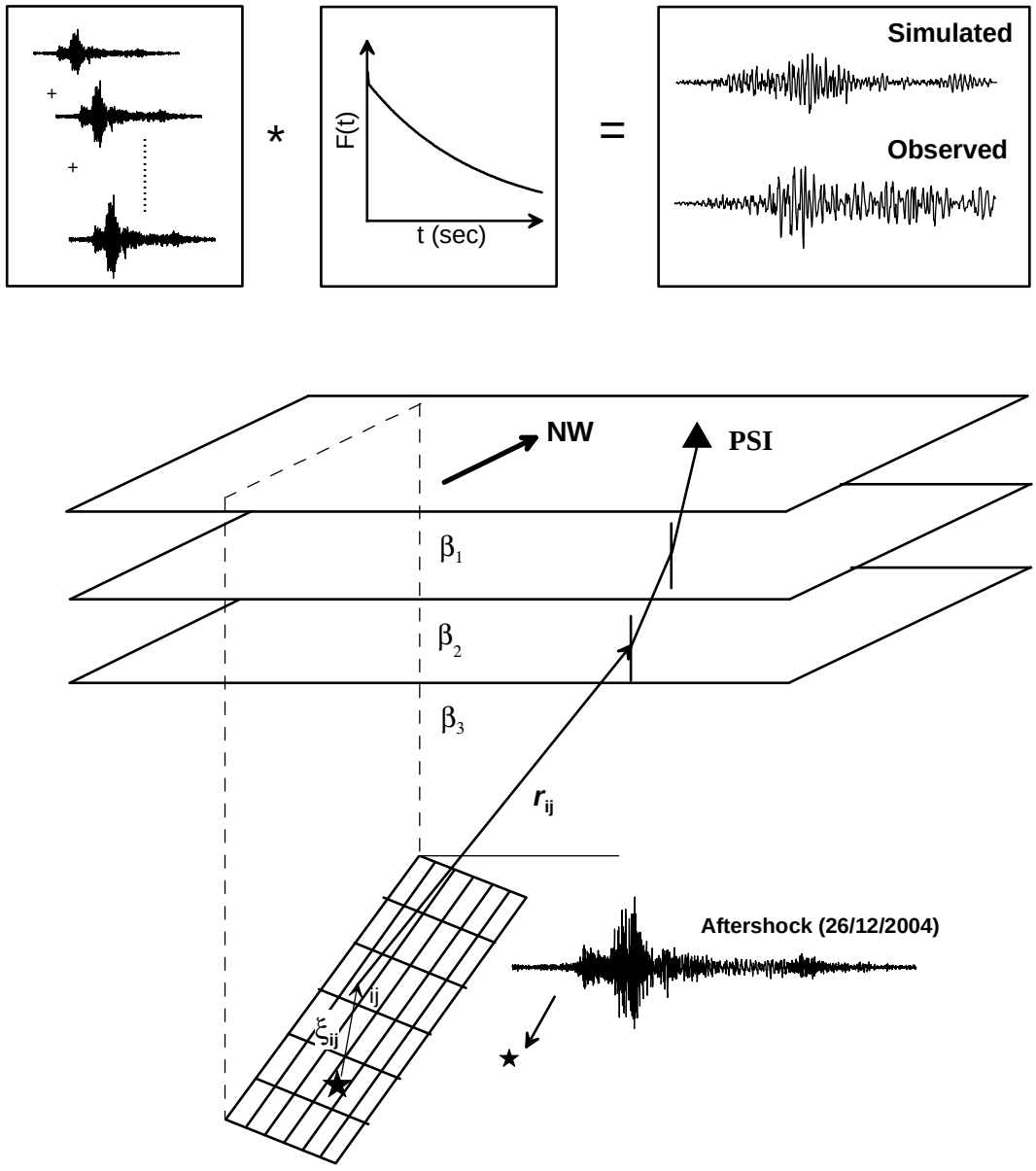

Figure 2.2 Illustration of Empirical Green's Function (EGF) simulation technique. Large and small star denotes the location of the hypocenter of target earthquake and the aftershock used as EGF. The parameters ξ_{ij} denotes the distance traveled by the rupture within the rupture plane of 6×6 sub-faults from nucleation point to the center of *ij*th sub-fault and r_{ij} is the distance traveled by energy from center of *ij*th sub-fault to the observation point. Subscript *i* and *j* denotes the location of sub-fault within the rupture plane and β_1, β_2 and β_3 are the shear wave velocities in the layered medium. Summation of all accelerograms from various sub-faults at the observation point is convolved with the correction factor *F*(*t*) gives the final simulated record, which has been compared with observed one

2.2 Modified Semi-Empirical Technique

The Empirical Green's Function (EGF) technique is one of the most reliable techniques used for simulation of strong motion but has limited applicability due to its major requirement of aftershock or foreshock of target earthquake to be modeled. In an attempt to remove dependency of EGF technique on aftershocks, Midorikawa (1993) proposed a semi-empirical Green's function approach in which the aftershocks are replaced by empirically generated Green's function. The theoretical development was made in such a way that this method satisfies the property of ω^{-2} source model given by Brune (1970). In recent years, the method of modified semi-empirical simulation of strong ground motion has evolved as an effective tool for simulation of strong ground motion. This method has advantages of both the empirical Green's function technique and the stochastic simulation technique. The simplified technique is based on modifications made in the semi-empirical technique given by Midorikawa (1993) and later modified by Joshi and Midorikawa (2004). In this technique synthetic records from different sub-faults within the rupture plane are used in place of aftershock records as Green's function. The advantage of the semi-empirical technique given by Midorikawa (1993) is that it require less time for computations and is based on simple attenuation relations and various parameters which are easy to predict. However, the dependency of semi-empirical method on the attenuation relationship itself poses strong constraint on its applicability, especially for the case of modeling great earthquake using empirically generated attenuation relationships. The semi-empirical method has been used for strong motion simulation of small to large earthquake in a broad frequency range (Joshi 2004; Joshi and Midorikawa 2004; Joshi et al. 2010), but the method has never been tested for simulating records due to great earthquakes.

In the semi-empirical technique, the rupture plane of the target earthquake is divided into several sub-faults. The concept of dividing the rupture plane of the target earthquake into sub-fault is same as followed in EGF technique. The modified semi-empirical method proposed by Joshi and Midorikawa (2004) uses the concept of stochastic simulation technique together with the semi-empirical technique for simulation of strong motion time series. In first part of this technique a time series having basic spectral shape of accelerogram has been simulated while in second part deterministic model of the rupture plane has been used to simulate the envelope of accelerogram. The modified semi-empirical method uses the time series obtained from stochastic simulation technique and the envelope function obtained from the semi-empirical technique. In stochastic

simulation technique, white Gaussian noise of zero expected mean and variance chosen to give unit spectral amplitude (Figure 2.3a and Figure 2.3b) is passed through number of filters representing the earthquake processes. In this process the amplitude spectrum of white noise is replaced by the acceleration spectra of the target earthquake. The acceleration spectra can be defined as (Boore 1983):

$$A(f) = CS(f) D_S(f) F_R(f, R) \tag{2.29}$$

where, C is a constant scaling factor given by:

$$C = M_o \cdot R_{\theta\varphi} \cdot FS \cdot PRTITN \Big/ 4\pi\rho\beta^3 \tag{2.30}$$

The terms used in equation (2.30) are defined by Boore (1983). In this expression, M_o is the seismic moment, $R_{\theta\varphi}$ is the radiation pattern, FS is the amplification due to the free surface, $PRTITN$ is the reduction factor that accounts for the partitioning of total shear-wave energy into two horizontal components, ρ is the density of the medium and β is the shear wave velocity. The radiation pattern $R_{\theta\varphi}$ is dependent on type of faulting mechanism and the geometry of earthquake source. In the present work following expression of the radiation pattern coefficient for SH wave given by Aki and Richards (2002) has been used:

$$\begin{aligned} R_{\theta\varphi} = {} & \cos\lambda.\cos\delta.\cos i_\xi.\sin(\varphi-\varphi_S) + \cos\lambda.\sin\delta.\sin i_\xi.\cos 2(\varphi-\varphi_S) \\ & + \sin\lambda.\cos 2\delta.\cos i_\xi.\cos(\varphi-\varphi_S) - \frac{1}{2}\sin\lambda.\sin 2\delta.\sin i_\xi.\sin 2(\varphi-\varphi_S) \end{aligned} \tag{2.31}$$

where, φ_s, δ, λ, i_ξ and φ are strike, dip, rake, takeoff angle and source-receiver azimuth of the rupture plane, respectively. The filter $S(f)$ in equation (2.29) is the source acceleration spectrum and is defined by Brune (1970) as follows:

$$S(f) = (2\pi f)^2 \Big/ \left[1 + (f/f_c)^2\right] \tag{2.32}$$

In Equation (2.29), filter $D_S(f)$ is the near-site attenuation of high-frequencies which is defined as (Boore 1983):

$$D_S(f) = 1 \Big/ \left[1 + (f/f_m)^8\right]^{1/2} \tag{2.33}$$

The parameter f_m in the above equation represents the high-frequency cutoff range of the high-cut filter. The filter $F_R(f, R)$ represents the effect of anelastic attenuation and is given as (Boore 1983):

$$F_R(f,R) = \left(e^{-\pi fR/\beta Q_\beta(f)}\right)\Big/ R \tag{2.34}$$

where, R denotes the hypocentral distance in kilometer and $Q_\beta(f)$ is the shear wave quality factor which defines the frequency-dependent attenuation during the shear wave propagation. The spectrum of white noise (Figure 2.3b) after multiplication with theoretical filters (Figure 2.3c) given in equation (2.29) represents basic spectral shape of acceleration spectra (Figure 2.3d). Time domain representation of acceleration spectra (Figure 2.3e) gives an acceleration record which has basic spectral properties of acceleration spectra. However, it is observed that the obtained records overestimate the high-frequency strong ground motion and underestimate low-frequency in the synthetic strong ground motion. This is due to the difference in the duration of slip of target and the small earthquake considered as sub-faults. A correction function $F(t)$ is convolved with the obtained acceleration records for correcting duration of the slip of target and element earthquake. Convolution of $F(t)$ with obtained acceleration record $a_{ij}(t)$ gives acceleration record $A_{ij}(t)$ (Figure 2.3f) as:

$$A_{ij}(t) = F(t) * a_{ij}(t) \tag{2.35}$$

where, subscript i and j are position of the sub-fault along length and width of the rupture plane, respectively. The accelerogram $A_{ij}(t)$ from different sub-faults reaches observation point at different time lags. The obtained accelerogram is further windowed by the envelope function $e_{ij}(t)$ defined in equation (2.37) as follows (Figure 2.3h and Figure 2.3i):

$$ac_{ij}(t) = e_{ij}(t) \cdot A_{ij}(t) \tag{2.36}$$

Boore (1983) pointed that although stochastic simulation technique give reliable simulation it require proper windowing of the obtained record through a function which is based on kinematic representation of model of finite rupture. Such deterministic time window can be obtained by the semi-empirical technique of Midorikawa (1993) in the form of resultant envelope of accelerogram obtained from a model of finite rupture plane divided into several sub-faults. The acceleration

envelope waveform $e_{ij}(t)$ is computed from the following functional form given by Kameda and Sugito (1978) and further modified by Joshi (2004):

$$e_{ij}(t) = T_{ss}(t/T_d) \cdot \exp(1 - t/T_d) \tag{2.37}$$

In this expression, T_d represents the duration parameter and T_{ss} represent the transmission coefficient of the incident shear waves. This coefficient is given by the following formula after Lay and Wallace (1995, p. 102) and was used by Joshi et al. (2001) for modeling the effect of transmission of energy in the shape of acceleration envelope as:

$$T_{ss} = 2\mu_2\eta_{\beta_2} \Big/ \left(\mu_1\eta_{\beta_1} + \mu_2\eta_{\beta_2}\right) \tag{2.38}$$

where, μ_1 and μ_2 are modulus of rigidity in the top and bottom layers, respectively, and β_1 and β_2 are shear wave velocities in the top and bottom layers, respectively. The parameters $\eta_{\beta 1}$ and $\eta_{\beta 2}$ are given as:

$$\begin{aligned} \eta_{\beta_1} &= \left(1 - p^2\beta_1^2\right)^{1/2} \Big/ \beta_1 \\ \eta_{\beta_2} &= \left(1 - p^2\beta_2^2\right)^{1/2} \Big/ \beta_2 \\ p &= \sin(i_a)/\beta_1 \end{aligned} \tag{2.39}$$

where, p and i_a are ray parameter and angle of incidence, respectively. The transmission coefficient contributes significantly to shaping the attenuation rate of the peak ground acceleration with respect to the distance from the source. Joshi and Midorikawa (2004) have observed that for the shallow focus earthquakes, the transmission coefficient is ≈1.0; however, for the intermediate to deep focus earthquake, this coefficient is ≠1.0. This means that this coefficient should be taken into consideration when modeling an intermediate to deep focus earthquake. The duration parameter T_d used in equation (2.37) can be calculated using following relation given by Midorikawa (1989):

$$T_d = 0.0015 \times 10^{0.5M_w} + aR^b \tag{2.40}$$

where, M_w and R are the moment magnitude of the target earthquake and the hypocentral distance in km, respectively. The coefficients a and b in above expression depends on the study area and is derived from regression analysis. The parameters required to define the model of the rupture plane are its length (L), width (W), length and width of the sub-faults (L_e, W_e), nucleation point, strike

and dip of the rupture plane (φ_s, δ), rupture velocity (V_r) and shear wave velocity in the medium. In the semi-empirical method the rectangular rupture plane of the target earthquake of seismic moment M_o is divided into $N \times N$ sub-faults of seismic moment M_o'. Once the rupture plane of target earthquake is divided into several sub-faults, one of the sub-faults is fixed from which the rupture initiates. The centre of this sub-fault is called the nucleation point, which may coincide with the focus of the earthquake. The rupture starts from the nucleation point, and propagates radially within the rupture plane. Each sub-faults releases energy whenever the rupture front approaches its centre. The energy is released in the form of acceleration record $ac_{ij}(t)$ obtained in equation (2.36). The record $ac_{ij}(t)$, released from different sub-faults reaches the observation point at different time. The arrival time at the observation point t_{ij} depends on the time taken by rupture from the nucleation point to the ijth sub-fault with rupture velocity V_r and time taken by energy released from ijth sub-fault to reach the observation point with the velocity β of propagation. The time t_{ij} is calculated using the following relation given by Joshi and Midorikawa (2004):

$$t_{ij} = r_{ij} / \beta + \xi_{ij} / V_r \tag{2.41}$$

where, r_{ij} is the distance from the observation point to the ijth sub-fault and ξ_{ij} is the distance travelled by the rupture from the nucleation point to the particular sub-fault. Summation of all records '$ac_{ij}(t)$' reaching the observation point at different time lag t_{ij} (Figure 2.3i) gives the resultant record '$Ac(t)$' at the observation point which is expressed as (Figure 2.3j):

$$Ac(t) = \sum_{i=1}^{N} \sum_{j=1}^{N} ac_{ij}\left(t - t_{ij}\right) \tag{2.42}$$

In this expression, $N \times N$ are the total number of sub-faults within the rupture plane. The methodology for simulating acceleration record $Ac(t)$ by using finite fault model is shown in Figure 2.3. Various parameters of the modelled rupture plane are selected on the basis of iterative modeling of the rupture plane and comparison of simulated record with observed record. Procedure of selection of various parameters of rupture plane using iterative modeling has been given in a flow graph shown in Figure 2.4.

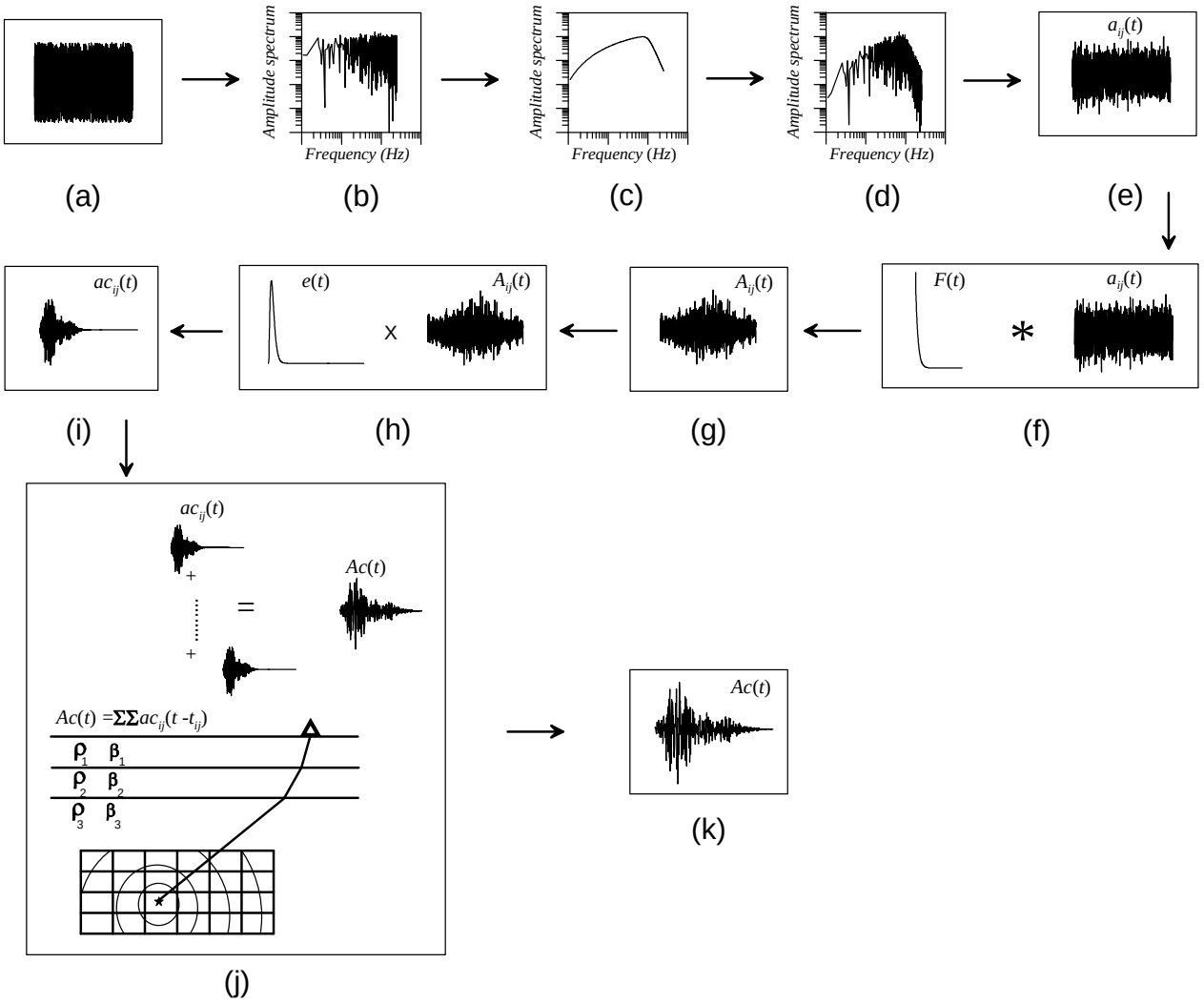

Figure 2.3 (a) White Gaussian noise, (b) its spectrum, (c) The theoretical spectrum of acceleration record including all filters, (d) Multiplication of theoretical spectrum of acceleration record with the spectrum of white Gaussian noise, (e) Filtered white Gaussian noise, (f) Convolution of the filtered accelerogram with the correction function $F(t)$ where $*$ is the convolution operator, (g) Obtained accelerogram after convolve with the correction function, (h) Multiplication of shaping window $e(t)$ with obtained accelerogram $A_{ij}(t)$, where $\times$ is the multiplication sign, (i) Obtained finite duration accelerogram $ac_{ij}(t)$ for ijth sub-fault, (j) Rupture model in a layered earth medium for radial rupture geometry. Star denotes nucleation point. Summation of accelerograms obtained from each sub-faults to simulate the acceleration record $Ac(t)$ of the target earthquake, (k) Simulated accelerogram

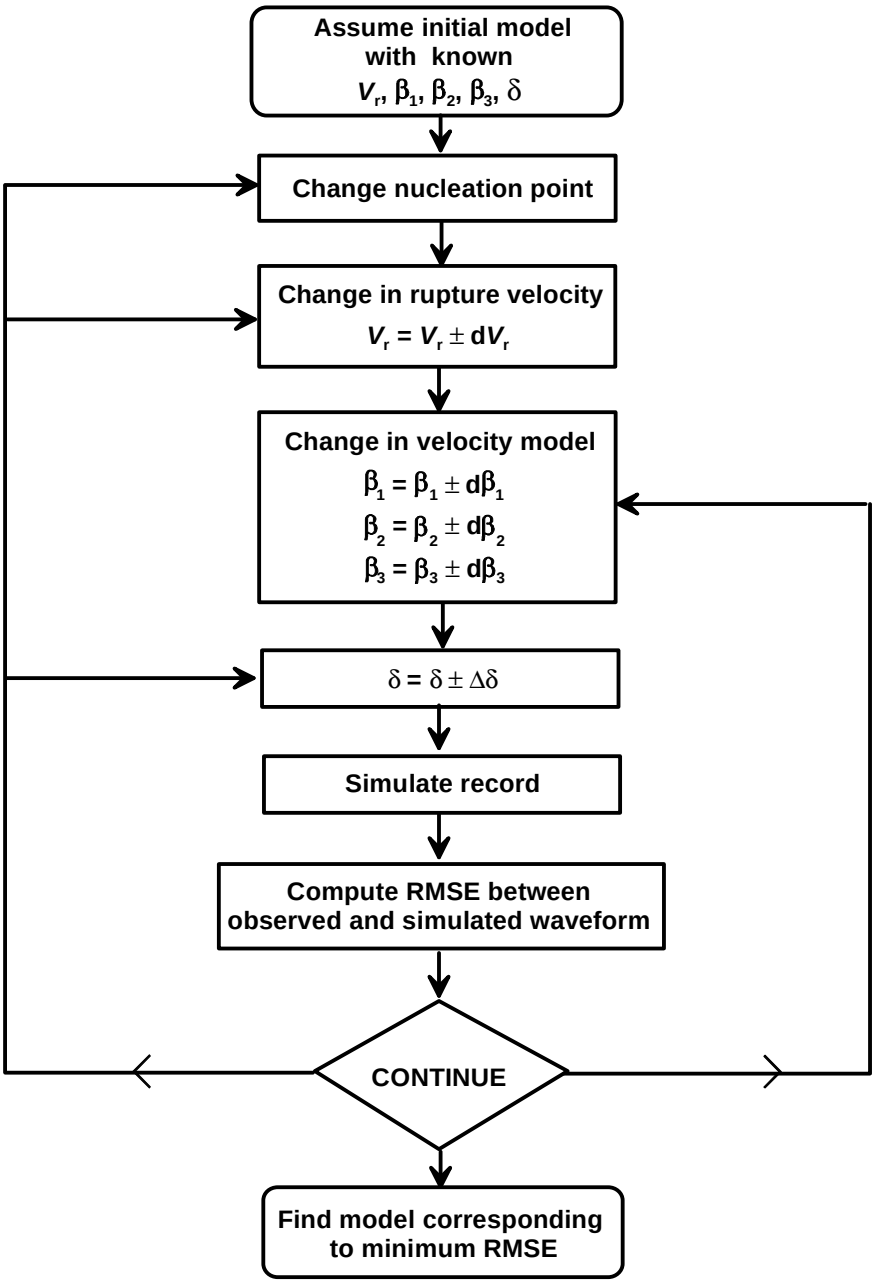

Figure 2.4 Flow graph for iterative selection of various modeling parameters

2.2.1 Numerical Experiments

Modified semi-empirical method has been extensively tested for its applicability in simulating strong ground motion by Midorikawa (1993) and Joshi and Midorikawa (2004). Directivity effects are considered to be one of the most important properties of strong motion

records. The approach of semi-empirical modeling technique given by Midorikawa (1993) clearly follows directivity effect. The modifications in the semi-empirical approach suggested by Joshi and Midorikawa (2004) for layering and correction function also confirm the presence of directivity effects in simulated records. In the present thesis seismic moment has been used for scaling the amplitude of accelerogram together with the radiation pattern. These modifications require an investigation regarding applicability of directivity effects in strong motion records. In order to check the effect of directivity in the modified technique, strong motion records are simulated on both sides of the rupture plane for both bilateral and unilateral rupture propagations. In this numerical experiment vertical rupture plane of length 750 km and downward extension of 150 km has been considered for modeling an earthquake of magnitude 9.0 (M_w). The rake of this rupture has been considered to be similar to the pure thrust mechanism. This rupture plane is further divided into 100 sub-faults, each of which corresponds to 7.0 (M_w) magnitude earthquake and is placed in a three layered velocity model. The three layer velocity model given by Sorensen et al. (2007) used for modeling of the rupture plane of Sumatra earthquake has been used in this experiment. Variation of peak ground acceleration (PGA) on both sides of the rupture plane in strike direction for unilateral rupture propagation and bilateral rupture propagation has been shown in Figure 2.5, which reveals that, in case of unilateral rupture propagation, PGA values are higher in the direction of rupture propagation as compared to PGA values in opposite direction of rupture propagation. In case of bilateral rupture propagation, symmetry has been observed in the contour around both side of rupture propagation. This confirms the presence of directivity effect in the modified semi-empirical technique which has been used for modeling of strong ground motion in the present thesis.

The stability of the modified technique of simulation of strong ground motion and its dependency on modeling parameter has been checked by dividing rupture plane of same modeling parameters into different number of sub-faults. Division of sub-fault is based on the self-similarity laws discussed in section 2.1.1. To check the dependency of number of sub-faults on the obtained simulated record at a selected site, the rupture plane of length and width of 750 and 150 km, respectively has been divided into 10×10, 14×7, 12×8 and 19×5 sub-faults. In all models location of nucleation point is almost same. Using self-similarity laws the magnitude of sub-faults needed to model the rupture of target earthquake into 10×10, 14×7, 12×8 and 19×5 sub-faults has been obtained as 7.0 (M_w), 6.8 (M_w), 6.8 (M_w) and 6.9 (M_w), respectively. Strong motions records at

same station have been simulated using these four models and are shown in Figure 2.6. It is observed that as long as self-similarity is obeyed, there is no drastic change in the shape of record and the PGA parameter also remains almost same for all simulations maintaining the applicability of self-similarity laws.

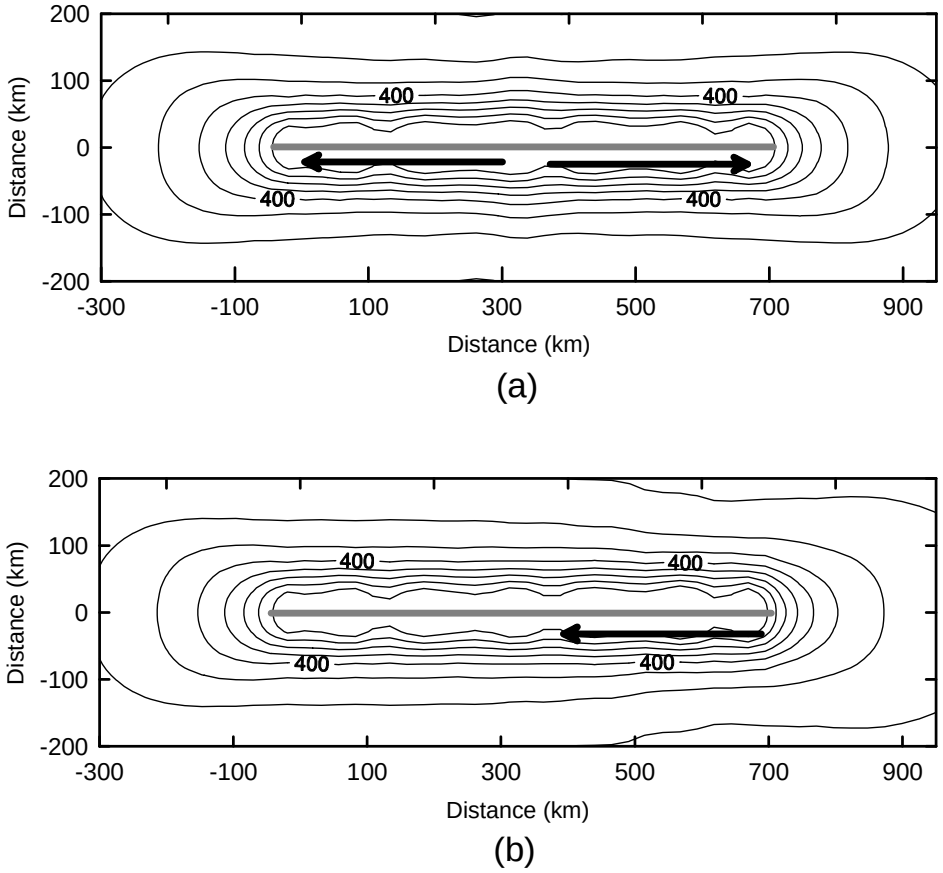

Figure 2.5 Contour of peak ground acceleration (PGA in gal) value in case of (a) bilateral and (b) unilateral rupture propagation. The rupture plane of dimension 750 km×150 km has been shown by thick gray line which placed in vertical direction. Thick arrow shows the rupture propagation direction

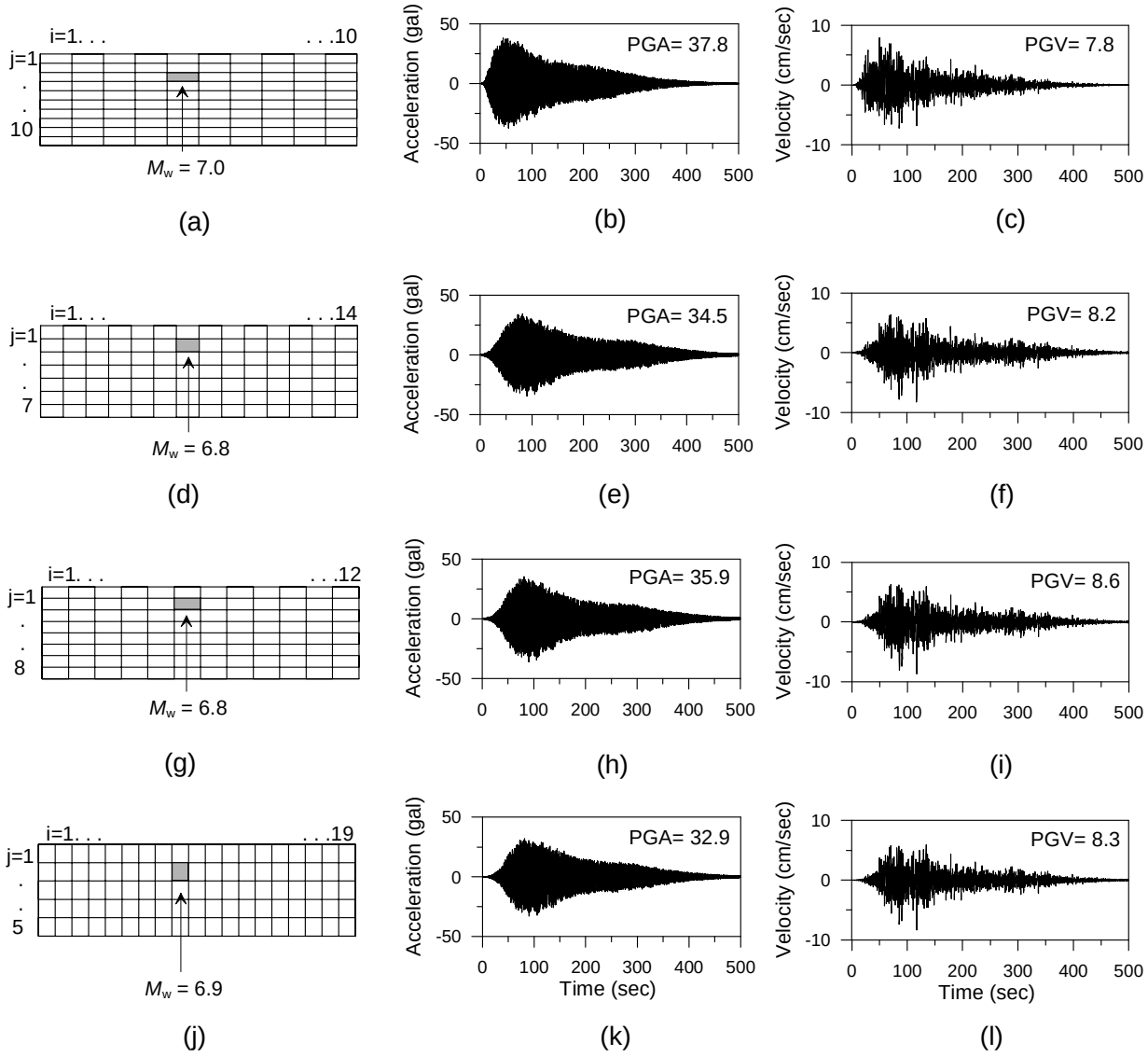

Figure 2.6 (a) Division of rupture plane into 10×10 sub-faults each of which represent 7.0 (M_w) magnitude, (b) simulated acceleration record and its (c) velocity record; (d) Division of rupture plane into 14×7 sub-faults each of which represent 6.8 (M_w) magnitude, (e) simulated acceleration record and its (f) velocity record; (g) Division of rupture plane into 12×8 sub-faults each of which represent 6.8 (M_w) magnitude, (h) acceleration record and its (i) velocity record; (j) Division of rupture plane into 19×5 sub-faults each of which represent 6.9 (M_w) magnitude, (k) acceleration record and its (l) velocity record. In all models the location of starting point of rupture is same

2.3 Component-wise Simulation using Modified Semi-Empirical Technique

The method of semi-empirical simulation technique given by Midorikawa (1993) and further modified by Joshi and Midorikawa (2004) depends heavily on attenuation relation. This method has been modified to remove its dependency on attenuation relation. In the present work the seismic moment and radiation pattern are used in place of attenuation relation for scaling of envelope of accelerogram. Various numerical experiments have been performed to check presence of the directivity effects in the simulated records and stability of simulated technique. The modified method still require component-wise simulation of strong ground motion which is required for the effective comparison of simulated records with the observed records. In the present thesis the modification in semi-empirical method are made to obtain simulated horizontal components of strong motion record.

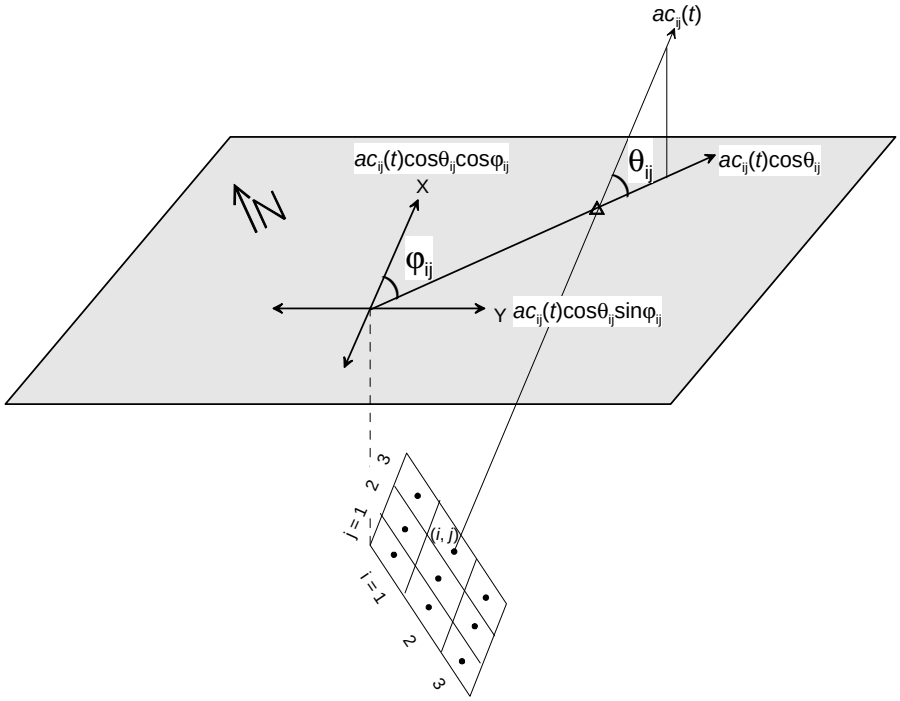

Figure 2.7 Illustration of method for simulation of NS and EW component of earthquake ground motion from *ij*th sub-fault. Triangle shows the recording station. θ_{ij} and φ_{ij} are represents angle made by resultant ground acceleration with the vertical and the angle made by horizontal projection of resultant ground motion acceleration from *ij*th sub-fault with the direction of strike of the modelled fault. X- and Y- axes follows the strike and dip direction of the rupture plane, respectively

Component-wise simulation of strong ground motion can be obtained by including simple vector notation in modified semi-empirical approach which has been explained in the earlier section. The acceleration record simulated using equation (2.35) is a resultant record. The direction of resultant component from each sub-fault with respect to the strike of fault is defined by an angle between a line joining centre of sub-fault to the recording station and strike of fault. This direction is different for different sub-faults and for obtaining contribution of horizontal component along strike and dip direction from each sub-fault, records from each sub-fault need separate treatment. Figure 2.7 shows the division of resultant acceleration record $ac_{ij}(t)$ released from *ij*th sub-fault into components along strike and dip directions. Following formula is used for obtaining the horizontal component of records along the direction of strike (X- axis) and the direction of dip (Y-axis) of the modelled fault, respectively, from resultant component $ac_{ij}(t)$ released by *ij*th sub-fault:

$$ac_{ij}^{X}(t) = ac_{ij}(t) \cdot \cos\theta_{ij} \cdot \cos\varphi_{ij} \tag{2.43}$$

$$ac_{ij}^{Y}(t) = ac_{ij}(t) \cdot \cos\theta_{ij} \cdot \sin\varphi_{ij} \tag{2.44}$$

In equations (2.43) and (2.44), $ac_{ij}^{X}(t)$ and $ac_{ij}^{Y}(t)$ are the acceleration records along X- and Y- axis, respectively. The parameter φ_{ij} in equations (2.43) and (2.44), represents the angle made by horizontal projection of resultant ground acceleration from *ij*th sub-fault with the direction of strike of the modelled fault, and θ_{ij} represents the angle made by resultant ground acceleration with the vertical. The angles θ_{ij} and φ_{ij} are different for different sub-faults and depend on the position of sub-fault within the rupture plane. Once the components of acceleration records are obtained along X- and Y- axes, it has been further rotated by angle ϕ using following matrix rotation formula to obtain components along NS and EW direction:

$$\begin{bmatrix} ac_{ij}^{NS}(t) \\ ac_{ij}^{EW}(t) \end{bmatrix} = \begin{bmatrix} \cos\phi & -\sin\phi \\ \sin\phi & \cos\phi \end{bmatrix} \begin{bmatrix} ac_{ij}^{X}(t) \\ ac_{ij}^{Y}(t) \end{bmatrix} \tag{2.45}$$

where, $ac_{ij}^{NS}(t)$ and $ac_{ij}^{EW}(t)$ are the components of acceleration record along NS and EW direction, respectively, and ϕ is the strike of the modelled rupture plane measured with respect to the geographic North. Summation of all NS and EW component of acceleration record released

from different sub-faults reaching the observation point at different time lag t_{ij} gives the final NS and EW component of acceleration record as follows:

$$Ac^{NS}(t) = \sum_{i=1}^{N}\sum_{j=1}^{N} ac_{ij}^{NS}\left(t - t_{ij}\right) \tag{2.46}$$

$$Ac^{EW}(t) = \sum_{i=1}^{N}\sum_{j=1}^{N} ac_{ij}^{EW}\left(t - t_{ij}\right) \tag{2.47}$$

where, $Ac^{NS}(t)$ and $Ac^{EW}(t)$ represent the north-south and east-west component of acceleration records, respectively. A FORTRAN code, named MSETCS (Modified Semi Empirical Technique for Component-wise Simulation) has been developed for component-wise simulation of strong ground motion using modified semi-empirical technique. Various parameters of the modelled rupture plane are selected on the basis of iterative modeling of rupture plane and comparison of simulated record with observed record. The flow graph showing procedure of iterative modeling and selection of final modeling parameters has been shown in Figure 2.8.

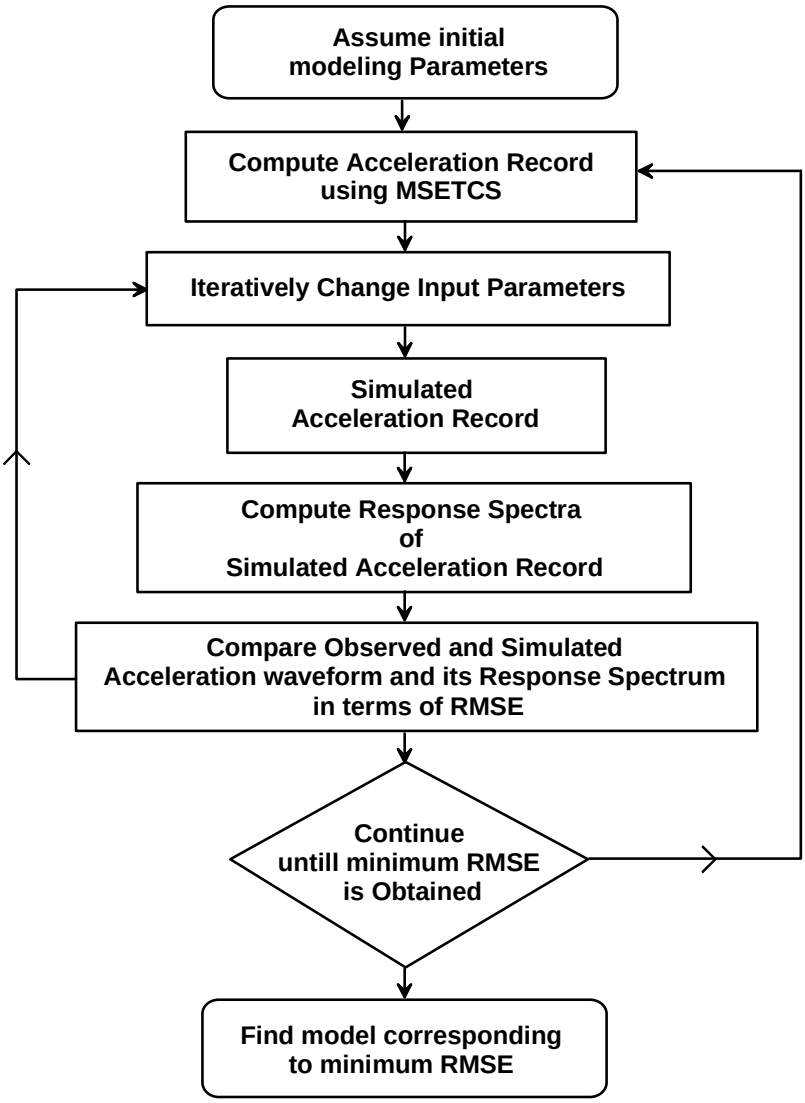

Figure 2.8 Flow graph of methodology for simulation of strong motion records of horizontal components

2.3.1 Numerical Experiments

It has been observed that modifications in the semi-empirical method favor directivity effects. The method modified for component-wise simulation of strong ground motion also requires an investigation regarding applicability of directivity effects in the simulated strong motion records. In order to check the effect of directivity in the modified technique, strong motion records are simulated on both sides of the rupture plane for bilateral and unilateral rupture propagations. In this numerical experiment, a simple vertical rupture plane of length 750 km and

downward extension 150 km has been considered. The dip and rake of this rupture is assumed to be 90° and 0° to consider pure strike-slip mechanism. This rupture plane is divided into 81 sub-faults, each of which corresponds to 7.1 (M_w) magnitudes and placed in a layered velocity model defined by Cotte et al. (1999).

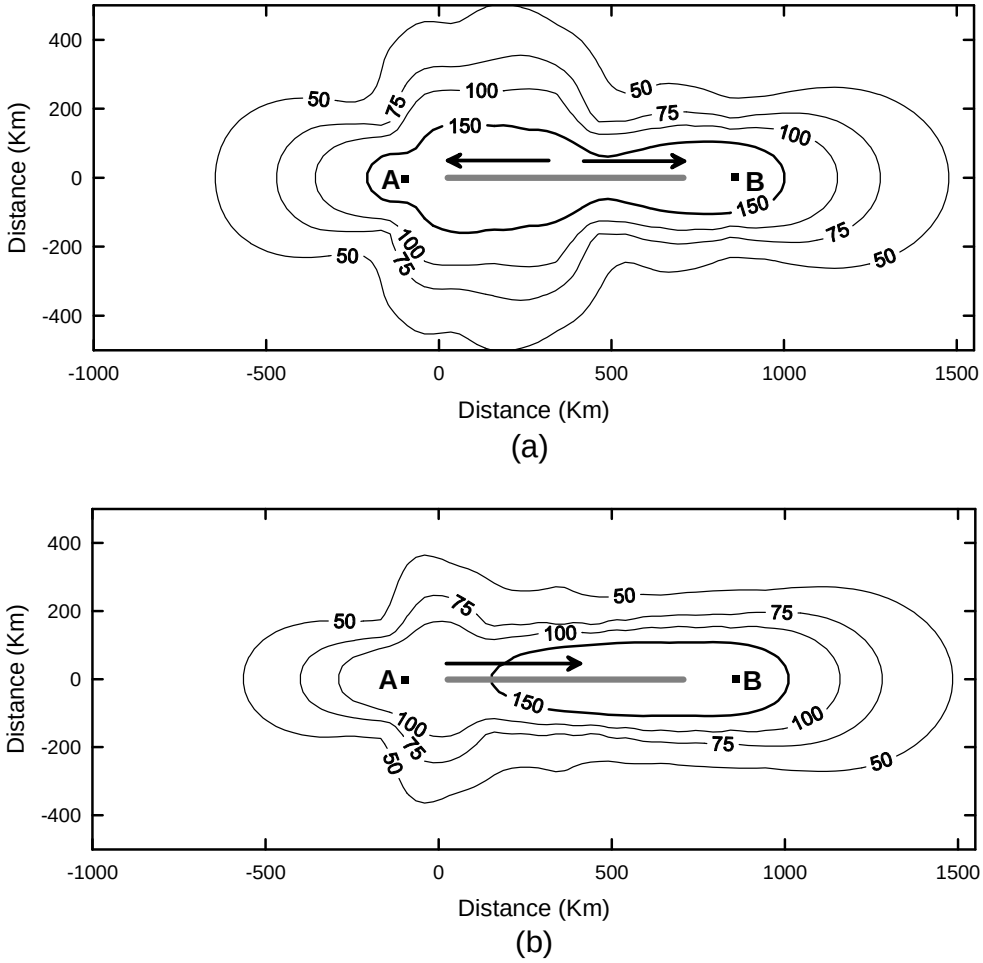

Figure 2.9 Contour of peak ground acceleration (PGA in gal) value in case of (a) bilateral and (b) unilateral rupture propagation. The rupture plane of dimension 750 km×150 km is shown by thick gray line which placed in vertical direction. Arrow shows the rupture propagation direction. Points A and B marked in the figure lies at equal distance from the vertical projection of fault plane

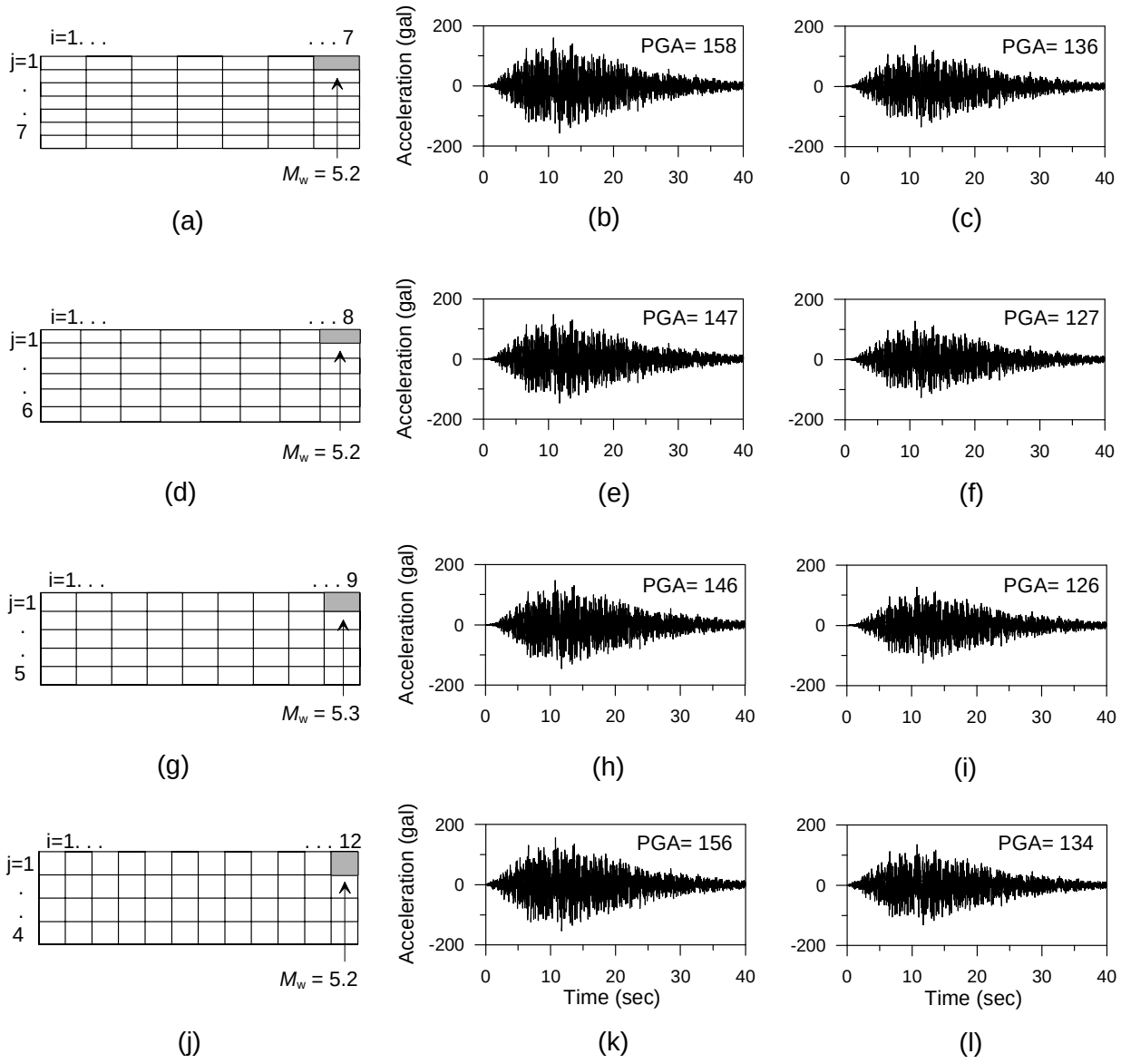

Figure 2.10 (a) Division of rupture plane into 7×7 sub-faults each of which represent 5.2 (M_w) magnitude, (b) simulated NS acceleration record and (c) EW acceleration record; (d) Division of rupture plane into 8×6 sub-faults each of which represent 5.2 (M_w) magnitude, (e) simulated NS acceleration record and (f) EW acceleration record; (g) Division of rupture plane into 9×5 sub-faults each of which represent 5.3 (M_w) magnitude, (h) NS acceleration record and (i) EW acceleration record; (j) Division of rupture plane into 12×4 sub-faults each of which represent 5.2 (M_w) magnitude (k) NS acceleration record and (l) EW acceleration record. In all models the location of starting point of rupture is same

Variation of PGA on both sides of the rupture plane in strike direction for bilateral rupture propagation and unilateral rupture propagation has been shown in Figure 2.9. It has been observed that due to inclusion of radiation pattern, transmission effect, and component-wise simulation, absolute symmetry is not obtained as in case of bilateral rupture propagation. However, it has been observed that two points equidistant from the corner of rupture plane have nearly same PGA for bilateral propagation. The PGA values are higher in the direction of rupture propagation in case of unilateral rupture propagation as compared to the PGA in the opposite direction of rupture propagation. This confirms the presence of directivity effect in the technique modified for component-wise simulation of strong ground motion.

Stability of modified technique and its dependency on modeling parameter has been checked by dividing rupture plane of target earthquake into different number of sub-faults. The parameters of target earthquake are considered to be same for all cases. Division of sub-fault is based on self-similarity laws. To check the dependency of number of sub-faults on the obtained simulated record, the rupture plane of target earthquake has been divided into 7×7, 8×6, 9×5 and 12×4 sub-faults. Location of nucleation point is almost same in all models. The magnitude of sub-faults needed to model rupture of target earthquake into 7×7, 8×6, 9×5 and 12×4 sub-faults have been calculated as 5.2 (M_w), 5.2 (M_w), 5.3 (M_w) and 5.2 (M_w), respectively using self-similarity laws. Strong motions records at same station have been simulated using these four models and are shown in Figure 2.10. It has been observed that as long as self-similarity is obeyed, there is no drastic change in the shape of record and the PGA parameter also remains same for all simulations maintaining the applicability of self-similarity laws in the modified technique.

2.4 Conclusion

This chapter discussed the well-known empirical Green's function technique in detail and modified semi-empirical technique for the simulation of strong ground motion at a site of interest. Modifications in the semi-empirical method have been made to remove its dependency on attenuation relation for scaling of envelope of acceleration in earlier method. Seismic moment and radiation pattern has been used to replace attenuation relationship. Modifications in this method have been made to simulate both horizontal components of strong ground motion by using simple vector law. Numerical tests have been performed to check the applicability of directivity effect and stability, in each modification introduced in semi-empirical technique.

Chapter – 3

SYNTHETIC GROUND MOTION FOR THE NIIGATA EARTHQUAKE OF OCTOBER 23, 2004 (M_W = 6.6)

The Niigata-ken Chuetsu, Japan earthquake was recorded on a dense network of strong motion recorders installed within entire Japan. This chapter presents the simulations of strong ground motion data of the Niigata-ken Chuetsu earthquake using modified semi-empirical approach presented in Chapter 2. The simulations obtained using developed techniques have been compared with the simulations obtained from the well-established EGF technique using the same rupture model.

3.1 Niigata Earthquake

Mid Niigata prefecture located at 80 km south of Niigata city on the West Coast of Honshu, Japan (Bardet 2004) was stuck by a strong earthquake (M_{JMA} = 6.8) on October 23, 2004 at 17:56 (JST). This earthquake is popularly named as Niigata-ken Chuetsu, earthquake. Parameters of this earthquake are given in Table 3.1. Location of the epicenter of this earthquake and stations that had recorded this earthquake is shown in Figure 3.1.

Table 3.1 Parameters of the Niigata-ken Chuetsu, Japan earthquake of October 23, 2004

Hypocenter	Size	Fault Plane Solution	Reference
08:56:4.8 s GMT	$M_o = 8.6\times10^{25}$ dyne-cm	NP1 $\varphi = 23°,\ \delta = 39°,\ \lambda = 86°$	Global CMT
37.31°N, 138.83°E	$M_w = 6.6$	NP2 $\varphi = 209°,\ \delta = 51°,\ \lambda = 93°$	
13 km	$M_{JMA} = 6.8$		
	$m_b = 6.4$		
17:56:00 s JST	$M_o = 7.5\times10^{25}$ dyne-cm	NP1 $\varphi = 27°,\ \delta = 43°,\ \lambda = 87°$	Kamae et al. (2005)
37.29°N, 138.86°E	$M_w = 6.6$	NP2 $\varphi = 212°,\ \delta = 47°,\ \lambda = 93°$	
13.1 km	$M_{JMA} = 6.8$		

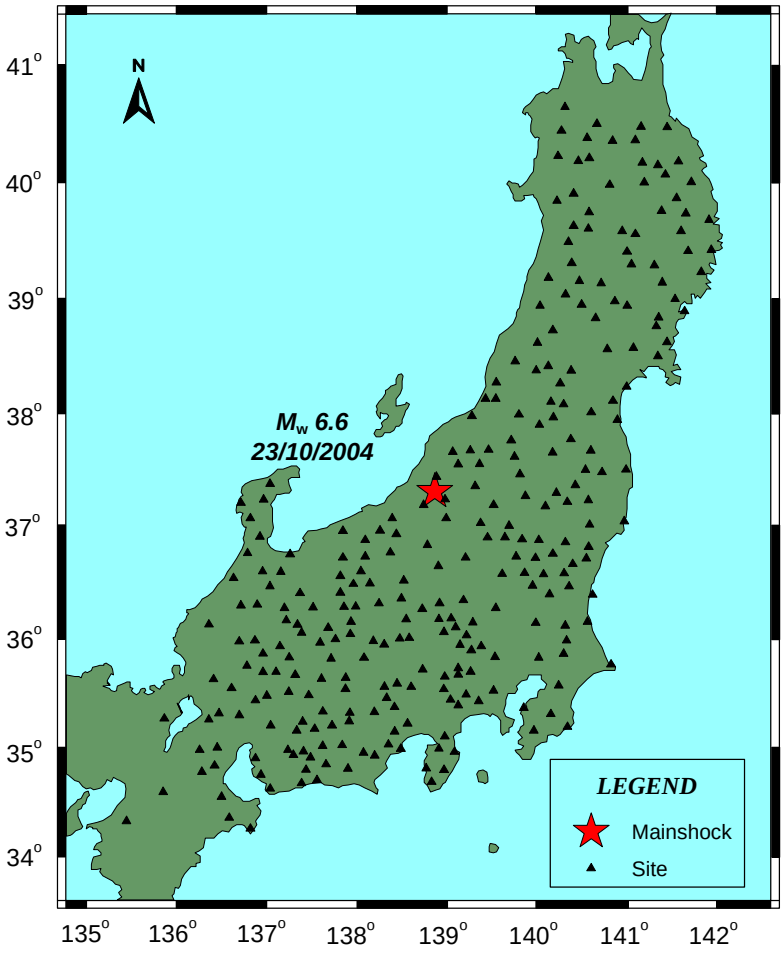

Figure 3.1 Map showing epicenter of the 2004 Niigata-ken Chuetsu, Japan earthquake and 286 sites of KiK-net network that has recorded this earthquake. Coordinates are taken from www.kyoshin.bosai.go.jp

3.2 Geology of the Region

Niigata Prefecture in Japan is located on the island of Honshu on the West Coast of the Sea of Japan. Niigata Prefecture stretches about 240 km along the Sea of Japan, from the southwest to the northeast, with a coastal plain between the mountains and the sea (Joshi and Mohan 2008). The epicentral area of the 2004 Niigata-ken Chuetsu earthquake consists of Neogenic and Quaternary deposits (Sato et al. 2003) and is shown in Figure 3.2. These Neogenic and Quaternary deposits overlay the pyroclastic volcanic basement rocks. The Quaternary deposits generally consist of clay, silt, sand and gravel. The Neogenic formations are heavily folded (Sato et al. 2003). The Shinano River flows through the syncline axis, and Tokamachi, Ojiya and Nagaoka are situated in the

Shinano valley. Another syncline, which has similar trends, is located in the east where Sumon, Koide, Yamato and Muikamachi towns are located on this syncline along which Uono Stream of Shinano River flows. The anticline and synclines axes are tilted to NE. Uono stream changes its flow direction from NE to NW at Koide town and joins Shinano River nearby Kawaguchi town. This segment of the stream seems to follow a sinistral fault segment, which starts from Yuno valley and extends to Kashiwazaki (Sato et al. 2003).

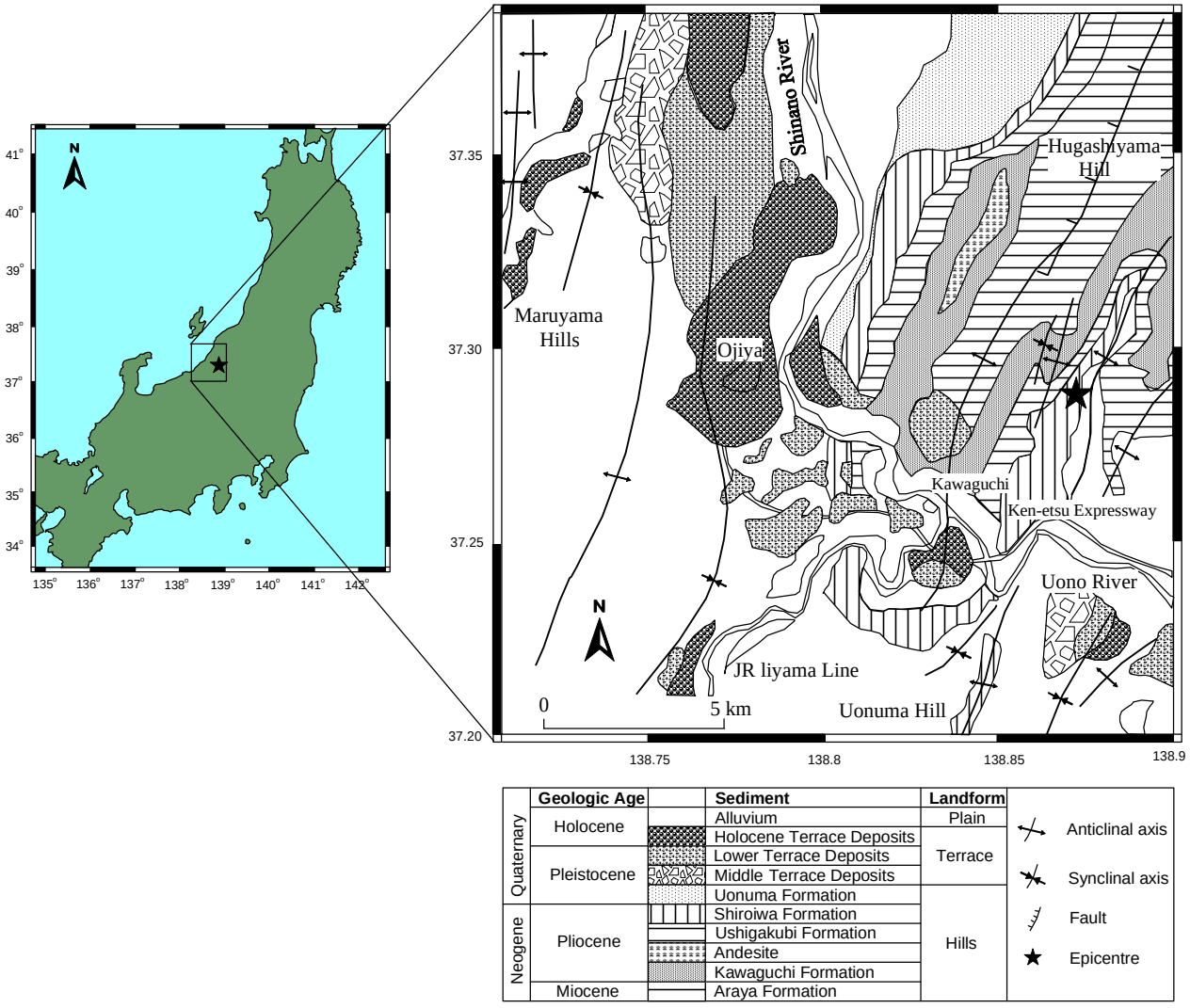

Figure 3.2 Geology around the epicentral region of the 2004 Niigata-ken Chuetsu earthquake (Figure modified after Sato et al. 2003)

3.3 Data

Niigata-ken Chuetsu earthquake of October 23, 2004 was recorded at 286 strong motion stations of Kiban-Kyoshin network (KiK-net) and 327 stations of Kyoshin network (K-NET). KiK-net and K-NET consists of total 660 and 1034 strong ground motion seismographs, respectively spreading all over Japan. Seismographs of the KiK-net network are deployed at surface as well as borehole at all stations whereas seismographs of the K-NET network are deployed at surface only. The average station-to-station distance for K-NET is about 20 km. Each station has a digital strong-motion seismograph with a wide frequency band and dynamic range required for measurable acceleration of 2000 gal. The maximum peak ground acceleration (PGA) recorded during this earthquake was 840 gal at Nagaoka station of KiK-net and was 1750 gal at Tohkamachi station of K-NET. Acceleration data recorded at three stations (NIGH01, NIGH13 and NIGH19) of KiK-net of the National Research Institute for Earth Science and Disaster Prevention (NIED) has been used in the present study. Details of these stations are given in Table 3.2. The records from the borehole sensor have been used for the purpose of comparison with synthetic records to avoid site amplifications which may present in sensor at the surface. The records downloaded from KiK-net site have been processed using basic processing steps given by Boore and Bommer (2005). The processing steps involves baseline correction, instrument correction and band pass filtering.

The modified semi-empirical method requires knowledge of the duration parameter. This parameter is needed in scaling the envelope function of accelerogram. The relation between duration parameter, magnitude and hypocentral distance is empirical in nature and was given by Midorikawa (1989). This relation was modified by different workers (Joshi and Patel 1997; Joshi and Midorikawa 2004; Joshi and Mohan 2008) for study of different earthquakes in different regions. The duration parameter given by Joshi and Mohan (2008) has been used in simulation of strong ground motion for the Niigata earthquake.

Table 3.2 Detail of observation stations used for simulation

Station Code	Latitude (in degree)	Longitude (in degree)	Hypocentral Distance (km)	Epicentral Distance (km)	Station Name
NIGH01	37.43	138.89	20.41	15	NAGAOKA
NIGH13	37.05	138.40	51.14	49	MAKI
NIGH19	36.81	138.78	55.50	54	YUZAWA

Source: www.kyoshin.bosai.go.jp

3.4 Simulation of Strong Ground Motion using Modified Semi-Empirical Technique

The Niigata earthquake was modeled by Joshi and Mohan (2008) with modified semi-empirical approach using attenuation relation of Abrahamson and Litehiser (1989). Several modifications in this technique have been made to remove its dependency on attenuation relationship. The semi-empirical technique has been modified for simulation of strong ground motion by using seismic moment in place of regional attenuation relation for scaling the envelope function. Another modification has been made to incorporate effect of radiation pattern in the simulation technique. Further, the semi-empirical technique has been modified for component-wise simulation of strong ground motion by using simple vector theory. The rupture model given by Honda et al. (2005) and tested by Joshi and Mohan (2008) has been used in the present work for simulation of strong ground motion. The parameters of the rupture plane are given in Table 3.3. The geometrical parameter of sub-faults has been calculated using the self-similarity laws given by Kanamori and Anderson (1975). Based on seismic moment of the mainshock, the rupture plane of dimension 42 km×24 km has been divided into 12 sub-faults of moment magnitude 5.5 (M_w). The velocity model given by Honda et al. (2005) has been used for simulation is given in Table 3.4.

Table 3.3 Parameters of the responsible rupture plane for the Niigata earthquake used for simulation

Modeling Parameter	Source
Length = 42 km	Honda et al. (2005)
Width = 24 km	Honda et al. (2005)
Dip = 39°	Global CMT
Strike = 211°	Honda et al. (2005)
N_L = 4, N_W = 3	Based on scaling relation by Kanamori and Anderson (1975)
V_r = 3.1 km/sec	Joshi and Mohan (2008)
β = 2.8 km/sec	
$Q_\beta(f) = 158.48f^{0.7}$	Kiyono (1992)
$M_o = 1.2\times10^{26}$ dyne-cm	Honda et al. (2005)

Table 3.4 Velocity model in source region of the Niigata earthquake (after Honda et al. 2005)

Thickness (km)	S-wave Velocity (km/sec)	Density (g/cm^3)
7.4	1.9	1.8
4.4	3.1	3.0
1.4	3.6	3.5

A software named MSETCS has been developed in FORTRAN for simulation of records using modified semi-empirical technique. This software is capable of simulating acceleration waveform caused by an earthquake generated by a finite fault. As discussed in earlier chapter this program requires coordinates of recording station in a Cartesian system in which the X- and the Y-axes follows the strike and dip direction of the rupture plane, respectively. In this section, acceleration records have been simulated for the Niigata earthquake at three rock site stations of KiK-net. Location of modeled rupture plane and recording stations used for simulation of strong ground motion has been shown in Figure 3.3. Final rupture model used for simulating records of the Niigata earthquake has been shown in Figure 3.4.

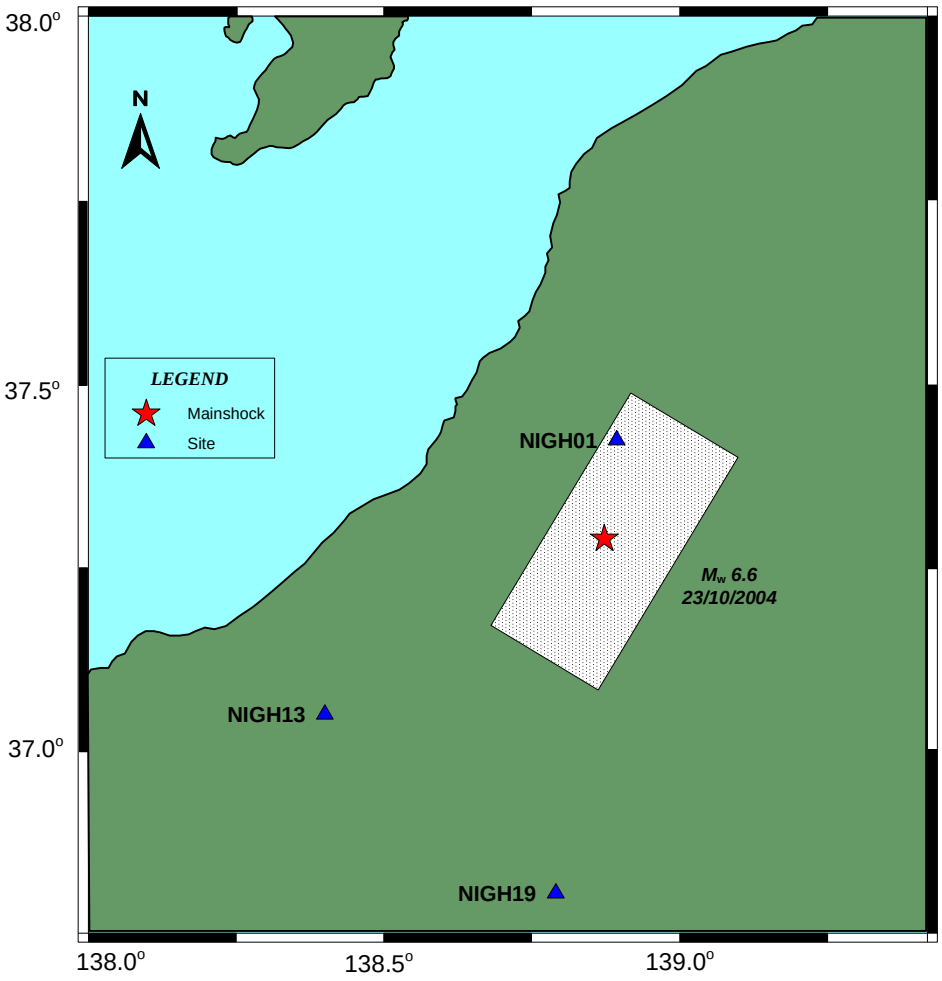

Figure 3.3 Location of rupture plane and stations at which simulations has been made for the Niigata earthquake

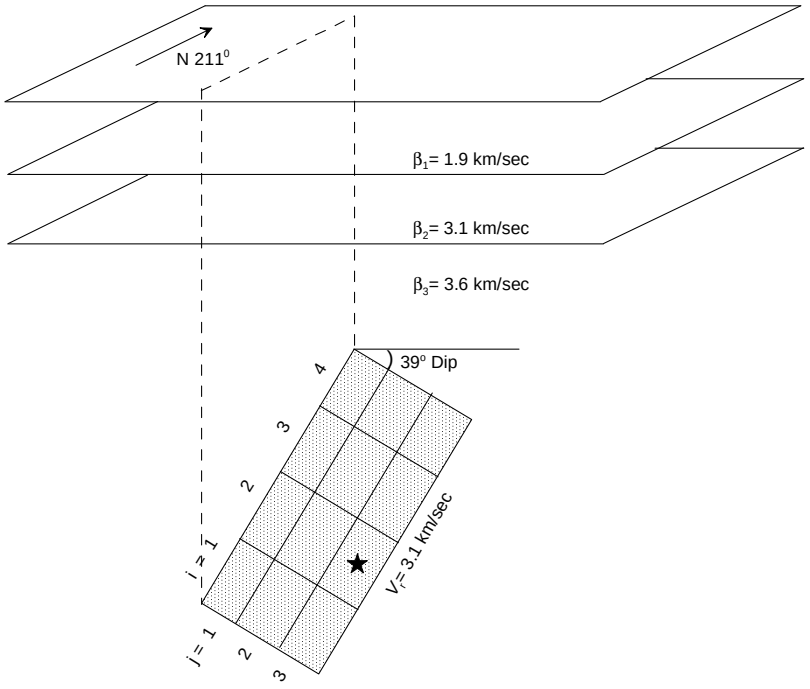

Figure 3.4 Final rupture model of the Niigata-ken Chuetsu earthquake consisting of 4×3 sub-faults in a layered medium with 211°N strike direction. Star shows the starting position of rupture

Present method requires knowledge of frequency dependent quality factor ($Q_\beta(f)$ relation) for region under study. In this work $Q_\beta(f)$ relation given by Kiyono (1992) has been used which is an average relation for Japan. Same relation was used by Joshi and Midorikawa (2004) for simulation of strong ground motion of the Geiyo earthquake using semi-empirical technique. The rupture plane of the Niigata earthquake has been divided into 12 sub-faults and the location of nucleation point is assumed at sub-fault numbered as (2, 3). The NS and EW components of strong motion records have been simulated at three different stations. Simulated records have been compared with the observed records and shown in Figure 3.5. It has been observed that acceleration records show almost similar trends in all simulated records. Pseudo-acceleration response spectra have been calculated from both observed and simulated acceleration records at these stations and are compared in Figure 3.6. Comparison of response spectra from both NS and EW component shows similar trend. This confirms the applicability of the modified semi-empirical technique for this earthquake.

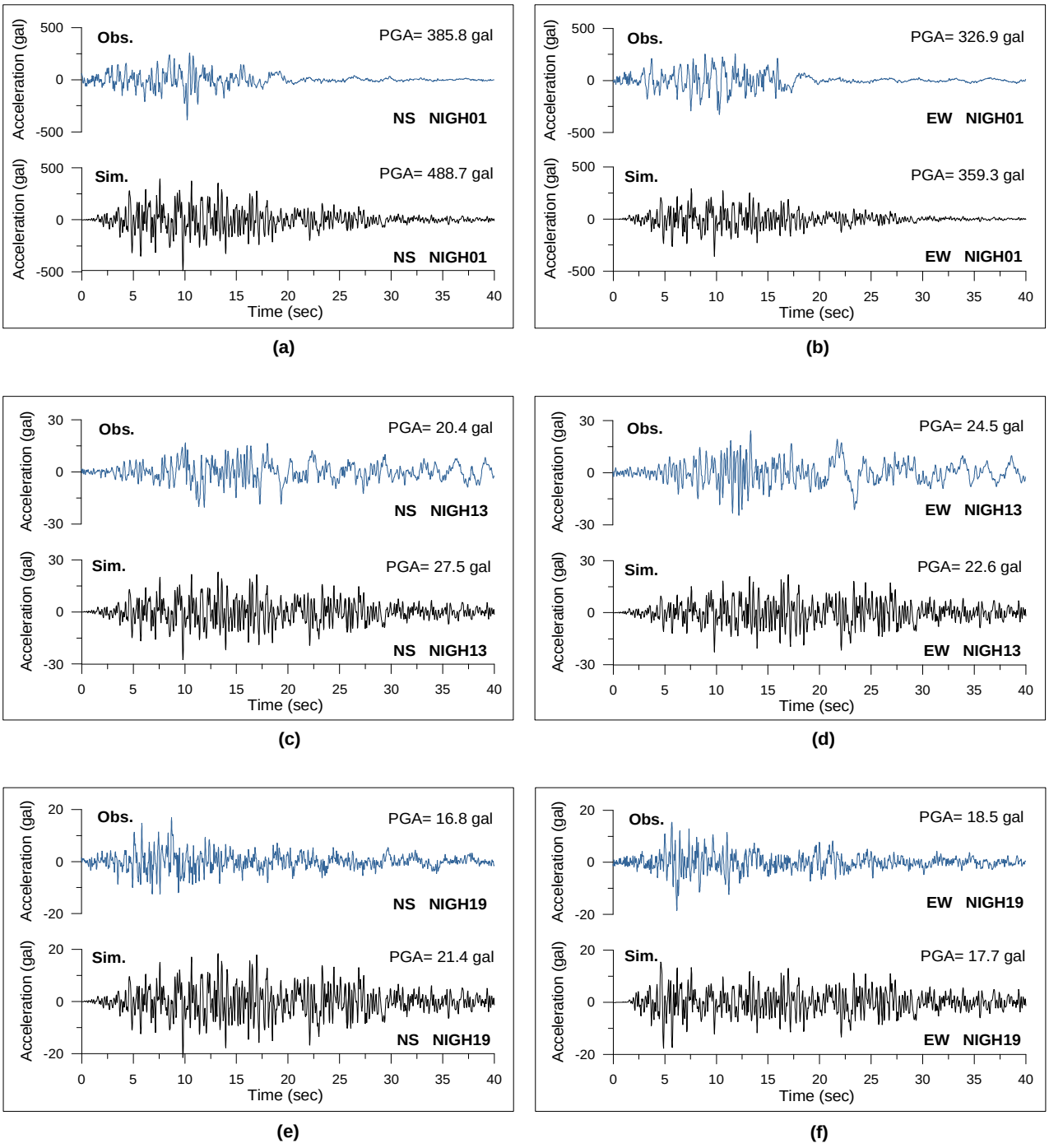

Figure 3.5 Comparison of observed (in blue) and simulated (in black) NS and EW components of acceleration record at NIGH01, NIGH13 and NIGH19 stations of rock site using modified semi-empirical technique

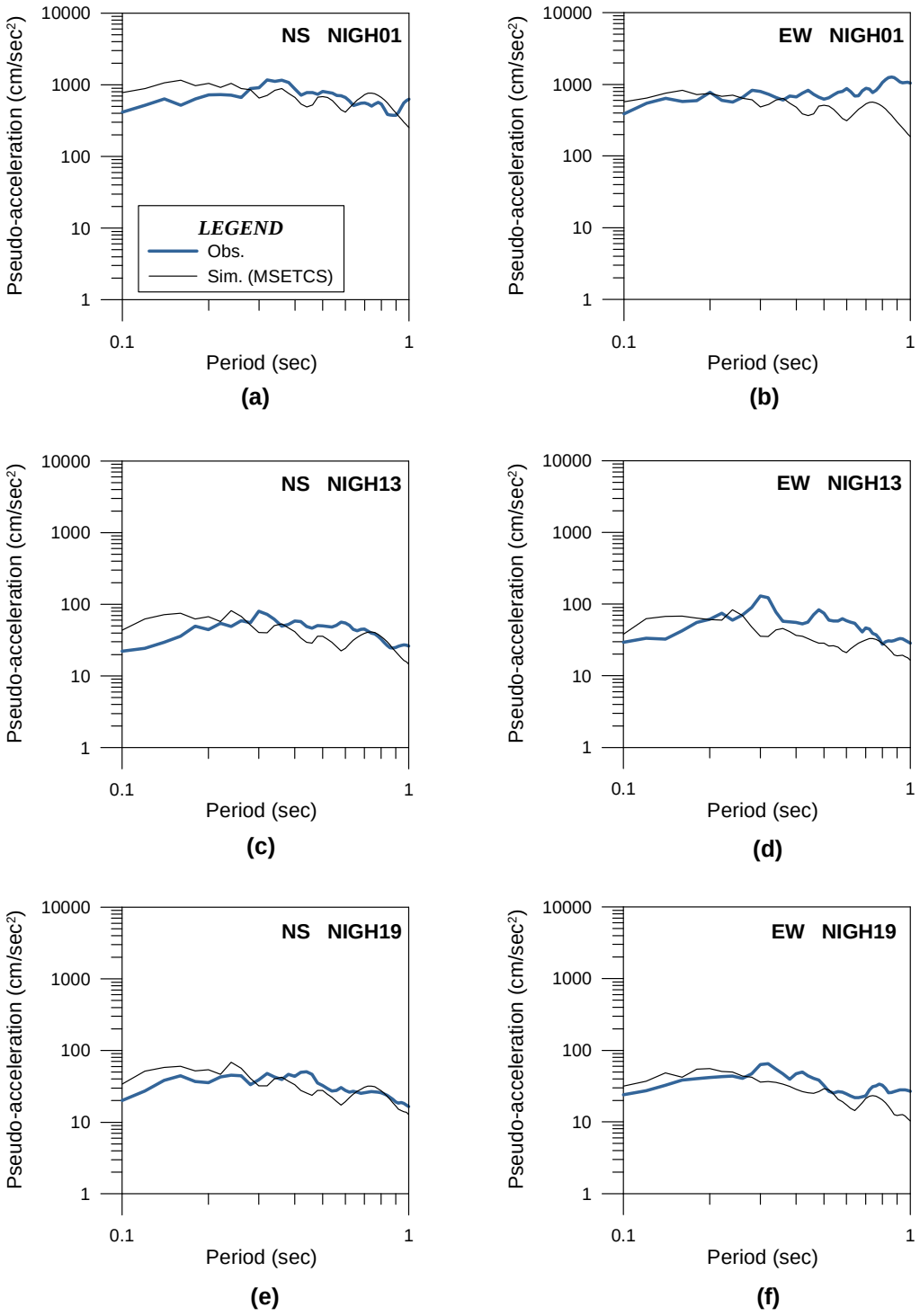

Figure 3.6 Comparison of pseudo-acceleration (PSA) response spectrum with 5% damping determined from NS and EW components of observed and simulated records at NIGH01, NIGH13 and NIGH19 stations

3.5 Discussion

Empirical Green's function technique is one of the most reliable technique for simulation of strong ground motion. This technique has advantage of not requiring the computation of the propagation and the local site effects (Joshi and Midorikawa 2004). Its main limitation is that it can be applied in cases only where appropriate records of small events considered as Green's function in the area of study are available (Joshi and Midorikawa 2004). Unfortunately, it is rare to have good records of such small events, especially in the source area of a future large earthquake (Kamae et al. 1998). It is observed that the Niigata earthquake was one of the well recorded earthquake and has sufficient strong motion data require for EGF simulations. Several aftershocks of the Niigata earthquake were also recorded by the KiK-net at same stations that has recorded the mainshock of the Niigata earthquake. Among several aftershocks the aftershock record of the Niigata-ken Chuetsu, Japan earthquake which occurred on October 23, 2004 of magnitude 5.5 (M_w) has been used as empirical Green's function in this work. Parameters of this aftershock are given in Table 3.5. This aftershock was recorded at 124 sites of KiK-net. This aftershock was recorded at all three stations that have been considered for strong motion simulation using modified semi-empirical approach in earlier section. Location of this aftershock with recorded strong motion data at these stations are shown in Figure 3.7.

Table 3.5 Parameter of an aftershock of the 2004 Niigata-ken Chuetsu, Japan earthquake

Hypocenter	Size	Fault Plane Solution	Reference
23/10/2004	$M_o = 2.47\times10^{24}$ dyne-cm	NP1 $\varphi = 221°,\ \delta = 41°,\ \lambda = 98°$	Global CMT
09:57:29.2s GMT	$M_w = 5.5$	NP2 $\varphi = 30°,\ \delta = 50°,\ \lambda = 83°$	
37.25°N, 138.91°E	$M_{JMA} = 5.7$		
13.6 km	$m_b = 5.2$		

One of the major requirements in the EGF simulation is the source parameters of both the target earthquake and the aftershock used as empirical Green's function. Source parameters which are required for EGF simulation are corner frequency, seismic moment and stress drop of the mainshock and the aftershock that used as empirical Green's function. In the present work the source parameters of the mainshock and aftershock has been estimated from the source displacement spectrum calculated from the borehole acceleration records recorded by seismographs installed by KiK-net network. Calculation of source displacement spectra is based on

the concept of source spectra given by Brune (1970). The calculation of source spectra from acceleration record requires corrections for propagation and high-cut filters. The propagation filter is dependent on frequency dependent quality factor. In the present work frequency dependent quality factor given by Kiyono (1992) has been used in the propagation filter.

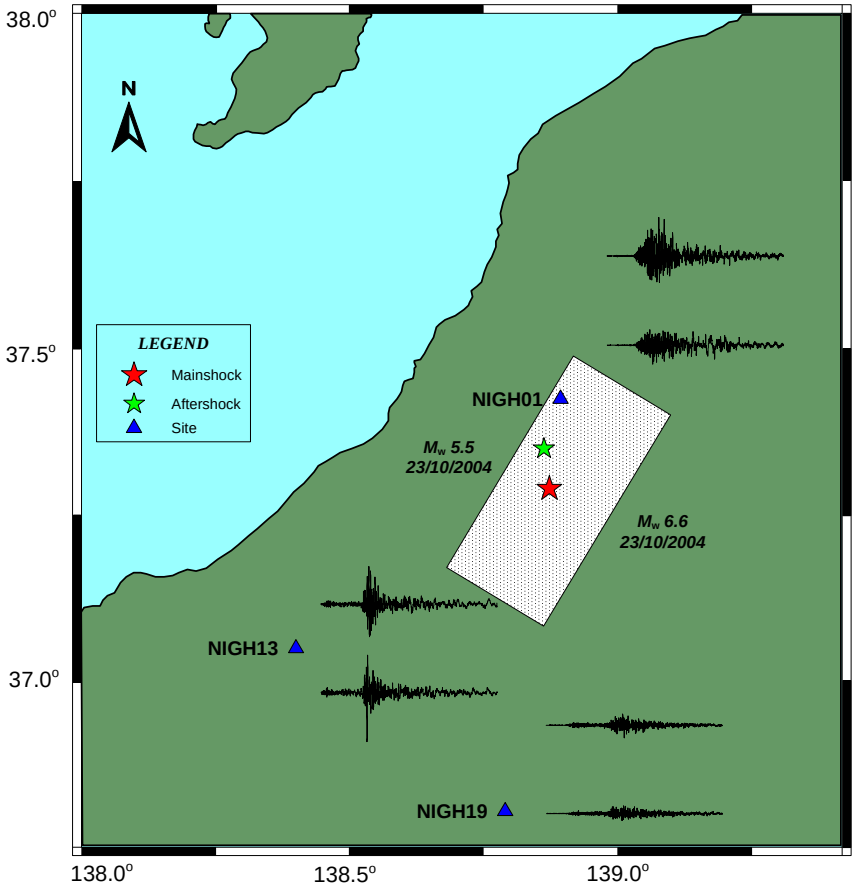

Figure 3.7 Location of rupture plane and stations at which simulations has been made for the Niigata earthquake using an aftershock of magnitude 5.5 (M_w). Aftershock records of NS and EW components used as empirical Green's function are shown along with their recording sites

The source displacement spectra has been calculated from the horizontal components of acceleration records of the aftershock and mainshock of the Niigata-ken Chuetsu earthquake recorded at NIGH01 station from a time window containing prominent S-phase. The corner

frequency and long term flat level have been estimated from the computed source spectrum by comparing it with theoretical spectrum given by Brune (1970). Estimated corner frequency and long term flat level calculated from source displacement spectra are further used for calculation of seismic moment, source radius and stress drop using equations defined in following section.

3.5.1 Estimation of Source Parameters

In computing source displacement spectrum the horizontal component of acceleration record at NIGH01 station has been used. The corner frequency and the long-term spectral level are estimated from the source displacement spectrum by comparing it with the theoretical source spectrum given by Brune (1970). These parameters are used further to compute the seismic moment and the stress drop parameters.

3.5.1.1 Seismic Moment

Seismic moment is related to the long term flat level observed in the source displacement spectrum by the following expression (Keilis-Borok 1959):

$$M_o = \frac{4\pi\rho R\beta^3\Omega_o}{R_{\theta\varphi}} \tag{3.1}$$

where, M_o is seismic moment in dyne-cm, ρ is the density in g/cm^3, β is mean S-wave velocity of the crust, $R_{\theta\varphi}$ is radiation pattern for the S-wave, R is hypocentral distance and Ω_o is long-period spectral level of the S-wave.

3.5.1.2 Stress Radius

The corner frequency is related to the radius of an equivalent circular crack that is used to model an earthquake source. The relation between radius of circular crack and corner frequency given by Brune (1970) is given as:

$$r_s = \frac{2.34\beta}{2\pi f_c} \tag{3.2}$$

where, β and f_c are the S-wave velocity and corner frequency, respectively.

3.5.1.3 Stress Drop

The stress drop is defined in a given point of a fault as the difference between in stress state before and after the rupture. Stress drop can be calculated by the knowledge of seismic moment and source radius. The average stress drop is defined as (Brune 1970):

$$\Delta\sigma = \frac{7M_o}{16r_s^3} \tag{3.3}$$

where, M_o is the seismic moment and r_s is the source radius.

The plot of the observed and the theoretical displacement spectrum of the Niigata-ken Chuetsu earthquake and its aftershock have been shown in Figure 3.8. The values of source parameters of the aftershock and mainshock computed from the source displacement spectra have been given in Table 3.6.

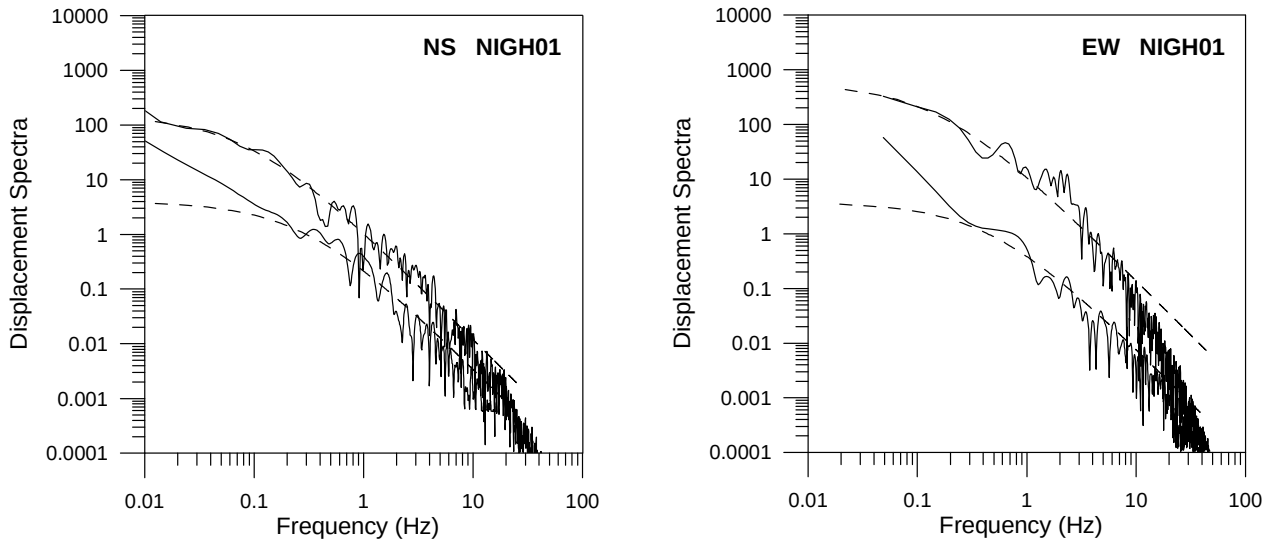

Figure 3.8 Displacement spectra of the mainshock and its aftershock of the Niigata-ken Chuetsu earthquake computed from the S-phase of NS and EW component of accelerogram recorded at NIGH01 borehole station of KiK-net. Theoretical Brune spectrum are represented by dashed line

Table 3.6 Ground motion parameters of the Niigata earthquake estimated from displacement spectra

Events	Ω_o	f_c (Hz)	$\Delta\sigma$ (bars)	M_o (dyne-cm)
Mainshock	150.0	0.1	119	4.24×10^{26}
Aftershock	4.0	0.3	105	1.01×10^{25}

3.6 Simulation of Strong Ground Motion using Empirical Green's Function Technique

The empirical Green's function technique has been used to simulate strong ground motion due to Niigata earthquake at three sites which were considered for simulations using modified semi-empirical approach. The parameters and rupture model are assumed to be same as that used for simulation of strong ground motion using modified semi-empirical approach in earlier section. Based on the self-similarity laws of fault parameters and source spectra the entire rupture plane has been divided into 12 sub-faults. Location of the rupture model is same as defined in Figure 3.3. Parameters of the rupture model are same as defined in Table 3.3, however the division of this rupture plane is based on the self-similarity law of seismic moment of aftershock and the mainshock. The velocity model used for simulation of strong ground motion using EGF technique is same as used in the modified semi-empirical technique and is given in Table 3.4. The stress drop ratio of the mainshock and the aftershock is 1.2 and this value has been used as input for simulation of strong ground motion using EGF technique. The north-south (NS) and east-west (EW) component of strong motion aftershock records recorded at NIGH01, NIGH13 and NIGH19 stations at the borehole have been used as EGFs for simulating NS and EW components of the target earthquake. The NS and EW component of the acceleration records have been simulated at NIGH01, NIGH13 and NIGH19 stations, respectively, by using EGF technique and has been shown in Figure 3.9. Comparison shows that the simulated records bear realistic appearance and the value of PGA from both actual and simulated records are comparable.

The pseudo-acceleration response spectrums have been calculated from both simulated and observed records. The comparison of pseudo-acceleration response spectrum determined from NS and EW components of the simulated record using modified semi-empirical and EGF technique with the observed records at these stations has been shown in Figure 3.10. It has been observed that the simulations obtained using modified semi-empirical technique presented here bear realistic appearance with that obtained from EGF technique.

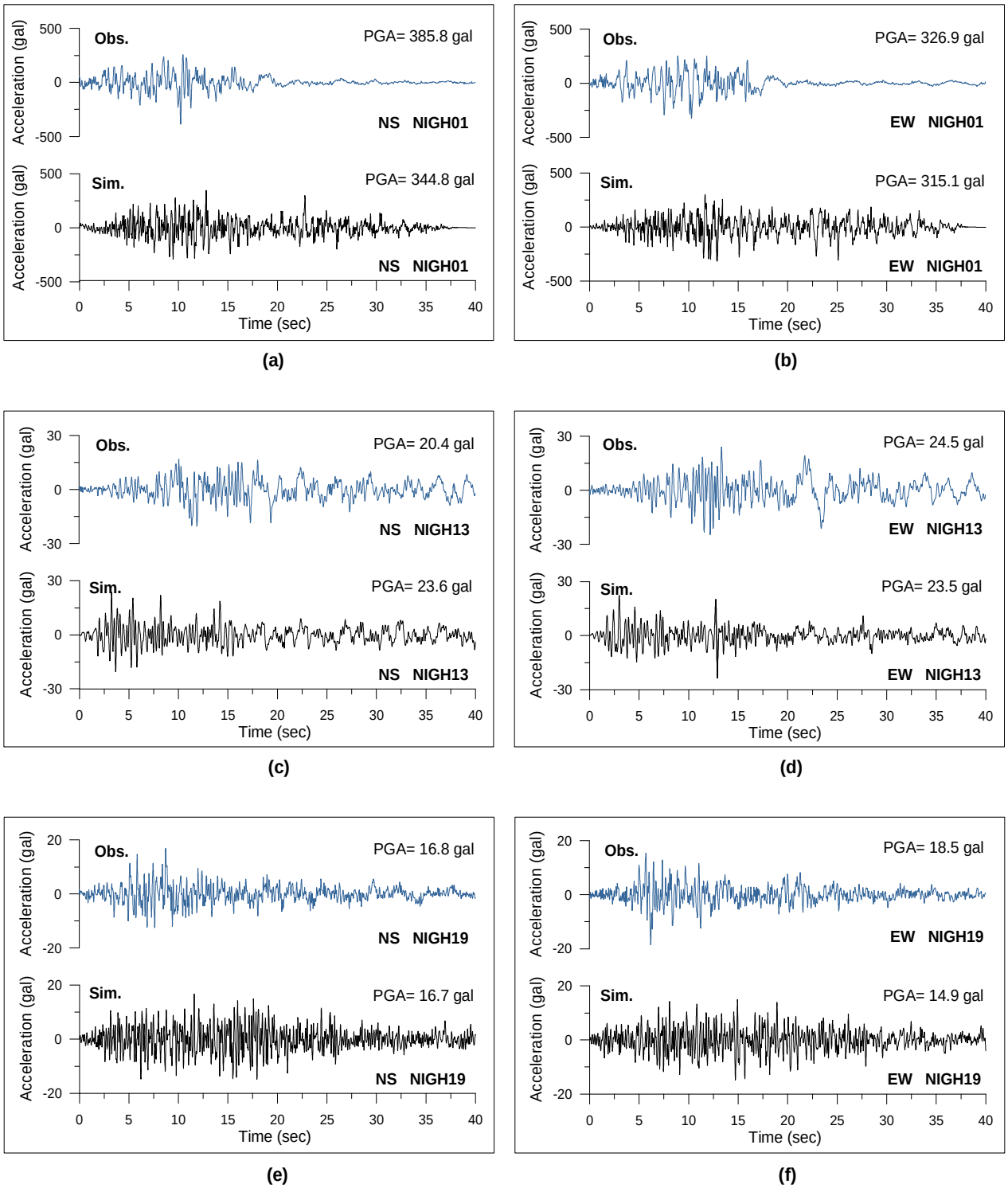

Figure 3.9 Comparison of observed (in blue) and simulated (in black) NS and EW components of acceleration record at NIGH01, NIGH13 and NIGH19 stations of rock site using empirical Green's function technique

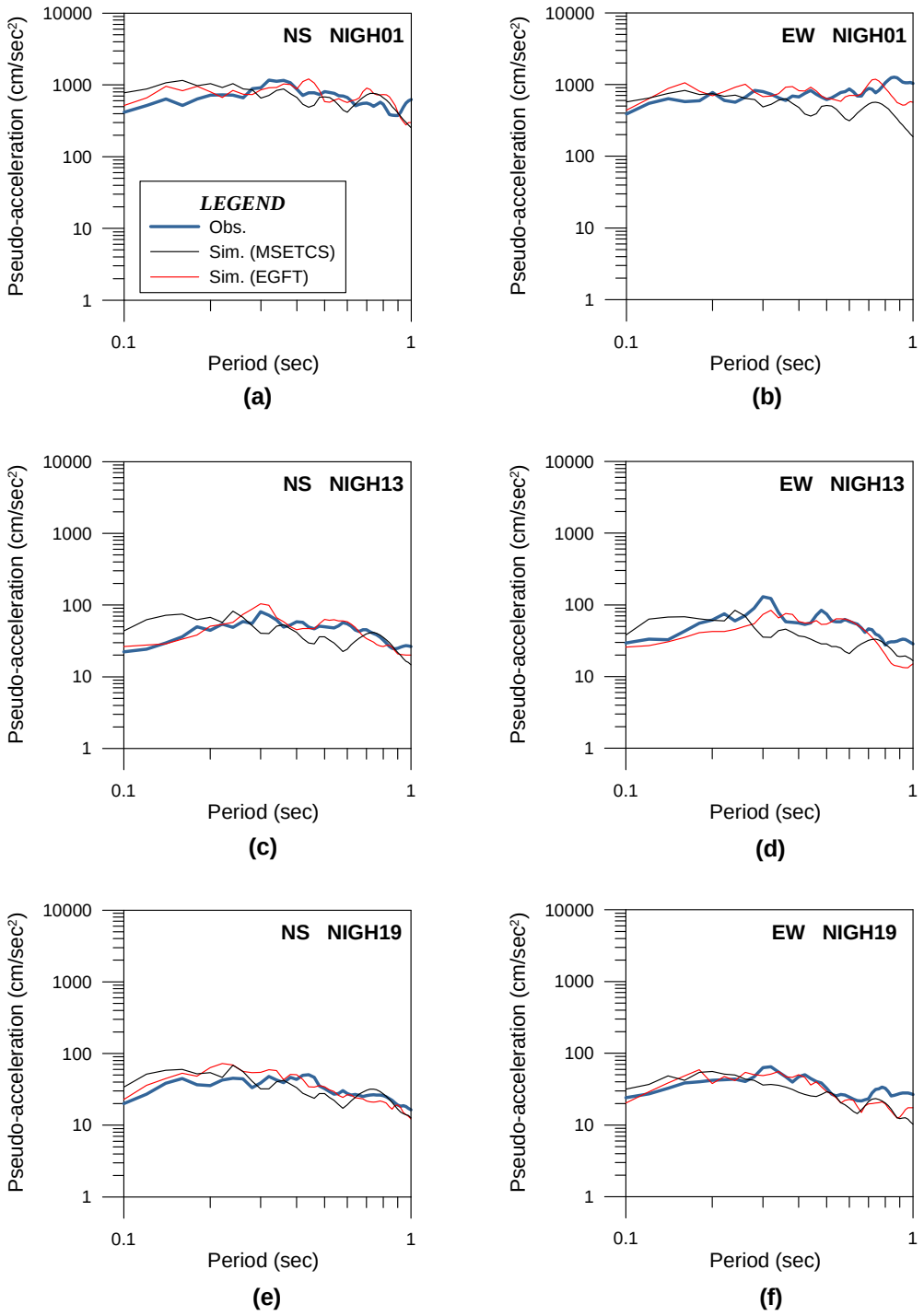

Figure 3.10 Comparison of pseudo-acceleration (PSA) response spectra with 5% damping determined from NS and EW components of observed and simulated records at NIGH01, NIGH13 and NIGH19 stations

The response spectra obtained from simulated record using modified semi-empirical and EGF technique have been compared in terms of root mean square error (RMSE) defined as:

$$RMSE = \sqrt{\frac{1}{N}\sum_{i=1}^{N}\left(\frac{a_f(i) - a_s(i)}{a_s(i)}\right)^2} \tag{3.4}$$

where in this relation, RMSE is root mean square error of N samples of observed $a_f(i)$ and simulated $a_s(i)$ pseudo-acceleration response spectra obtained from observed and simulated acceleration records. The comparison of RMSE between pseudo-acceleration response spectra calculated from observed and simulated acceleration records for the NS and EW components have been listed in Table 3.7. It has been observed that although RMSE is less in the simulations by EGF technique, the simulation by modified semi-empirical technique also gives comparable match at some stations.

Table 3.7 Comparison of RMSE calculated from pseudo-acceleration response spectra obtained from observed and simulated NS and EW components of acceleration records of the Niigata-ken Chuetsu earthquake using modified semi-empirical and EGF technique

Station	RMSE (MSETCS)		RMSE (EGFT)	
	NS	EW	NS	EW
NIGH01	0.6	0.7	0.4	0.4
NIGH13	0.6	0.6	0.4	0.6
NIGH19	0.4	0.4	0.4	0.4

The quantitative comparison of observed and simulated strong motion record has been made in terms of various strong motion parameters. Various strong motion parameters that have been used for quantitative comparison in this work are defined as:

I. Peak Ground Acceleration (PGA):

This parameter defines maximum contribution in the acceleration record and is calculated as follows:

$$PGA = \max\left|a(t)\right| \tag{3.5}$$

where, $a(t)$ is the acceleration record.

II. Peak Ground Velocity (PGV):

This parameter defines maximum contribution in the velocity record that is obtained after integration of acceleration record and is calculated as follows:

$$PGV = \max\left|v(t)\right| \tag{3.6}$$

where, $v(t)$ is the velocity record.

III. Peak Ground Displacement (PGD):

This parameter defines maximum contribution in the displacement record obtained after integration of velocity record and is calculated as follows:

$$PGD = \max\left|d(t)\right| \tag{3.7}$$

where, $d(t)$ is the displacement record.

IV. Ratio of peak velocity and peak acceleration ($v_{\max}/a_{\max}$):

The velocity record is prepared from acceleration record after numerical integration. It is observed that peak velocity and peak acceleration are usually associated with different frequencies (Newmark 1973; Seed et al. 1976; McGuire 1978). The ratio of peak velocity and peak acceleration is defined as:

$$v_{\max}/a_{\max} = \frac{\max\left|v(t)\right|}{\max\left|a(t)\right|} \tag{3.8}$$

where, $v(t)$ is the velocity record obtained after integration of acceleration record $a(t)$.

V. Arias Intensity (I_a):

It is a parameter which is closely related to the root mean square acceleration (Arias 1970). This parameter is calculated by using following formula (Kramer 1996):

$$I_a = \frac{\pi}{2g}\int_0^{T_d}\left(a(t)\right)^2 dt \tag{3.9}$$

where, $a(t)$ is the acceleration time-history, T_d is the duration of the ground motion. The unit of Arias intensity is same as that of velocity and is usually expressed in meter per second (Kramer 1996).

VI. Effective Design Acceleration (EDA):

It is seen that, pulses of high acceleration at high frequencies induce little response in most structures Kramer (1996). This parameter corresponds to the peak acceleration value found after low-pass filtering the acceleration time history with a cutoff frequency of 9 Hz (Benjamin and Associates 1988).

VII. Predominant Period (T_p):

The predominant period T_p is the period at which the maximum spectral acceleration occurs in an acceleration response spectrum calculated at 5% damping. It is calculated as:

$$T_P = \max\left[A_{RS}(T)\right] \tag{3.10}$$

where, $A_{RS}(T)$ is acceleration response spectrum at 5% damping.

VIII. Bracketed Duration:

The duration is defined as the time between the first and last exceedance of a threshold value (Bolt 1969). In the present work the threshold value taken for computing duration parameter is 0.05 g.

IX. Significant Duration:

This definition of duration was given by Trifunac and Brady (1975) and is based on the time interval between the points at which 5% and 95% of total energy has recorded (Kramer 1996).

These nine strong motion parameters have been extracted from both horizontal components of simulated and observed records at different stations and are listed in Table 3.8, Table 3.9 and Table 3.10. Extensive comparison of several strong motion parameters of the observed record and simulated record with that from EGF technique confirms that the simulated records using modified semi-empirical technique bear realistic appearance and give various parameters which closely match with observed record. The comparison of simulations with EGF technique shows that the modified semi-empirical technique is capable of simulating realistic records for cases where direct use of aftershock record is not possible.

Table 3.8 Comparison of ground motion parameters at NIGH01 station calculated from observed and simulated NS and EW components of acceleration records of the Niigata-ken Chuetsu, Japan earthquake

S. No.	Strong Motion Parameters	Observed		Simulated Using			
				MSETCS		EGFT	
		NS	EW	NS	EW	NS	EW
1.	Peak Ground Acceleration (PGA) (gal)	385.8	326.9	488.7	359.3	344.8	315.1
2.	Peak Ground Velocity (PGV) (cm/sec)	57.4	54.3	49.8	36.6	45.2	42.8
3.	Peak Ground Displacement (PGD) (cm)	40.5	34.1	26.1	17.4	22.2	19.8
4.	v_{max}/a_{max} (sec)	0.14	0.16	0.10	0.10	0.13	0.13
5.	Arias Intensity (I_a) (m/sec)	2.08	2.68	5.29	2.67	3.35	3.85
6.	Effective Design Acceleration (EDA) (gal)	388.6	332.9	486.2	357.5	323.1	319.5
7.	Predominant Period (T_p) (sec)	0.32	0.86	0.22	0.22	0.44	0.74
8.	Bracketed Duration (sec)	170.6	170.7	79.9	79.6	52.8	51.2
9.	Significant Duration (sec)	16.0	14.4	19.8	18.3	23.1	25.9

Table 3.9 Comparison of ground motion parameters at NIGH13 station calculated from observed and simulated NS and EW components of acceleration records of the Niigata-ken Chuetsu, Japan earthquake

S. No.	Strong Motion Parameters	Observed		Simulated Using			
				MSETCS		EGFT	
		NS	EW	NS	EW	NS	EW
1.	Peak Ground Acceleration (PGA) (gal)	20.4	24.5	27.5	22.6	23.6	23.5
2.	Peak Ground Velocity (PGV) (cm/sec)	5.8	8.6	3.9	4.3	3.1	2.8
3.	Peak Ground Displacement (PGD) (cm)	5.4	5.65	2.3	2.5	1.9	1.9
4.	v_{max}/a_{max} (sec)	0.28	0.35	0.14	0.19	0.13	0.12
5.	Arias Intensity (I_a) (m/sec)	0.02	0.03	0.02	0.02	0.01	0.01
6.	Effective Design Acceleration (EDA) (gal)	20.5	24.6	27.3	22.5	23.5	23.7
7.	Predominant Period (T_p) (sec)	0.30	0.30	0.26	0.26	0.30	0.32
8.	Bracketed Duration (sec)	172.7	170.7	79.6	79.7	54.9	59.4
9.	Significant Duration (sec)	112.0	92.2	25.9	29.0	37.7	37.0

Table 3.10 Comparison of ground motion parameters at NIGH19 station calculated from observed and simulated NS and EW components of acceleration records of the Niigata-ken Chuetsu, Japan earthquake

S. No.	Strong Motion Parameters	Observed		Simulated Using			
				MSETCS		EGFT	
		NS	EW	NS	EW	NS	EW
1.	Peak Ground Acceleration (PGA) (gal)	16.8	18.5	21.4	17.7	16.7	14.9
2.	Peak Ground Velocity (PGV) (cm/sec)	3.2	2.8	3.3	2.6	1.4	1.7
3.	Peak Ground Displacement (PGD) (cm)	2.1	1.5	2.0	1.5	0.9	0.8
4.	v_{max}/a_{max} (sec)	0.19	0.15	0.15	0.15	0.08	0.11
5.	Arias Intensity (I_a) (m/sec)	0.01	0.01	0.01	0.01	0.01	0.01
6.	Effective Design Acceleration (EDA) (gal)	16.9	17.9	21.3	17.4	16.1	15.0
7.	Predominant Period (T_p) (sec)	0.44	0.32	0.26	0.38	0.22	0.18
8.	Bracketed Duration (sec)	172.4	172.2	79.6	79.7	78.5	76.9
9.	Significant Duration (sec)	40.1	31.1	28.4	31.9	49.8	48.6

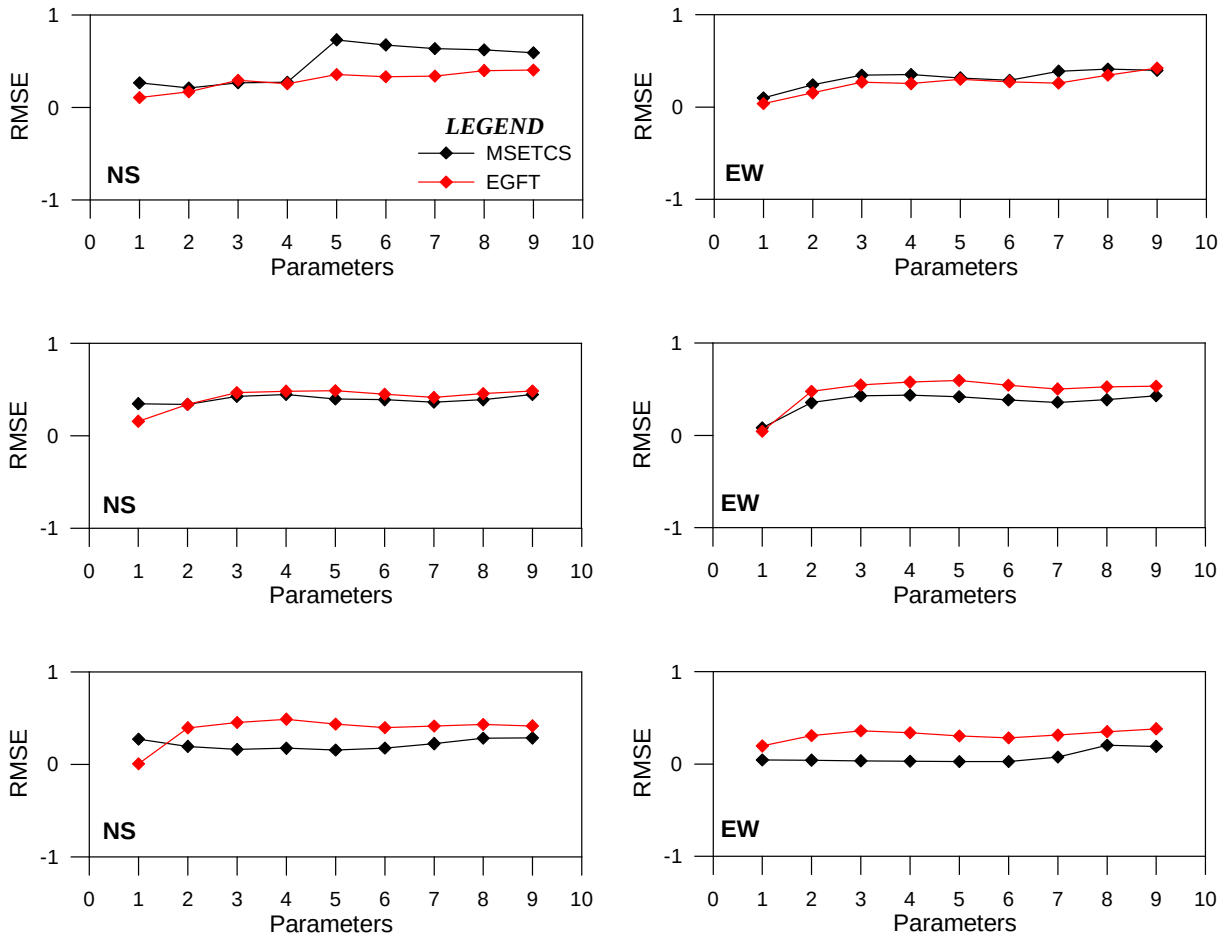

Figure 3.11 Comparison of root mean square error (RMSE) for nine parameters, estimated between observed and simulated strong motion parameters using both the modified semi-empirical and empirical Green's function technique from NS and EW components of observed and simulated records at NIGH01 (in upper panel), NIGH13 (in middle panel) and NIGH19 (in lower panel) stations

Root mean square error has been calculated for these nine strong motion parameters between the observed and simulated acceleration records obtained using modified semi-empirical technique and EGF technique. These errors have been plotted with respect to nine strong motion parameters in Figure 3.11 for both NS and EW components of three KiK-net stations. It has been observed that almost similar trends in RMSE obtained by using simulated records from EGF and modified semi-empirical technique.

3.7 Conclusion

The modified semi-empirical technique and empirical Green's function technique have been used for simulation of strong motion data of the Niigata-ken Chuetsu earthquake using similar rupture model. The parametric comparison of simulated and observed records confirms the efficacy of the developed modified semi-empirical technique and its utility for cases where direct use of empirical Green's function technique is not possible.

Chapter – 4

SYNTHETIC GROUND MOTION FOR THE SIKKIM EARTHQUAKE OF SEPTEMBER 18, 2011 (M_W = 6.9)

Recently the northeastern part of India was shaken by Sikkim earthquake (M_w = 6.9) on September 18, 2011. This earthquake was recorded at various near-field and far-field strong motion stations. The modified semi-empirical technique has been used to simulate near-field and far-field strong motion records due to an identified rupture plane responsible for this earthquake. Strong motion record obtained from the iterative modeling of the rupture plane has been compared with available strong motion records at both near as well as far-field stations in terms of RMSE between the observed and simulated records.

4.1 Seismotectonics of Region

Sikkim Himalaya lies in the eastern region of Indian subcontinent with well-mapped geological and tectonic units (Figure 4.1) having classic inverted Himalayan metamorphism. Sikkim lies in zone IV of the Indian Seismic Code (IS 1893: 2002). Geologically, the Sikkim Himalaya exhibits a vast terrain of proterozoic continental crust on the Indian plate, which is remobilized into vast slab-like Higher Himalayan Crystallines (HHC) due to Himalayan collision tectonics. This unit is bounded by the Main Central Thrust (MCT) at the base and the South Tibetan Detachment Zone (STDZ) at the top (Figure 4.1). The Lesser Himalayan Sedimentary Zone (Buxa, Permian Ranjit Pebble Slate/Damuda Formation) occurs in the Ranjit window and the Outer Lesser Himalayan Belt, as well. The whole sequence overrides the outermost Sub-Himalayan Siwalik Belt along the Main Boundary Trust (MBT).

The state of Sikkim in north-eastern part of India was struck by a strong earthquake of magnitude 6.9 (M_w) near the boundary between the Indian and Eurasian tectonic plates on September 18, 2011. Parameters of this earthquake are given in Table 4.1. Sikkim Himalaya is surrounded by three countries namely Nepal, China and Bhutan. The shaking effects were more

severe in eastern Nepal, which is closer to the epicenter. The earthquake was felt most strongly in northern Bangladesh. In this region, the Indian plate converges with Eurasian plate at a rate of approximately 5 cm/year toward the north-northeast (Tapponnier and Molnar 1977). There are many transverse faults in the Sikkim region and mainly two thrust faults in the south of the Sikkim region. Kayal (2001) has found the seismic activity in this area is mostly clustered in the north of the MBT, where earthquake occurs at a depth range of 0–50 km. Although the regional tectonic framework of the Sikkim region indicates compressional thrust tectonic regime, the CMT fault plane solution of this earthquake indicate predominantly strike-slip motion on a steep fault (Mahajan et al. 2012).

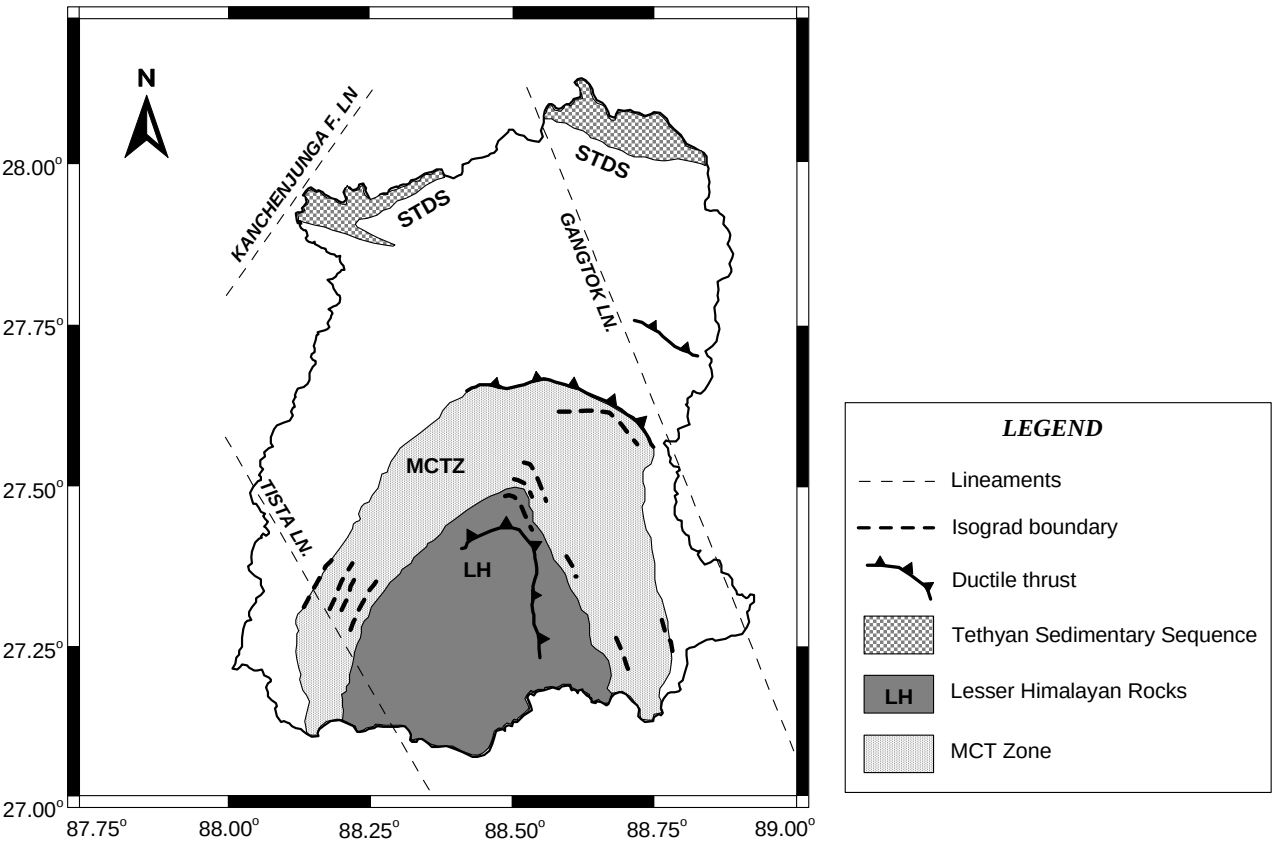

Figure 4.1 Geological map of Sikkim Himalaya. MCTZ: Main Central Thrust Zone, LH: Lesser Himalaya, STDS: South Tibetan Detachment System (Tectonic is taken from Nath et al. 2005 and Geology is taken from Dasgupta et al. 2004)

Table 4.1 Parameters of the Sikkim, India earthquake of September 18, 2011

Hypocenter	Size	Fault Plane Solution	Reference
12:41:02 s UTC 27.43°N, 88.33°E 47.4 km	$M_o = 2.78\times10^{26}$ dyne-cm $M_w = 6.9$	NP1 $\varphi = 313°,\ \delta = 73°,\ \lambda = -163°$ NP2 $\varphi = 217°,\ \delta = 74°,\ \lambda = -18°$	Global CMT
12:41:18 s UTC 27.74° N, 88.11°E 35 km	$M_o = 2.7\times10^{26}$ dyne-cm $M_w = 6.9$	NP1 $\varphi = 220°,\ \delta = 78°,\ \lambda = 0°$ NP2 $\varphi = 130°,\ \delta = 90°,\ \lambda = 168°$	USGS

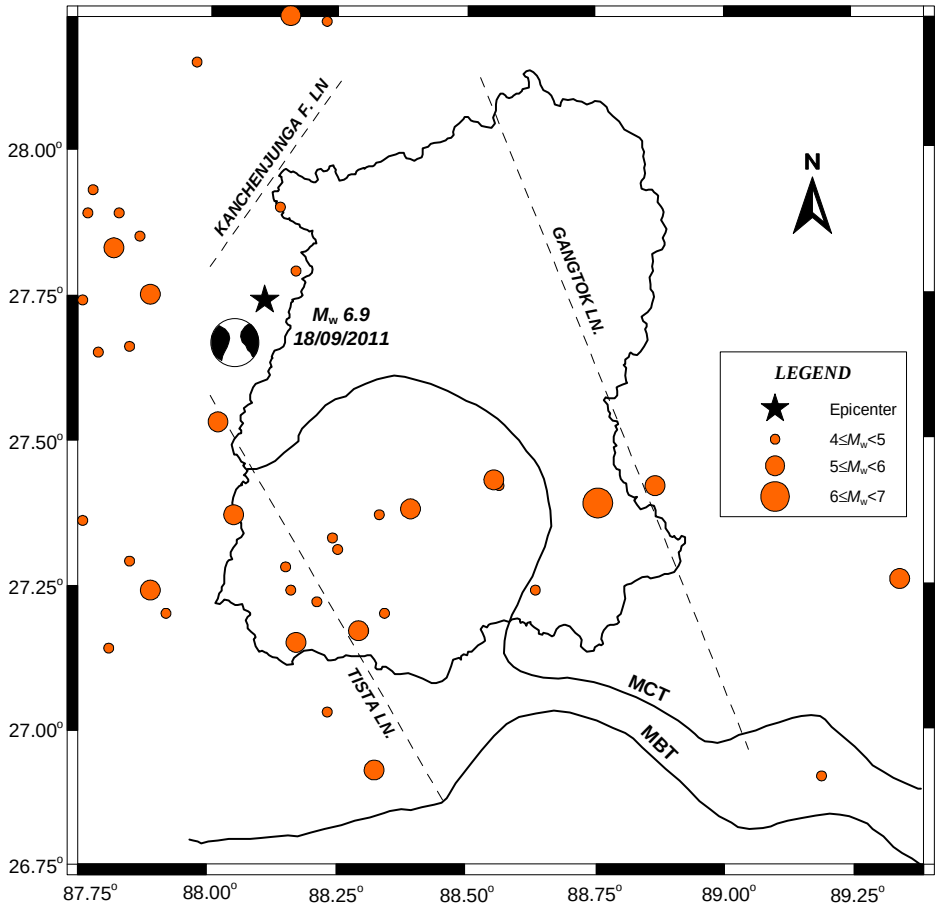

Figure 4.2 Seismotectonic map of the Sikkim Himalaya including location of epicenters of earthquakes during 1973 to 2011 of magnitude 4<M_w<7 from USGS catalog. Epicenter of the September 18, 2011 earthquake is denoted by star with its fault plane solution. MCT: Main Central Thrust, MBT: Main Boundary Thrust (Figure modified after Nath et al. 2005)

In this region, entire Himalayan front is generally characterized by shallow-angle thrust faulting. Most of the earthquakes in this region are predominantly strike-slip type and occur along north-west trending Tista and Gangtok lineaments (Hazarika et al. 2010). Figure 4.2 shows that the epicenter of the Sikkim earthquake lays between Tista and Gangtok lineaments. Distribution of past earthquakes in this region have been shown in Figure 4.2, suggests that it has experienced relatively moderate seismicity over past 38 years of magnitude > 4 within 140 km radius of the epicenter of the Sikkim earthquake.

4.2 Data

The Sikkim earthquake was recorded by several strong motion near-field as well as far-field stations. This event was recorded at near-field stations by the network installed by the Department of Earthquake Engineering, Indian Institute of Technology Roorkee, Uttarakhand. These stations were installed in states of Himachal Pradesh, Punjab, Haryana, Rajasthan, Uttarakhand, Uttar Pradesh, Bihar, Sikkim, West Bengal, Meghalaya, Arunachal Pradesh, Mizoram, Assam and Andaman and Nicobar Islands. The Sikkim earthquake of magnitude 6.9 (M_w) was recorded at nine station of this network at an epicentral distance between 66 and 903 km. A very dense network of fourteen stations has been maintained by the Department of Earth Sciences, Indian Institute of Technology Roorkee in the Uttarakhand state of India. This earthquake was recorded at six stations of this network. Acceleration records have been simulated at three near-field source stations from network of entire Himalaya within the range of 200 km and at twelve far-field stations within the epicentral distance of 900 km from the network of Uttarakhand Himalaya. Generation of synthetic accelerogram for Sikkim earthquake using modified semi-empirical approach requires various scaling laws. The modified semi-empirical technique of simulation of the envelope of accelerogram is dependent on the duration parameter. The regression relation for duration parameter used in the present work is that given by Midorikawa (1989) in equation (2.40). In this equation, the coefficients *a* and *b* for distance parameter have been derived from the actual duration parameter estimated from 13 ground motion records of the Sikkim earthquake. Following relation for duration parameter has been obtained for the study of Sikkim earthquake:

$$T_d = 0.0015\times10^{0.5M_w} + 1.08R^{0.41} \tag{4.1}$$

In this expression, M_w and R, are the moment magnitude and hypocentral distance, respectively. The residual sum of square for this relation is 0.45.

Table 4.2 Parameters of the aftershock of September 18, 2011 Sikkim, India earthquake

Hypocenter	Size	Reference
18/09/2011 at 13:11:59 s UTC 27.48°N, 88.50°E 35 km	m_b = 4.8	USGS

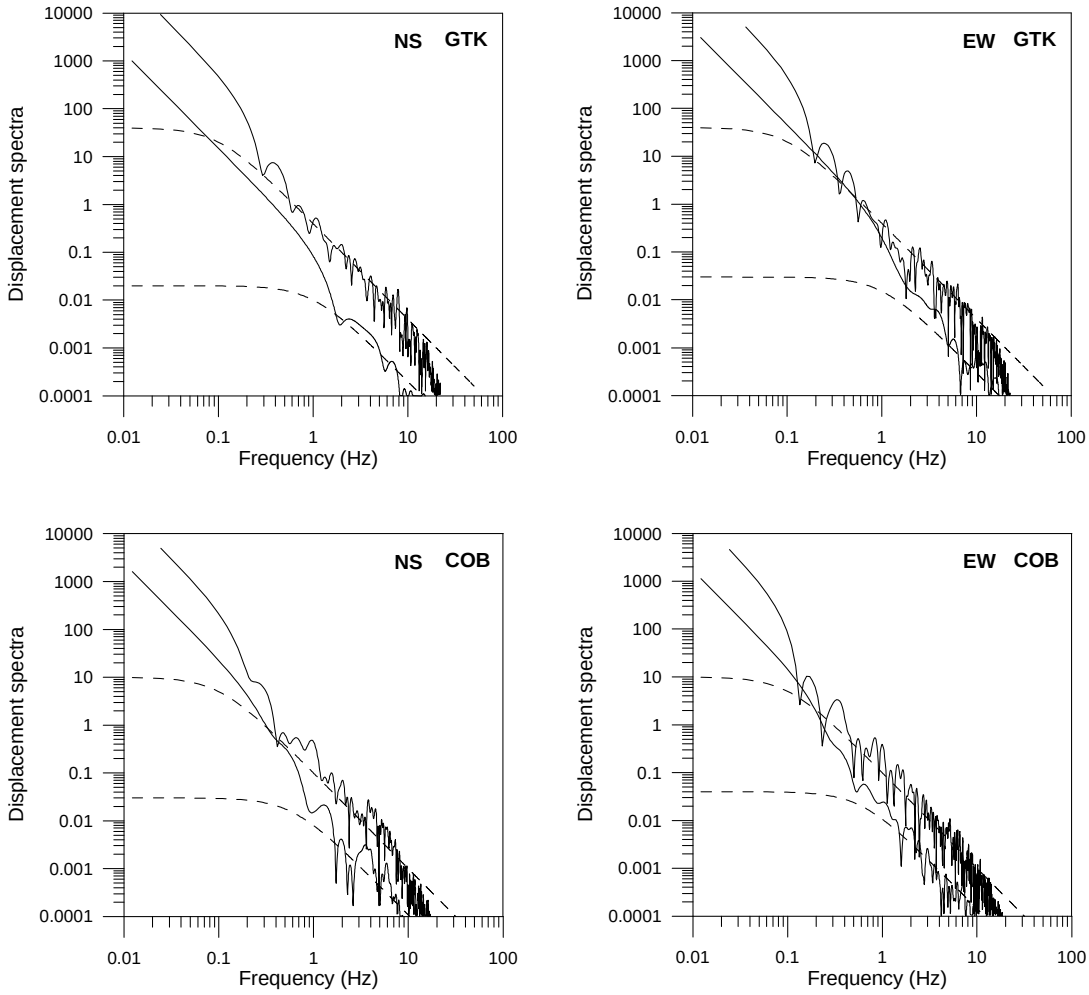

Figure 4.3 Displacement spectra of S-phase of recorded mainshock and aftershock acceleration record along with their theoretical spectra (in dashed line) for NS and EW component of Sikkim earthquake at GTK and COB stations

Table 4.3 Ground motion parameters of the Sikkim earthquake estimated from displacement spectra

Events	Ω_o	f_c (Hz)	$\Delta\sigma$ (bars)
Mainshock	25.0	0.1	61.5
Aftershock	0.03	0.8	41.2

The modified semi-empirical technique for generation of strong ground motion is based on ω^{-2} source model given by Brune (1970). In order to divide the finite rupture plane of target earthquake, self-similarity laws given by Kanamori and Anderson (1975) and explained in Chapter 2 has been used. The scaling of source spectra of target and elementary earthquake requires estimate of stress drop ratio of target and elementary earthquake. According to Kanamori and Anderson (1975), the seismic moment of target earthquake M_o and seismic moment of elementary earthquake M_o' are related as $M_o / M_o' = C'N^3$; where, C' is stress drop ratio of target and elementary earthquake. The stress drop of target and sub-fault earthquake has been calculated from the data of mainshock and aftershock, respectively, recorded at Gangtok and Cooch Bihar stations. The parameters of aftershock used as sub-fault is given in Table 4.2. The source displacement spectrum of the target and sub-fault earthquake has been shown in Figure 4.3. Parameters of mainshock and aftershock estimated from source displacement spectra have been given in Table 4.3. The stress drop ratio calculated from displacement spectra is obtained as 1.5. This ratio has been used for scaling of Brune's source pulse released by different sub-faults.

4.3 Rupture Model of the Sikkim Earthquake

The causative fault of the Sikkim earthquake has been decided on the basis of location of epicenter of this earthquake and seismic activity in the region. Most of the earthquakes in this region are predominantly strike-slip type and occur along north-west trending Tista and Gangtok lineaments (Hazarika et al. 2010). The rupture responsible for this earthquake has been placed at a depth of 44 km between Tista and Gangtok lineaments. The length and width of the rupture plane responsible for the Sikkim earthquake has been calculated using the relation given by Wells and Coppersmith (1994). This gives the length and width of rupture plane as 51 and 13 km, respectively. The strike of the rupture plane is assumed to be parallel to the Tista lineament and is 328°N which is close to that obtained from fault plane solution of this earthquake given by Global

CMT. The seismic moment of the aftershock of the Sikkim earthquake used as sub-fault has been calculated from source displacement spectra is 7.9×10^{23} dyne-cm. This value has been used for dividing the rupture plane of the target earthquake into several sub-faults. The rupture plane of the target earthquake has been divided into 7×7 sub-faults of magnitude 5.2 (M_w) on the basis of self-similarity laws given by Kanamori and Anderson (1975). Parameters of the rupture plane responsible for the Sikkim earthquake used for simulation are listed in Table 4.4. The velocity model used for simulation of ground motion at different sites is that given by Cotte et al. (1999) and given in Table 4.5. Density value used in the velocity model has been decided on the basis of relation between P-wave velocity and density of earth medium given by Brocher (2005). The rupture plane of the target earthquake has been placed in second layer of the velocity model at a depth of 44 km.

Table 4.4 Parameters of the rupture plane for the Sikkim earthquake used for simulation

Modeling Parameter	**Source**
Length = 51 km	Wells and Coppersmith (1994) relation
Width = 13 km	Wells and Coppersmith (1994) relation
Dip = 76°	
Strike = 328°	
N_L = 7, N_W = 7	Based on scaling relation by Kanamori and Anderson (1975)
V_r = 2.9 km/sec	
β = 3.6 km/sec	
$Q_\beta(f) = 167f^{0.47}$	Nath and Thingbaijam (2009)
$M_o' = 5.2$	

Table 4.5 Velocity model (after Cotte et al. 1999)

Depth (km)	**S-wave Velocity (km/sec)**	**Density (g/cm^3)**
0–40	3.5	2.7
40–70	3.8	2.8

The parameters of final rupture model have been decided on the basis of quantitative comparison of observed and simulated acceleration waveform in terms of RMSE of waveform comparison. The calculation of RMSE between observed and simulated record is based on following formula given by Joshi and Midorikawa (2004):

$$RMSE = \sqrt{\frac{1}{N}\sum_{i=1}^{N}\left(\frac{a_f(i) - a_s(i)}{a_s(i)}\right)^2} \tag{4.2}$$

where in this relation, RMSE is root mean square error of N samples of observed $a_f(i)$ and simulated $a_s(i)$ records.

Table 4.6 Details of the near-field strong motion recording stations which has recorded the Sikkim earthquake

Station Code	Latitude (in degree)	Longitude (in degree)	Hypocentral Distance (km)	Station Name
GTK	27.352	88.627	81.84	Gangtok
SLG	26.712	88.428	127.59	Siliguri
COB	26.319	89.440	210.98	Cooch Bihar

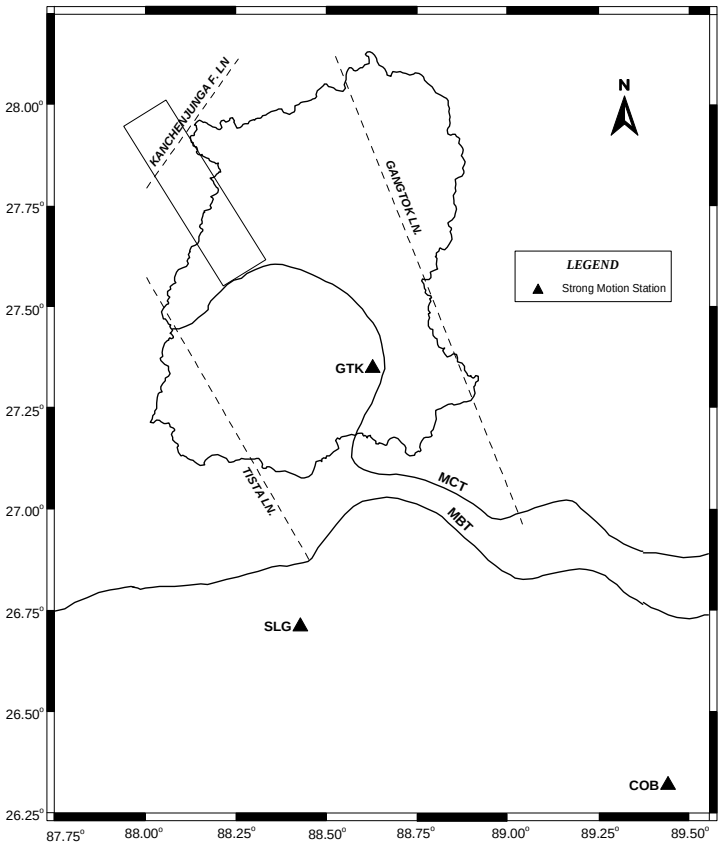

Figure 4.4 Location of the fault rupture plane responsible for the Sikkim earthquake of magnitude 6.9 (M_w) has been shown by rectangle region. MCT: Main Central Thrust, MBT: Main Boundary Thrust (Figure modified after Nath et al. 2005)

Simulations have been made at GTK, SIL and COB stations that lie within an epicentral distance of 206 km. Details of these stations are given in Table 4.6 and its location has been shown in Figure 4.4. Location of nucleation point is an important parameter in strong motion simulation; therefore, final selection of nucleation point is based on comparison of observed and simulated NS component of acceleration records obtained from various models at GTK station. In order to compare the simulated record with the observed acceleration record, the simulated acceleration records have been band-passed through a filter in a frequency range of 0.01–20.0 Hz which has been used for the processing of observed acceleration record at different stations. Root mean square error between observed and simulated waveform has been calculated for each cases.

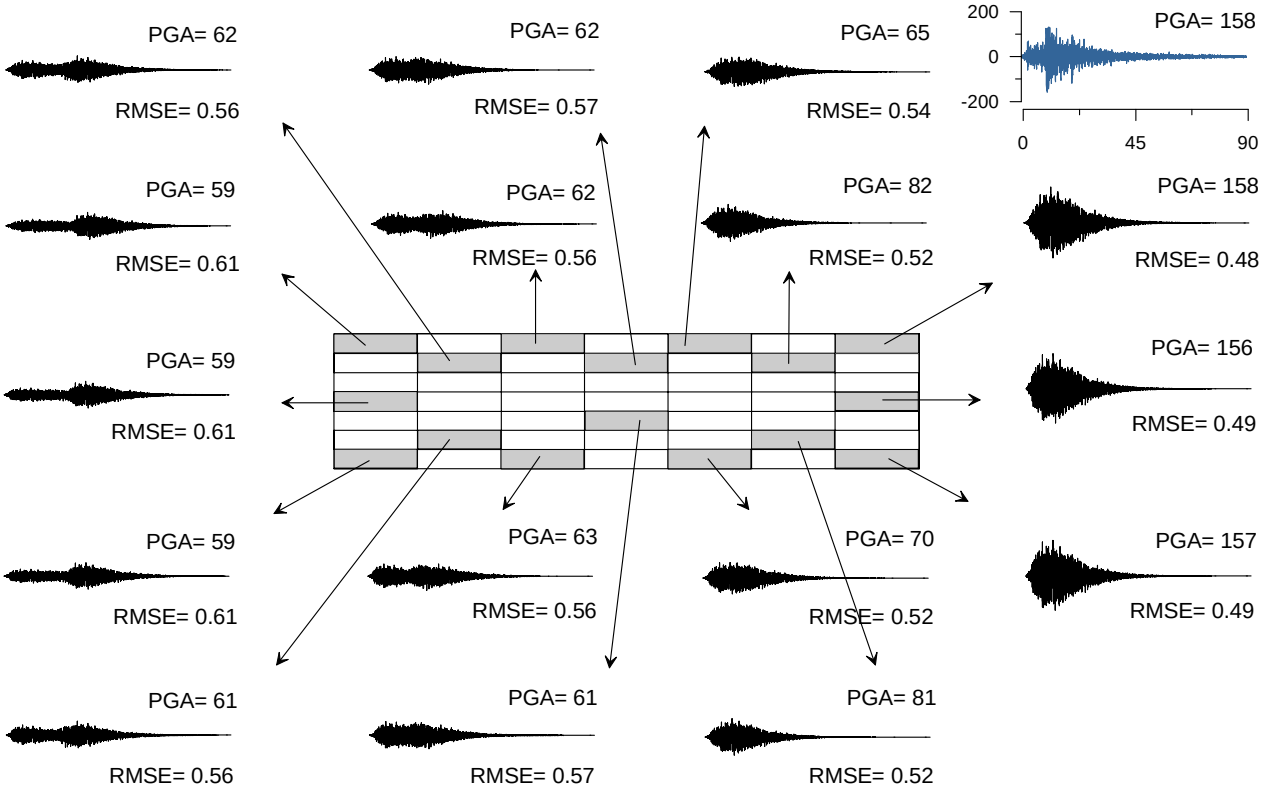

Figure 4.5 Filtered observed (in blue) and simulated NS acceleration record at GTK station for different possibility of nucleation points. Nucleation points have been shown by arrows. Both observed and simulated record has been filtered in a frequency range of 0.01–20.0 Hz

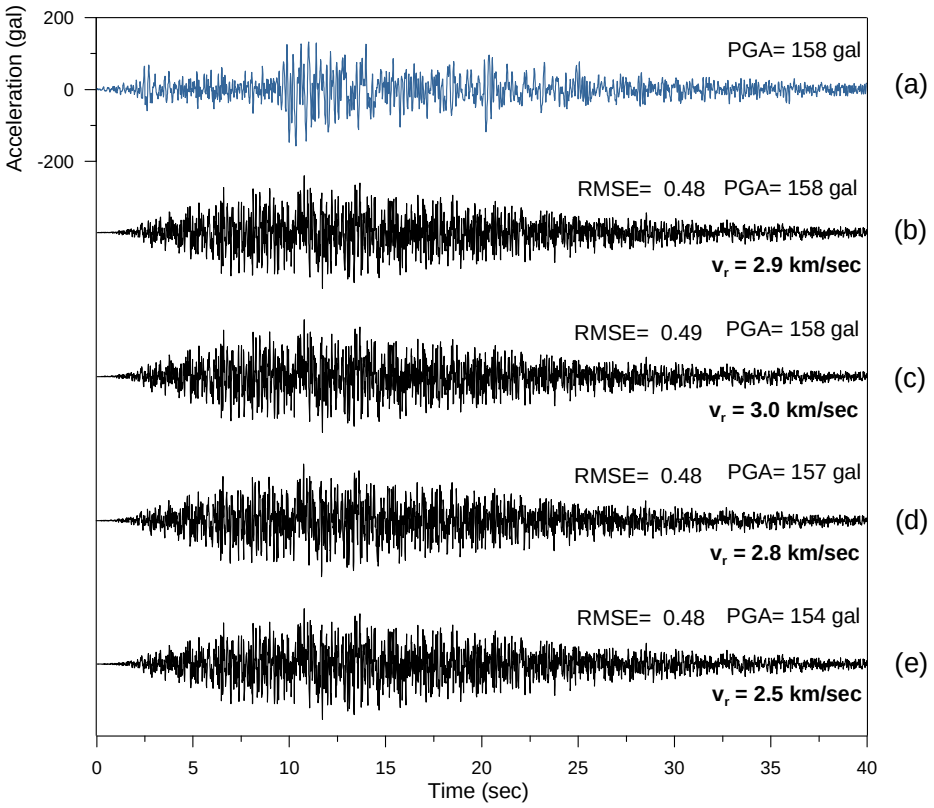

Figure 4.6 Filtered NS component of (a) observed acceleration record; simulated acceleration record for different rupture velocity (b) 2.9 km/sec, (c) 3.0 km/sec, (d) 2.8 km/sec and (e) 2.5 km/sec at GTK station. Both observed and simulated record has been filtered in a frequency range of 0.01–20.0 Hz

Various simulated records and its comparison with the observed record in terms of RMSE for different possibilities of nucleation point have been shown in Figure 4.5. The comparison in terms of RMSE suggests location of the nucleation point in the extreme north-west corner of rupture plane at a depth of 47 km and has been retained for further use. In all models considered for selecting nucleation point, the rupture velocity and dip angle have been assumed as 2.9 km/sec and 76°, respectively. The effect of rupture velocity and the dip angle in the rupture model has been checked for their validation through simulation of ground motion. Various rupture velocity ranging from 2.5 to 3.0 km/sec have been considered for simulating NS component of acceleration record at GTK station. Figure 4.6 shows the comparison of observed and simulated acceleration record obtained after considering rupture velocity as 2.5, 2.8, 2.9 and 3.0 km/sec.

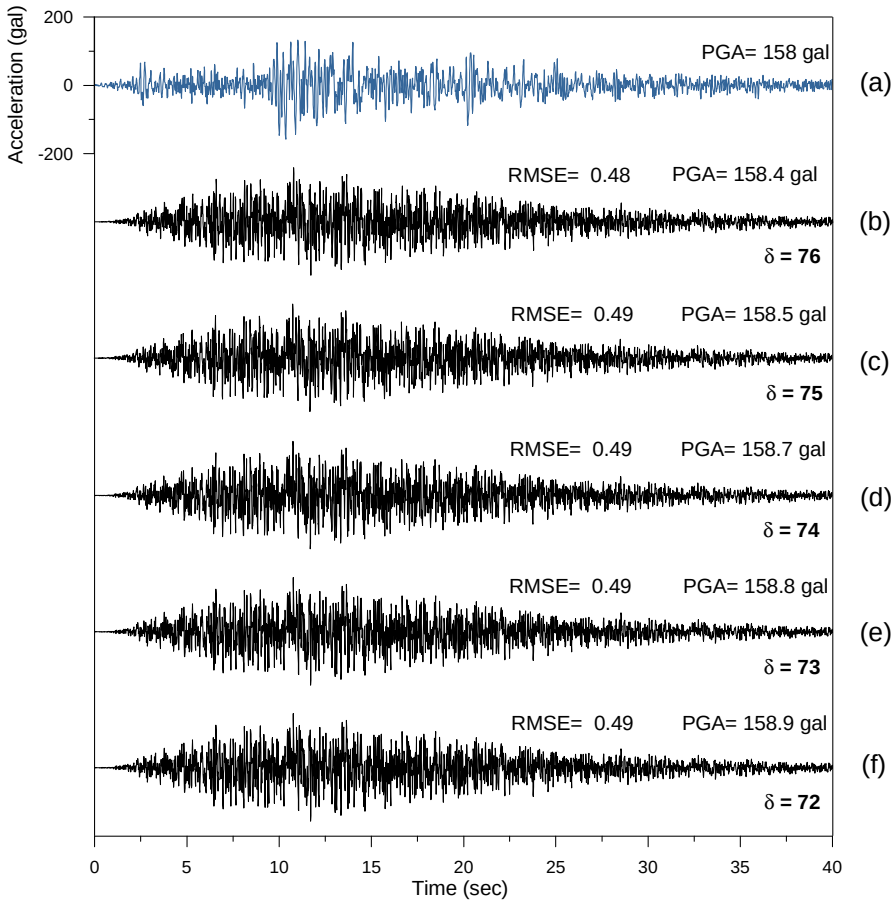

Figure 4.7 Filtered NS component of (a) observed acceleration record; simulated acceleration record for different dip angle (b) 76°, (c) 75°, (d) 74°, (e) 73° and (f) 72° at GTK station. Both observed and simulated record has been filtered in a frequency range of 0.01–20.0 Hz

Based on minimum RMSE, rupture velocity 2.9 km/sec has been used as final rupture velocity for further simulations. In order to check the dependency of dip angle in the entire simulation procedure, rupture model has been tested for dip angles ranging from 72° to 76°. It has been observed from Figure 4.7 that there is no drastic change in the PGA parameter and in the RMSE due to change in dip of rupture plane within this range. Among all obtained simulations minimum RMSE has been obtained for dip angle 76°. This dip angle has been selected as final parameter for simulation of ground motion of the Sikkim earthquake. Several simulations from different source models and their comparisons with observed records indicate that this earthquake was generated by a rupture originating at a depth of 47 km and propagating in southward direction

with rupture velocity of 2.9 km/sec. Final rupture model of the Sikkim earthquake obtained after several iterative comparisons has been shown in Figure 4.8.

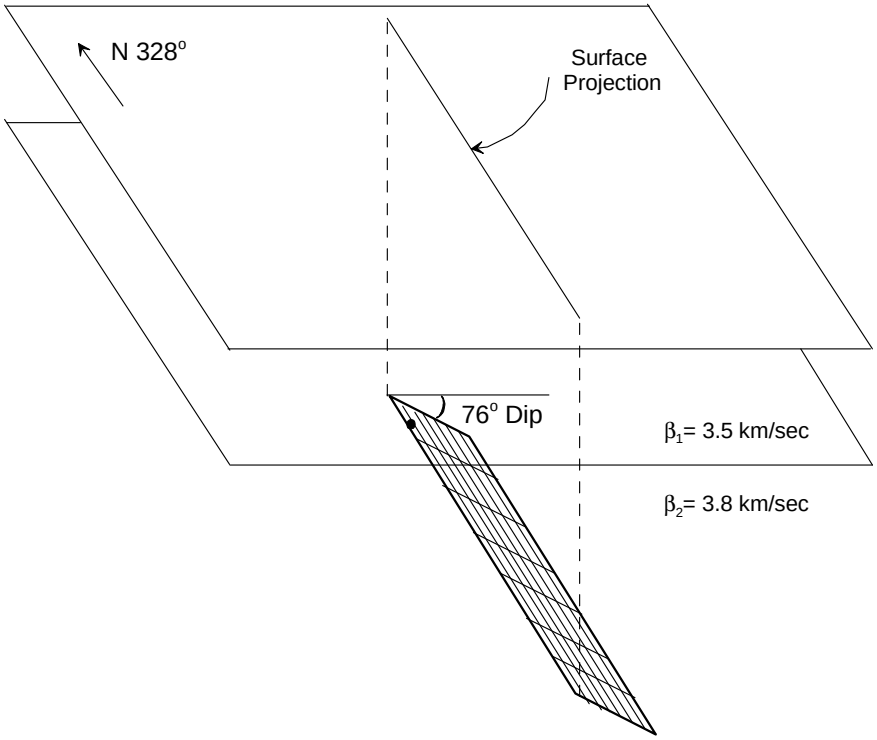

Figure 4.8 Source model of the Sikkim earthquake consisting of 7×7 sub-faults in a layered medium with 328°N strike direction. Solid circle shows the starting position of rupture

4.4 Near-field Simulation of Strong Motion Record

Acceleration records have been simulated at three near-field stations using final rupture model shown in Figure 4.8. These stations lie within epicentral distance of 206 km and their details are given in Table 4.6. Location of these stations is shown in Figure 4.4. Comparison of observed and simulated acceleration record at these three stations have been shown in Figure 4.9 and it shows that simulated record bears realistic shape as that of observed record and the PGA of observed and simulated record is also comparable. Pseudo-acceleration response spectra at 5% damping determined from NS and EW component of observed and simulated acceleration record and have been compared in Figure 4.10.

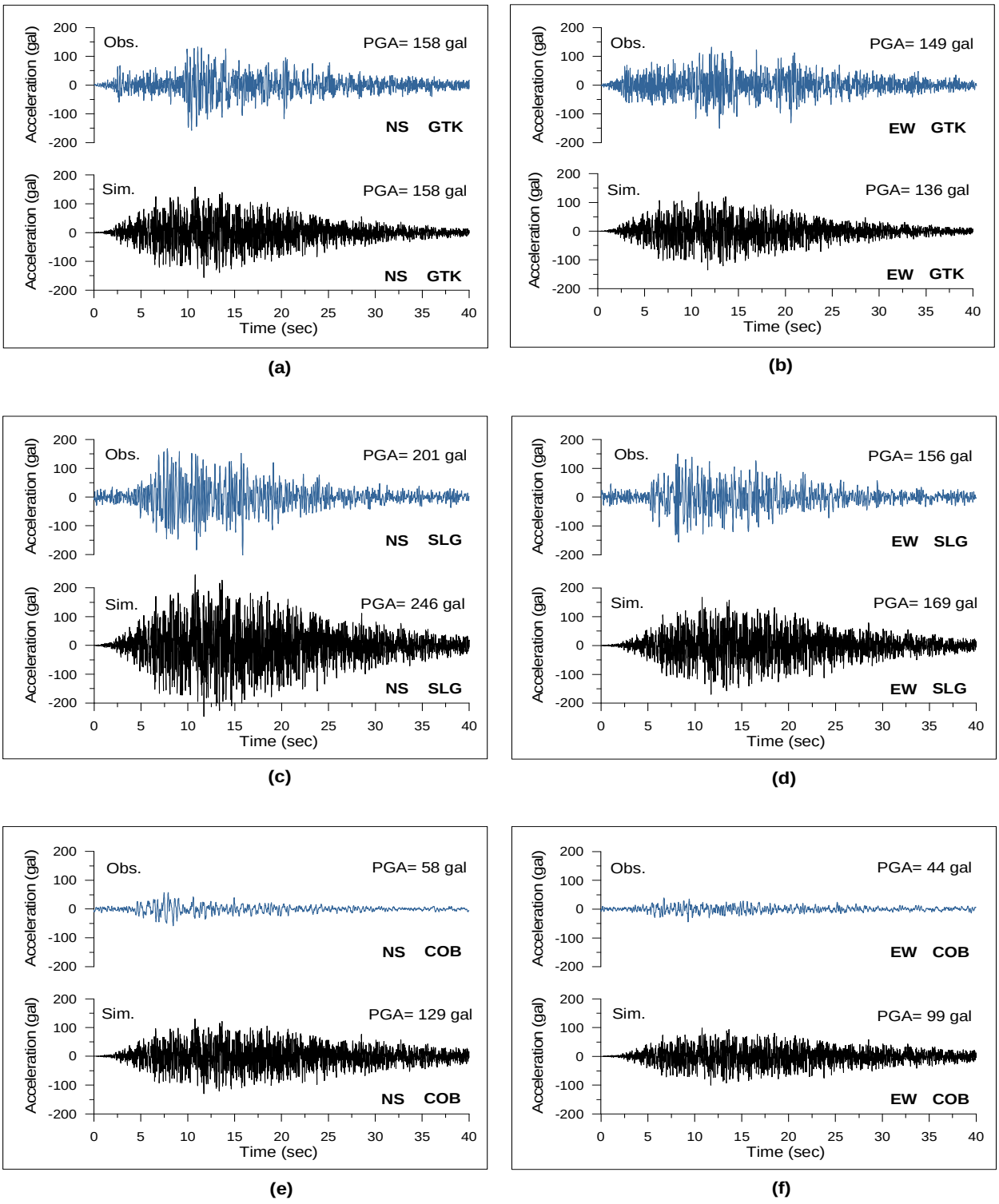

Figure 4.9 Comparisons of observed (in blue) and simulated (in black) acceleration record of NS and EW component for the Sikkim earthquake of magnitude 6.9 (M_w) at near-field stations

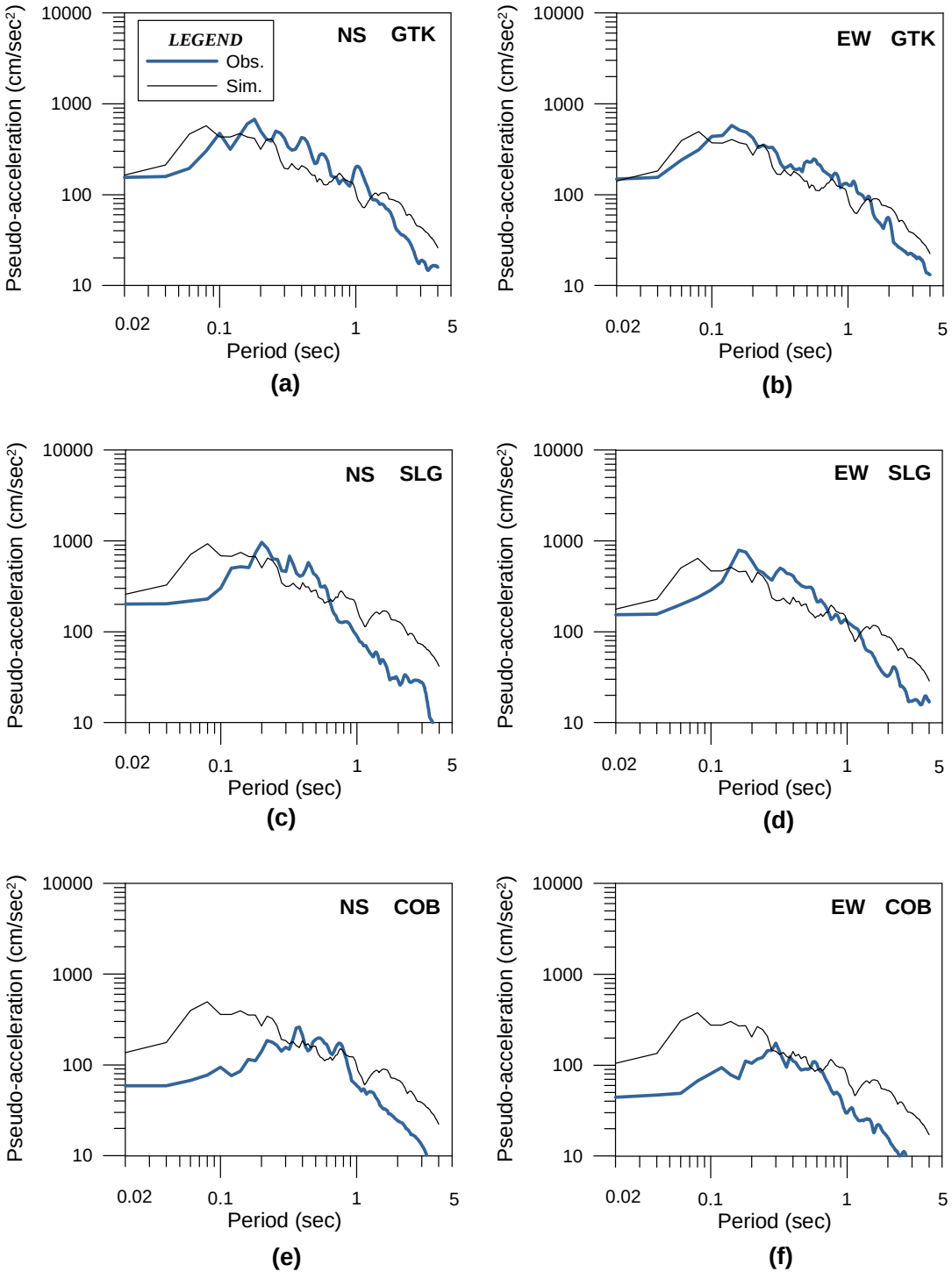

Figure 4.10 Comparisons of pseudo-acceleration response spectra with 5% damping determined from NS and EW component of observed and simulated acceleration record for the Sikkim earthquake of magnitude 6.9 (M_w) at GTK, SLG and COB stations

Table 4.7 Comparison of ground motion parameters at GTK station calculated from observed and simulated NS and EW components of acceleration records of the Sikkim earthquake

S. No.	Strong Motion Parameters	Observed		Simulated	
		NS	EW	NS	EW
1.	Peak Ground Acceleration (PGA) (gal)	158.0	149.1	158.4	136.6
2.	Peak Ground Velocity (PGV) (cm/sec)	12.4	11.3	16.2	14.0
3.	Peak Ground Displacement (PGD) (cm)	7.1	4.9	40.0	33.2
4.	v_{max}/a_{max} (sec)	0.07	0.07	0.10	0.10
5.	Arias Intensity (I_a) (m/sec)	0.61	2.63	0.78	0.58
6.	Effective Design Acceleration (EDA) (gal)	151.1	138.3	106.2	91.7
7.	Predominant Period (T_p) (sec)	0.18	0.14	0.08	0.08
8.	Bracketed Duration (sec)	39.6	39.7	38.8	38.4
9.	Significant Duration (sec)	23.4	25.4	21.0	20.9

Table 4.8 Comparison of ground motion parameters at SLG station calculated from observed and simulated NS and EW components of acceleration records of the Sikkim earthquake

S. No.	Strong Motion Parameters	Observed		Simulated	
		NS	EW	NS	EW
1.	Peak Ground Acceleration (PGA) (gal)	201.6	155.7	246.2	169.5
2.	Peak Ground Velocity (PGV) (cm/sec)	10.3	10.4	26.6	18.8
3.	Peak Ground Displacement (PGD) (cm)	28.3	61.6	81.2	53.3
4.	v_{max}/a_{max} (sec)	0.05	0.06	0.10	0.11
5.	Arias Intensity (I_a) (m/sec)	1.16	0.77	2.11	1.0
6.	Effective Design Acceleration (EDA) (gal)	192.5	160.0	173.7	120.9
7.	Predominant Period (T_p) (sec)	0.20	0.16	0.08	0.08
8.	Bracketed Duration (sec)	39.9	39.8	38.9	38.3
9.	Significant Duration (sec)	18.1	21.4	23.0	22.9

Table 4.9 Comparison of ground motion parameters at COB station calculated from observed and simulated NS and EW components of acceleration records of the Sikkim earthquake

S. No.	Strong Motion Parameters	Observed		Simulated	
		NS	EW	NS	EW
1.	Peak Ground Acceleration (PGA) (gal)	57.9	44.2	129.9	99.5
2.	Peak Ground Velocity (PGV) (cm/sec)	6.3	3.6	13.9	10.6
3.	Peak Ground Displacement (PGD) (cm)	45.0	17.5	60.5	47.1
4.	v_{max}/a_{max} (sec)	0.11	0.08	0.10	0.10
5.	Arias Intensity (I_a) (m/sec)	0.08	0.05	0.69	0.40
6.	Effective Design Acceleration (EDA) (gal)	58.1	40.3	92.8	71.2
7.	Predominant Period (T_p) (sec)	0.38	0.30	0.08	0.08
8.	Bracketed Duration (sec)	39.9	39.9	38.2	37.8
9.	Significant Duration (sec)	22.0	27.7	25.9	25.9

Nine Strong motion parameters explained in Chapter 3 have been extracted from both horizontal components of observed and simulated acceleration records at these near-field stations. The comparison of strong motion parameters at different stations have been listed in Table 4.7, Table 4.8 and Table 4.9. Parametric comparison of extracted parameters from observed and simulated records indicate that simulation at near-field stations like GTK and SLG gives comparable match in many extracted parameters. However, at COB, medium heterogeneity played an important role in reducing PGA and other energy related parameters in the observed record. Comparisons of response spectrum and strong motion parameters suggest that both simulated and observed response spectra give a comparable match at all near-field stations. This confirms the suitability of the final model and its selected parameters for generation of strong ground motion for both NS and EW components.

4.5 Far-field Simulation of Acceleration Record

Simulations at twelve far-field stations have been made using the same rupture model. These includes six stations managed by the Department of Earthquake Engineering, Indian Institute of Technology Roorkee and six in the Kumaon network managed by the Department of Earth Sciences, Indian Institute of Technology Roorkee. Stations managed by Department of Earth Sciences lies at an epicentral distance ranging between 886 and 944 km of the Sikkim earthquake. Information of these far-field stations is given in Table 4.10 at which ground motion records have been simulated by using the technique described in Chapter 2. Location of these stations is shown in Figure 4.11. Simulations at twelve far-field stations have been made from final rupture model of the Sikkim earthquake. The simulated NS and EW component of acceleration record has been compared in Figure 4.12 with the observed acceleration record in the same frequency range as used for its processing. Pseudo-acceleration response spectrums have been computed from the simulated and observed records and their comparison have been shown in Figure 4.13.

Table 4.10 Information of far-field strong motion stations at which simulation of accelerogram of the Sikkim earthquake have been made. Data has been taken from DEQ network and from the network of Kumaon region

S. No.	Station Code	Latitude (in degree)	Longitude (in degree)	Hypocentral Distance (km)	Station Name
1.	KOK	26.40	90.26	264	Kokhrajhar
2.	MLD	25.00	88.14	307	Malda
3.	RAX	26.98	84.84	336	Raxaul
4.	CHP	29.33	80.09	803	Champawat
5.	UDH	28.99	79.40	863	Udham Singh Nagar
6.	CMO	30.41	79.32	904	Chamoli
7.	BAL	29.79	80.42	887	Baluakot
8.	JAUL	29.75	80.38	888	Jauljibi
9.	PITH	29.58	80.21	894	Pithoragarh
10.	MUAV	29.74	80.13	909	Muavani
11.	BERI	29.77	80.05	917	Berinag
12.	BHAG	29.83	79.77	944	Bhageshwar

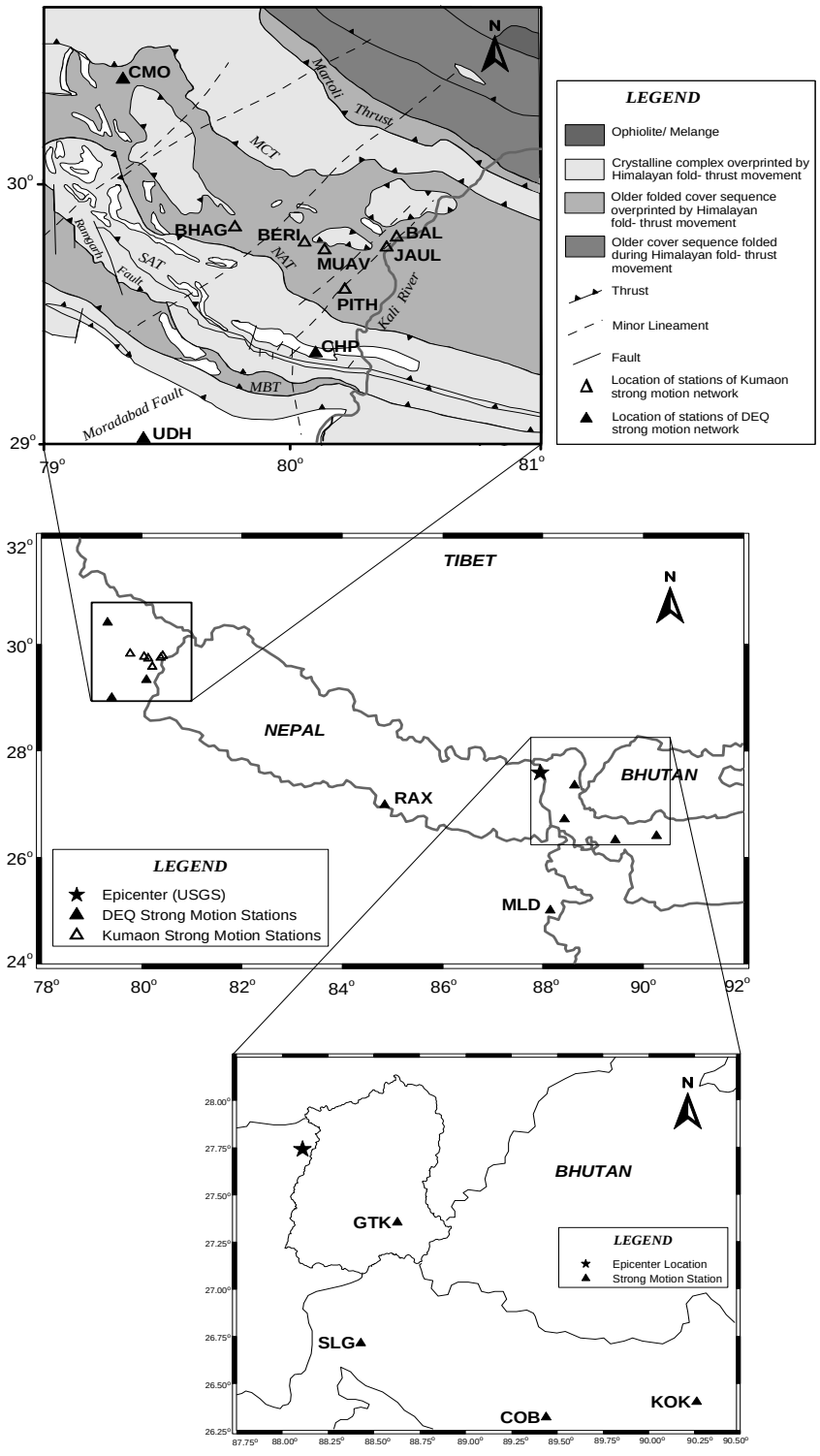

Figure 4.11 Location of near and far-field strong motion stations which have recorded the Sikkim earthquake of magnitude 6.9 (M_w). Geology of the Kumaon region has been taken after GSI (2000)

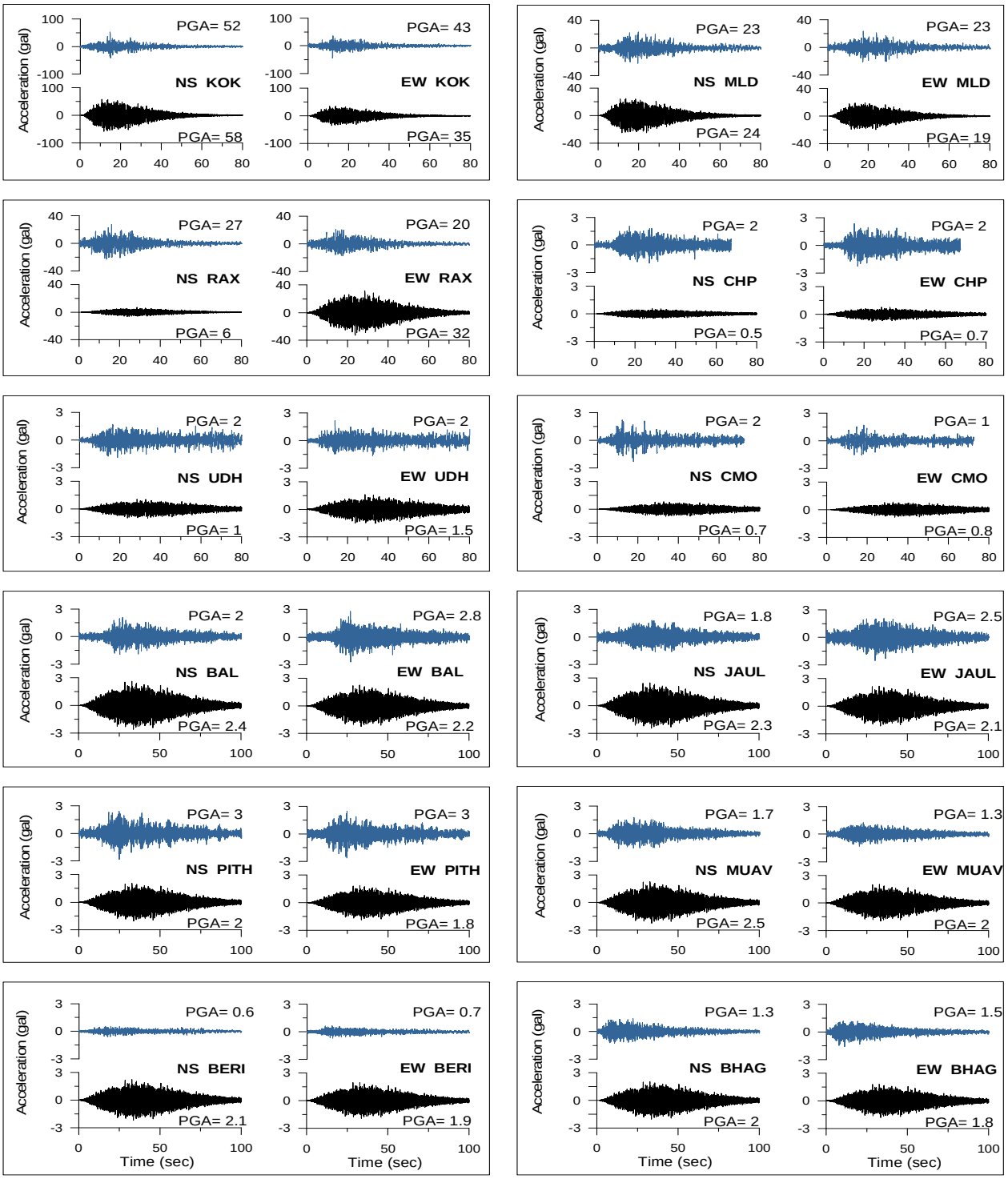

Figure 4.12 Comparison of NS and EW component of observed (in blue) and simulated (in black) acceleration record at different strong motion stations placed at an epicentral distance of 260–903 km range. Station codes and PGA values for observed and simulated record have been indicated in different plot

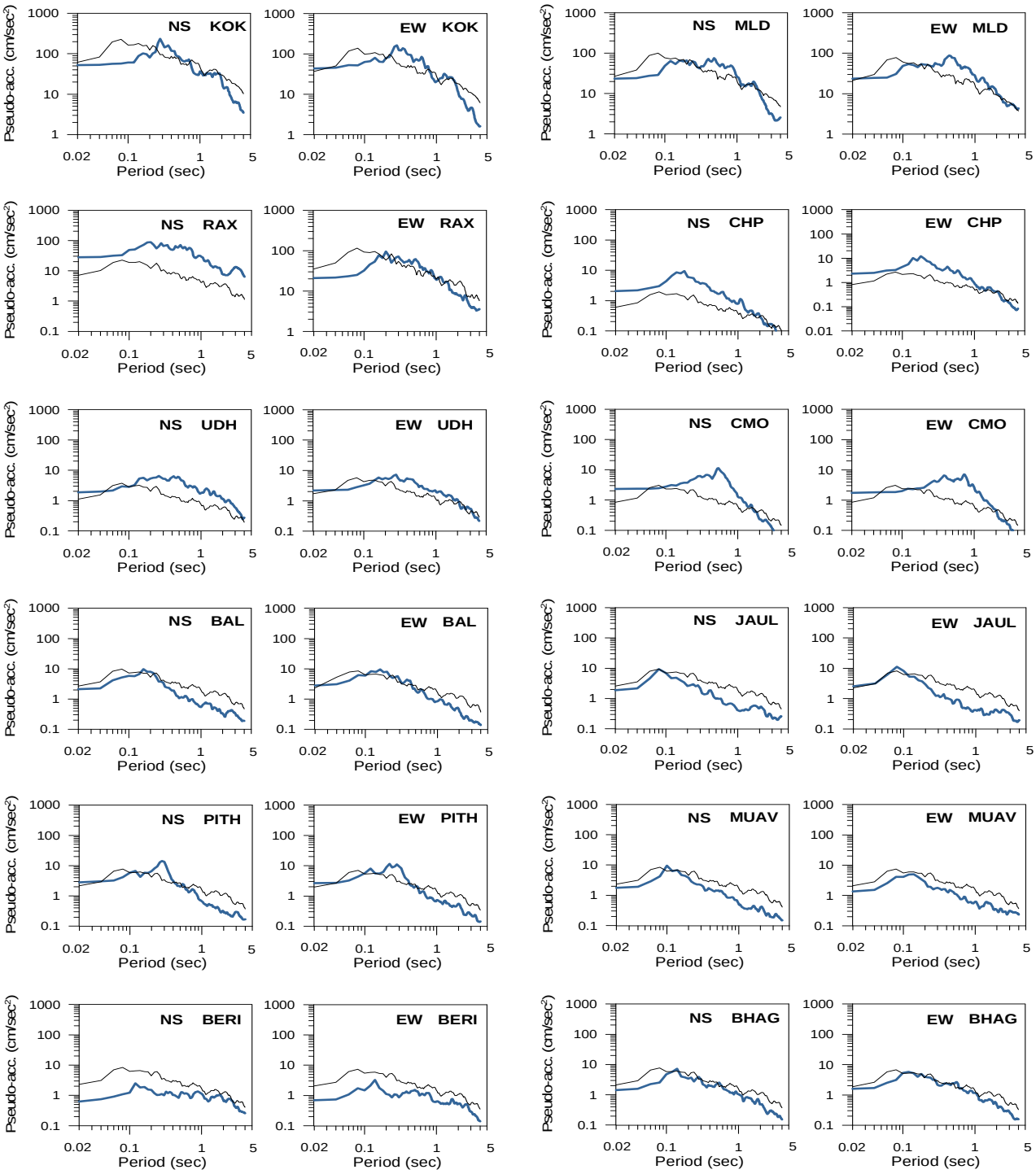

Figure 4.13 Comparison of pseudo-acceleration response spectra calculated from NS and EW component of observed and simulated acceleration record at different strong motion stations in a frequency range of 0.01–20.0 Hz. Station codes are shown with each plot. Thick blue line shows the pseudo-acceleration response spectra calculated from observed acceleration record

Root mean square error of waveform comparison has been estimated at each station using acceleration record and its response spectra. The estimated RMSE between observed and simulated records and its response spectra have been given in Table 4.11. Root mean square error between observed and simulated accelerograms varies from 0.46 to 0.56 at the near-field stations and from 0.32 to 0.62 at the far-field stations. The RMSE between response spectrums of observed and simulated records varies from 0.65 to 2.58 and from 0.34 to 2.28 at the near-field and far-field stations, respectively.

Peak ground acceleration values calculated from NS and EW component of simulated and observed records at near-field and far-field stations have been compared in Figure 4.14. The comparison shows that the modified semi-empirical technique is effectively capable of predicting PGA parameter of both components in near-field as well as far-field stations. The ratio of simulated and observed PGA of NS and EW components in Figure 4.15 indicates that the ratio of PGA is close to unity at most of the stations. This confirms the efficacy of approach and suitability of the final model to the prediction of PGA parameters for the Sikkim earthquake.

Table 4.11 Estimated RMSE between observed and simulated acceleration record and its response spectrum

S. No.	Stations	RMSE between observed and simulated Acceleration record		RMSE between observed and simulated Response Spectrum	
		NS	EW	NS	EW
1.	GTK	0.48	0.46	0.87	0.65
2.	SLG	0.46	0.56	2.58	1.19
3.	COB	0.53	0.52	1.84	2.28
4.	KOK	0.57	0.58	1.18	1.55
5.	MLD	0.47	0.47	1.03	0.34
6.	RAX	0.62	0.43	0.78	0.81
7.	CHP	0.46	0.45	0.49	0.65
8.	UDH	0.35	0.32	0.54	0.38
9.	CMO	0.54	0.55	1.03	0.74
10.	BAL	0.42	0.43	2.08	1.96
11.	JAUL	0.46	0.48	2.00	2.28
12.	PITH	0.37	0.37	1.84	1.40
13.	MUAV	0.39	0.40	2.20	1.51
14.	BERI	0.54	0.55	1.30	1.40
15.	BHAG	0.50	0.53	1.27	1.08

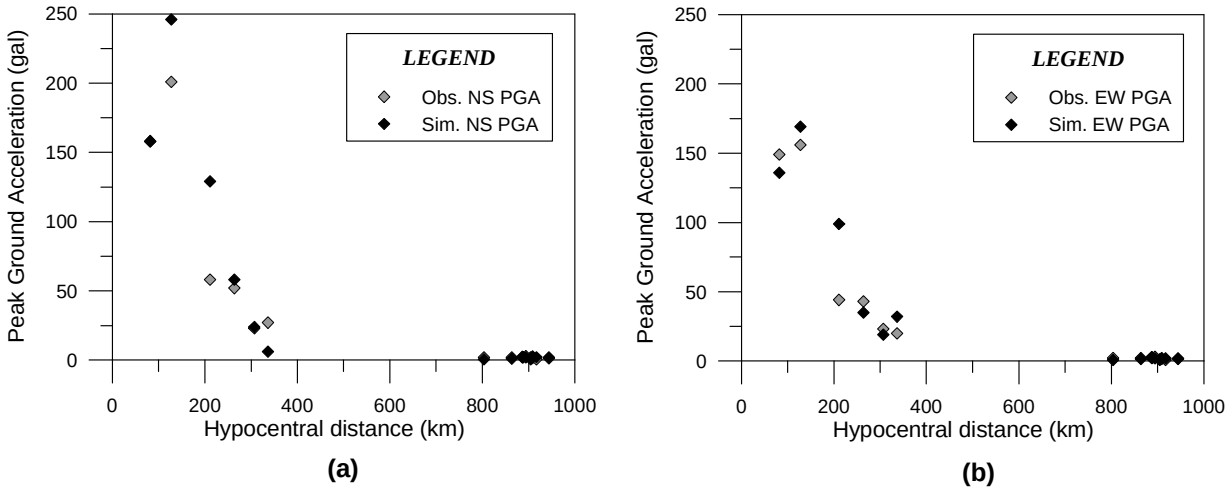

Figure 4.14 Comparison of peak ground acceleration (PGA) value of (a) NS and (b) EW component of the observed and simulated acceleration record at near and far-field stations

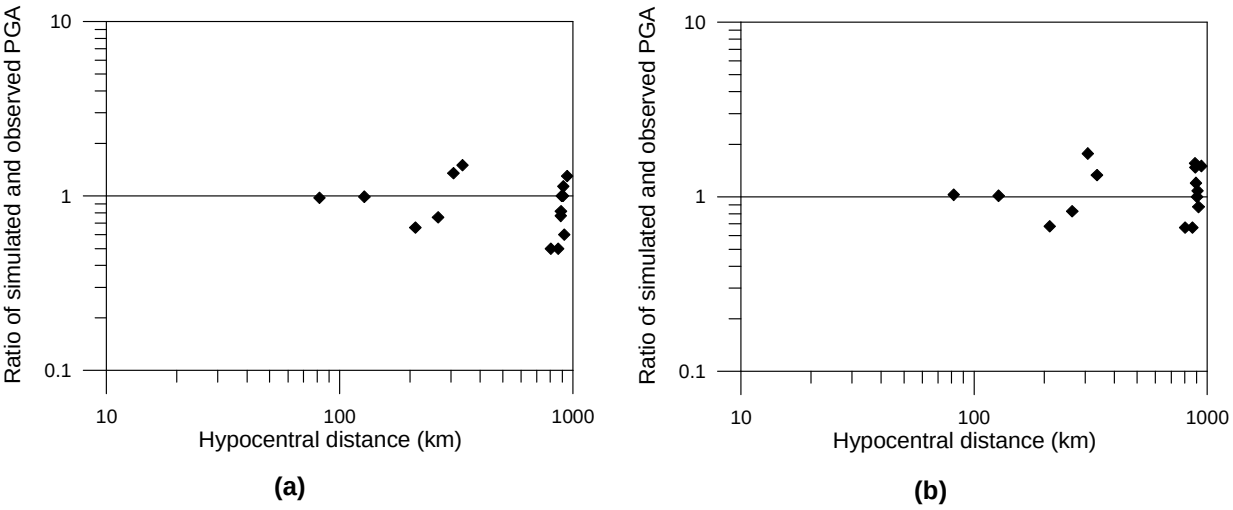

Figure 4.15 Ratio of peak ground acceleration (PGA) value for (a) NS and (b) EW component of the observed and simulated acceleration record for all fifteen stations

The quantitative comparison indicates that the range of uncertainty in simulated and observed acceleration record at far-field stations are higher as compared to the near-field stations. This may be resulted from several factors which are actually present in the ray path between source

and far-field recording stations and which have not been included in the present approach of simulation. These effects include large-scale crustal deformation and heterogeneities present in the path between source and receiver for far-field stations.

4.6 Conclusion

Modified semi-empirical approach has been used for component-wise simulation of strong ground motion due to the Sikkim earthquake. The method has been applied and tested for simulation of near-field and far-field acceleration records of the Sikkim earthquake (M_w = 6.9) of September 18, 2011. Several possibilities of modeling parameters like position of nucleation point, rupture velocity and dip of the rupture plane have been considered before arising to a final model. The selection of final model is based on RMSE of simulated and observed waveform. Comparison of simulated and observed record suggests that the method is capable of simulating record which bears realistic appearance in terms of shape and strong motion parameters. The results show that this technique gives records which match in a wide frequency range for the Sikkim earthquake and that too from simple and easily accessible parameters of the rupture plane.

Chapter – 5

SYNTHETIC GROUND MOTION FOR THE SUMATRA EARTHQUAKE OF DECEMBER 26, 2004 (M_W = 9.0)

A great earthquake (M_w = 9.0) occurred on December 26, 2004 in the Sumatra region has devastated entire south Asia. It marked a massive destruction with approximately 2,50,000 casualties (Chadha et al. 2005) and has raised concern over the safety of structures in the coastal region of various south Asian countries including India. This event has generated fault slip of up to 15 m near Banda Aceh, Sumatra (Jaiswal et al. 2011). This earthquake was recorded at several broadband stations worldwide. The simulation technique used to model such great earthquake needs to be effective in synthesizing both low-frequency ground motion in the velocity records as well as high-frequency ground motion in the acceleration record for comparing the simulated records with observed data. This chapter describes the applicability of empirical Green's function and modified semi-empirical technique discussed in Chapter 2 for simulation of records due to this earthquake at various stations. Broadband data of the Sumatra earthquake are used for comparing the simulated record obtained from the empirical Green's function and modified semi-empirical techniques.

5.1 Sumatra Earthquake

The coastal region of the Sumatra Island in Indonesia was struck by a devastating great earthquake of magnitude 9.0 (M_w) on December 26, 2004. It was one of the largest earthquake instrumentally recorded. This earthquake has released energy of about 4.3×10^{18} J and has triggered a devastating tsunami in entire south Asia (Ammon et al. 2005; Bilham 2005; Lay et al. 2005). Effect of this earthquake was felt in the Indian subcontinent in terms of destruction caused by Tsunami in the coastal regions. Tsunami height at different locations along the eastern coast of Indian peninsula was studied in detail by Chadha et al. (2005) and Dimri and Srivastava (2007).

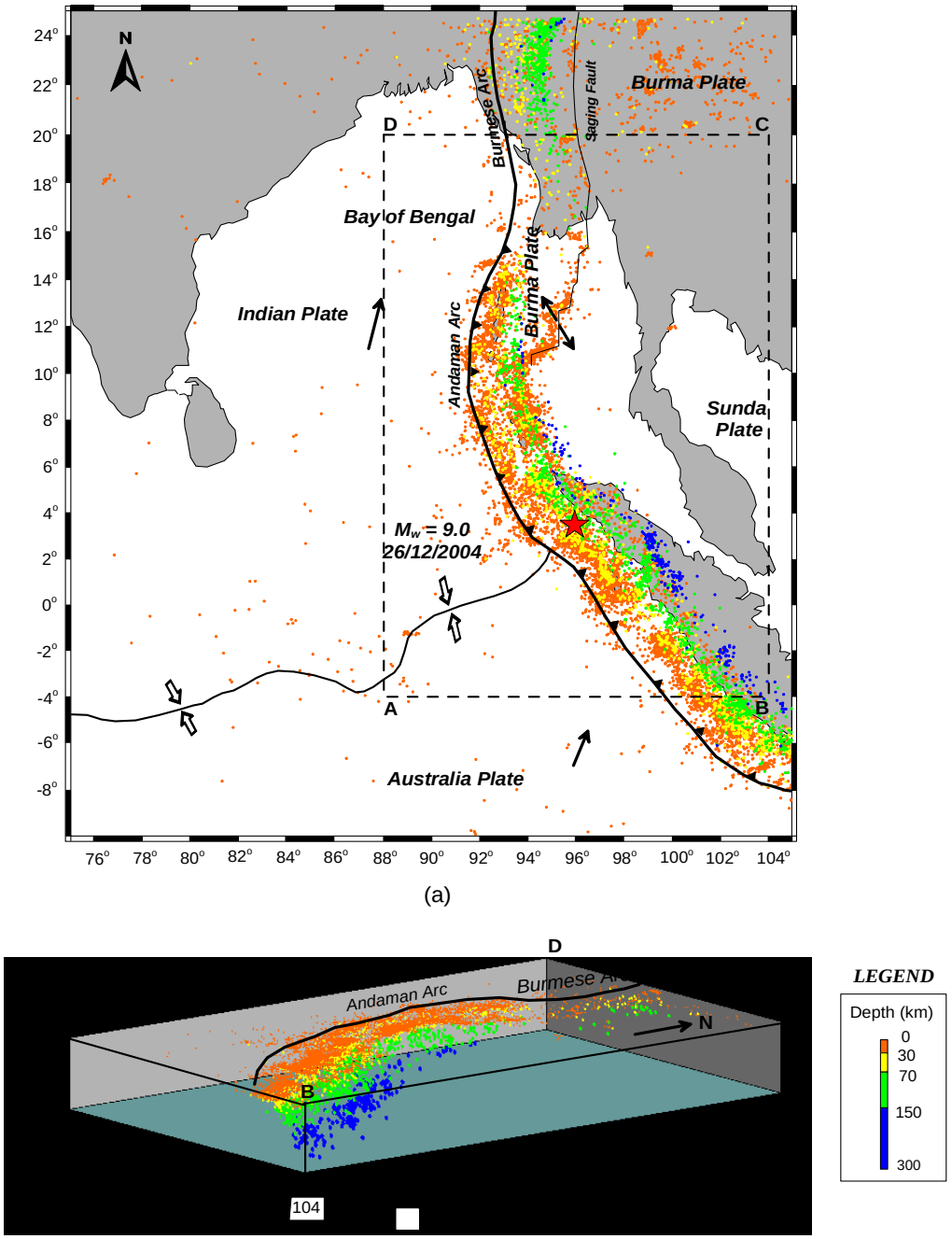

(a)

(b)

Figure 5.1 (a) Distribution of past seismicity along the Andaman–Burmese arc from 1973 to 2010 using USGS database (Figure modified after Rao and Chary 2005). Epicenter of December 26, 2004 event is shown with red star. The rectangular block ABCD marked in this figure is used to show the seismic activity in this area in a depth section. (b) Depth-wise distribution of different events from 1973 to 2010 in the rectangular block ABCD. Depth of events has been shown by different colors in legend

Table 5.1 Parameters of the Sumatra, Indonesia earthquake of December 26, 2004

Hypocenter	Size	Fault Plane Solution	Reference
00:58:50 s UTC 3.09°N, 94.26°E 29 km	$M_o = 4.0\times10^{29}$ dyne-cm $M_w = 9.0$	NP1 $\varphi = 329°,\ \delta = 8°,\ \lambda = 110°$ NP2 $\varphi = 129°,\ \delta = 83°,\ \lambda = 87°$	Global CMT
3.298°N, 95.779°E 30 km	$M_o = 2.5\times10^{29}$ dyne-cm $M_w = 8.2$	$\varphi = 274°,\ \delta = 13°,\ \lambda = 55°$	USGS
3.09°N, 94.26°E 29 km	$M_o = 6.5\times10^{29}$ dyne-cm $M_w = 9.1$	$\varphi = 340°,\ \delta = 14°,\ \lambda = 110°$	Lay et al. (2005)

The epicenter of this earthquake was approximately 155 km west of Sumatra and about 255 km south-east of Banda Aceh, Indonesia. It has ruptured along the boundary between the Indo-Australian plate and the Eurasian plate along the northwestern Sumatra, Nicobar Island and Andaman Island (Sorensen et al. 2007). The region is one of the most seismically active regions. Location of this event together with the past seismicity is shown in Figure 5.1a. The depth-wise distribution of seismicity in Figure 5.1b of the region shows the nature of movement of two different plates. Parameters of this earthquake are given in Table 5.1. The focus of this earthquake was at a depth of 30 km and ruptured length was estimated to be 750 km by Sorensen et al. (2007). Different studies indicated different rupture speeds varying from 1.5 km/sec (de Groot Hedlin 2005) to 2.5 ± 0.5 km/sec (Yagi 2005, Ammon et al. 2005) and the dip of rupture plane ranging from 8° given by Global CMT to 13° given by USGS.

5.2 Data

In order to simulate and compare the strong motion data of the Sumatra earthquake, broadband data collected by different agencies has been used. Several agencies operate broadband networks worldwide and have different format of their data dissipation. The collected data from different agencies need to be converted into ASCII format for further processing. Several software and programs have been used for this purpose. Since the record of the Sumatra earthquake has large number of data points, special processing software has been made to obtain corrected record at different stations. Under Ocean Hemisphere network Project (OHP), twenty broadband seismographs were installed in the north-west pacific region. Location of some of these stations maintained under this project is shown in Figure 5.2. The Sumatra earthquake of December 26,

2004 was recorded at fourteen stations of OHP. The closest broadband station out of fourteen stations which has recorded this earthquake is PSI station that lies at an epicentral distance of 355 km. The sensor at PSI station has sensitivity 0.75×10^{8} count/m/sec with the sampling frequency of 20 samples/sec. The velocity record at PSI station was provided in SEED format which have been processed after proper conversion into readable format. The removal of noise from data requires various signal processing tools. Broadband seismic data contain signal in broad frequency range which include both low and high-frequencies. Special consideration is required to avoid the incorrect representation of noise as signal for processing of high-frequency signal. Software has been developed in FORTRAN language in the present work which can handle the enormous data size obtained of this great earthquake. The algorithm used for processing of data is based on that given by Boore and Bommer (2005) which includes linear correction, instrumental scaling, padding, acausal band pass filtering and instrument response. The record at PSI station has been band-passed in a frequency range of 0.3–2.0 Hz for correctly representing particle ground motion at this station. The processed record at PSI station has been shown in Figure 5.3.

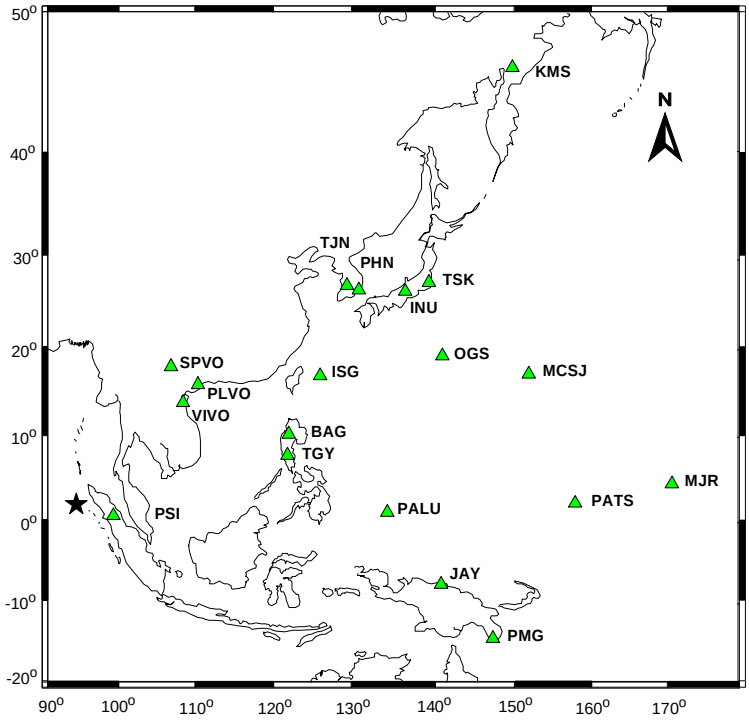

Figure 5.2 Location of some of seismic stations in the north-west pacific region maintained by OHP network shown by green triangle that has recorded the Sumatra earthquake of December 26, 2004. Epicenter of this event is shown with star

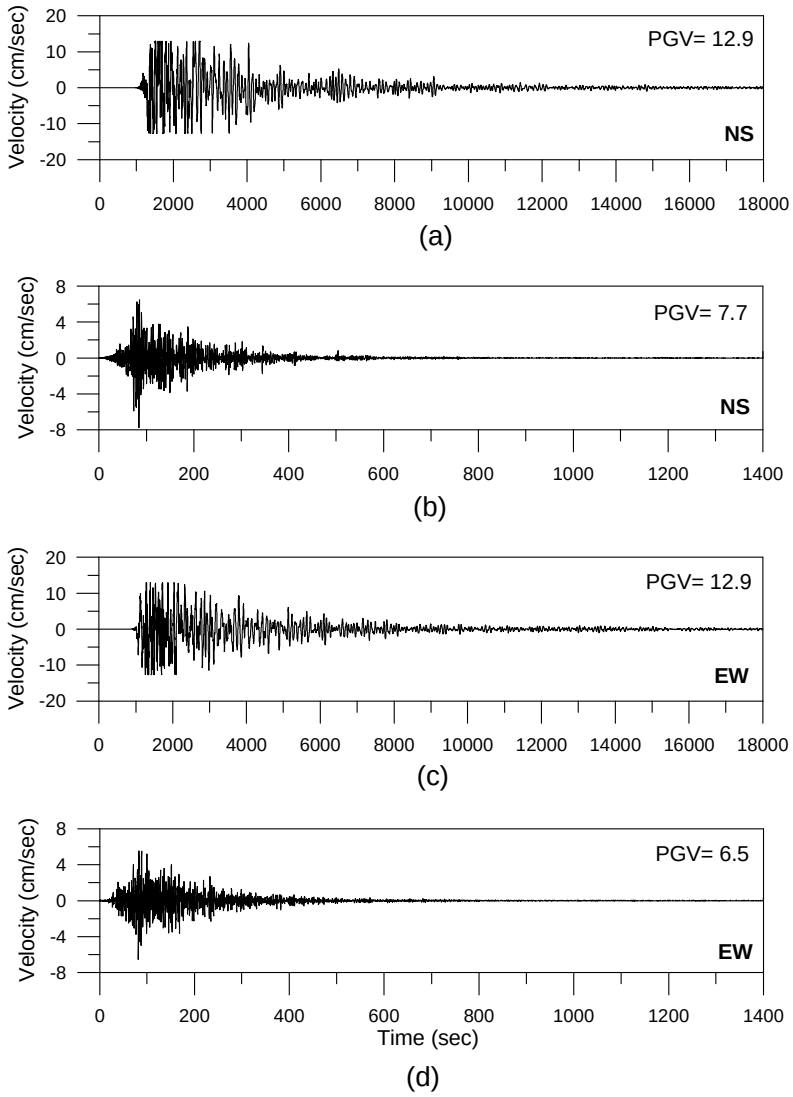

Figure 5.3 (a) Observed NS component, (b) filtered NS component, (c) observed EW component and (d) filtered EW component of velocity record of the great Sumatra earthquake of December 26, 2004 at PSI station. The range of band-pass Butterworth filter is 0.3–2.0 Hz

It has been observed from Figure 5.3a that recorded ground motion at PSI station is clipped for amplitude larger than 12.9 cm/sec due to the dynamic range of the instrument. Although this clipped record is not used as an input in the simulations in this work, it is required for comparison with the simulated record. In an attempt to check the frequencies present in the record that remain unaffected by clipping, the velocity records have been clipped experimentally at the PSI station at

amplitudes larger than 12.9, 12.5, 12.0, 11.5, 10.0 and 8.0 cm/sec, respectively. The amplitude spectra of records obtained after different level of clipping has been shown in Figure 5.4. The comparison of amplitude spectrum of clipped records at various clipping level shows that amplitude spectrum of record remains almost unaffected by clipping in a frequency range of 0.3–2.0 Hz. For this reason, the observed record is band-passed through a Butterworth filter in a frequency range of 0.3–2.0 Hz and is used for comparison with the simulated record generated in the same frequency range.

The simulation of record using EGF technique requires aftershock of the target earthquake recorded at the site of simulation as empirical Green's function, which is the main input in EGF simulation technique. The aftershock of the Sumatra earthquake that occurred on December 26, 2004 has been considered as empirical Green's function. Parameters of this earthquake are given in Table 5.2 and velocity record of this aftershock is shown in Figure 5.5. This record has been processed using the same steps used for processing of record of the target earthquake.

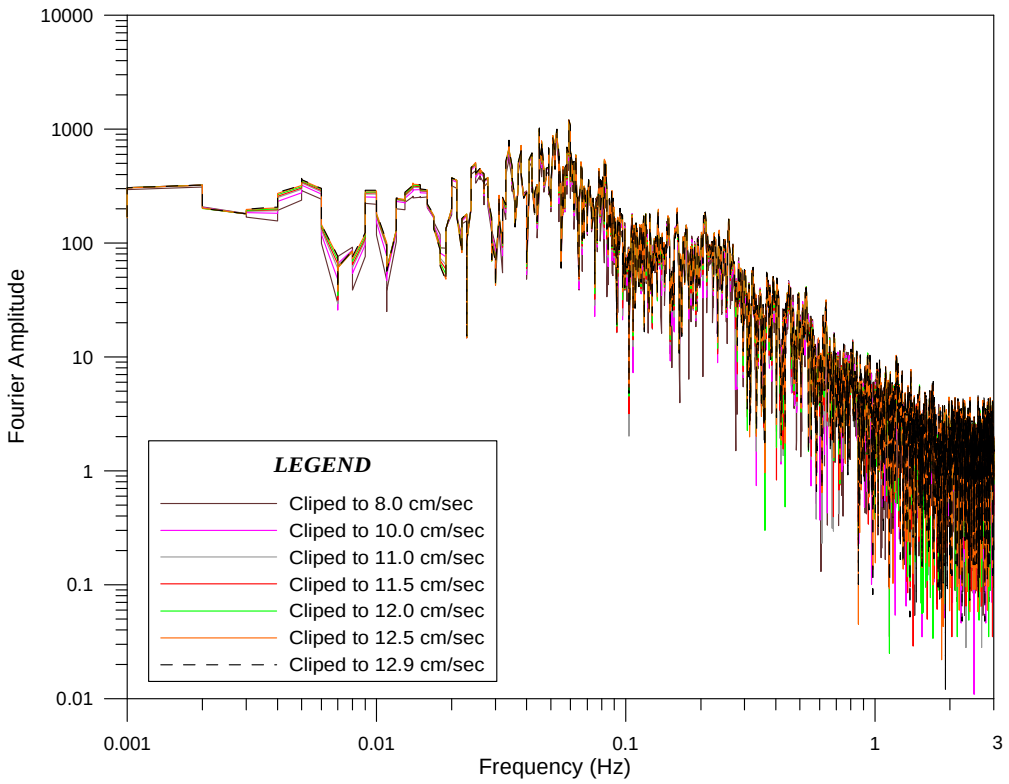

Figure 5.4 Comparison of Fourier amplitude spectra of records obtained from different level of clipping of NS component of observed velocity record at PSI station

Table 5.2 Parameters of the selected aftershock of December 26, 2004 used as empirical Green's function

Hypocenter	Size	Fault Plane Solution	Reference
26/12/2004 04:21:36.5 s GMT 06.61°N, 92.79°E 13.6 km	$M_o = 7.23\times10^{26}$ dyne-cm $M_w = 7.2$	NP1 $\varphi = 351°,\ \delta = 27°,\ \lambda = 121°$ NP2 $\varphi = 137°,\ \delta = 67°,\ \lambda = 75°$	Global CMT

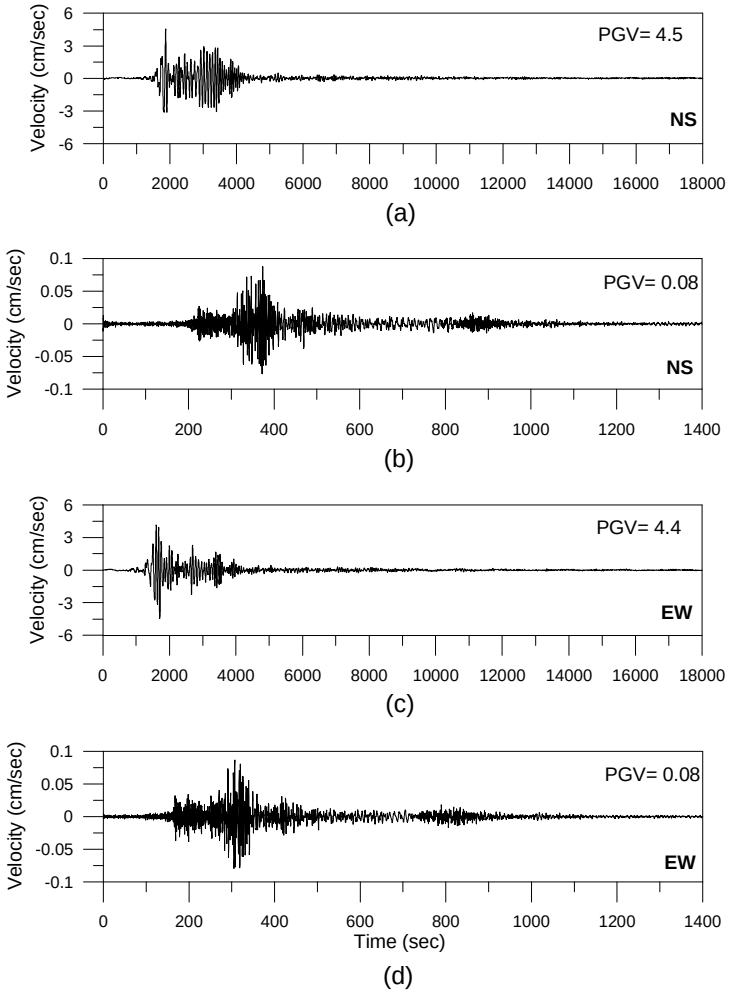

Figure 5.5 (a) Observed NS component, (b) filtered NS component, (c) observed EW component and (d) Filtered EW component of velocity record of the great Sumatra earthquake of December 26, 2004 at PSI station. The range of band-pass Butterworth filter is 0.3–2.0 Hz

India Meteorological Department (IMD) is the nodal agency of the Government of India which is responsible for monitoring seismic activity in and around the country. Among 17 broadband seismic stations, MDRS station has been used for simulation of ground motion of the Sumatra earthquake. These stations are under Real Time Seismic Monitoring Network (RTSMN) which was set up by India Meteorological Department. The network is capable of monitoring and reporting in least possible time, the occurrence of earthquakes capable of generating Tsunami likely to affect the Indian coastal regions. Processed record of the Sumatra earthquake at MDRS station after passing through Butterworth filter in a frequency range of 0.3–2.0 Hz has been shown in Figure 5.6.

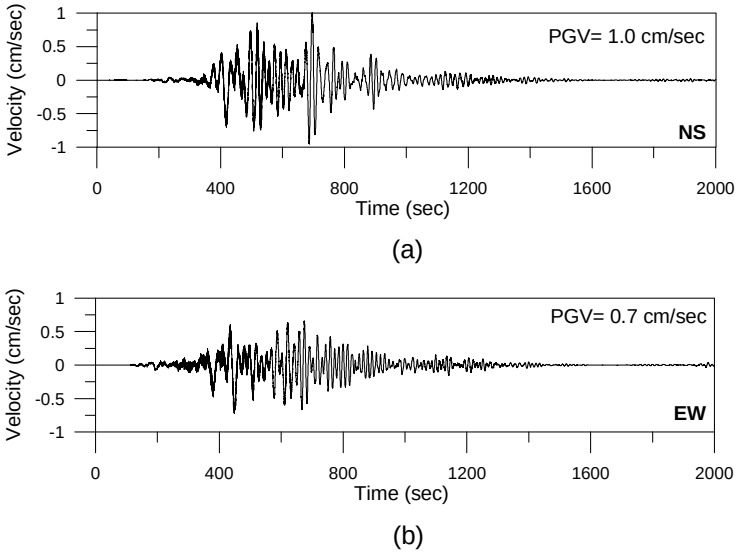

Figure 5.6 Processed velocity record of (a) NS and (b) EW component from broadband data recorded at MDRS station of IMD for December 26, 2004 Sumatra earthquake

Simulations of strong ground motion using modified semi-empirical technique require empirical relation of duration parameter. This duration parameter has been calculated using data from 23 records of the Sumatra earthquake and is given as:

$$T_d = 0.0015 \times 10^{0.5M_w} + 0.2R^{0.81} \tag{5.1}$$

where, M_w and R, are moment magnitude and hypocentral distance, respectively. The residual sum of square for this relation is 0.58.

5.3 Simulation of Ground Motion for the Sumatra Earthquake

5.3.1 Modified Semi-Empirical Technique

In order to understand the high-frequency nature of ground motion produced during this great earthquake, records have been simulated in this section by using modified semi-empirical technique. Due to complexities of slip mechanism of this mega-thrust earthquake and dependency of other simulation methods on slip distribution, modified semi-empirical technique have been used for simulation of strong motion data of this earthquake. In the modeling approach, a modification in semi-empirical technique has been made to remove its dependency on attenuation relation which has many constraints. It has been observed that the semi-empirical approach is dependent on simple modeling parameters which are easily available. This approach of ground motion simulation does not require complete slip distribution within the rupture plane which itself is difficult to model. The present study is aimed to use modified semi-empirical method to provide estimate of rupture velocity and rupture propagation of the Sumatra earthquake by simulating its record at various observation points. Strong motion modeling of the rupture plane using modified semi-empirical approach is dependent on various parameters like, length, width, nucleation point, velocity structure, rupture velocity, location and geometry of rupture plane and its sub-faults. The geometrical parameters of sub-faults have been calculated using the self-similarity laws given by Kanamori and Anderson (1975). The modeling parameters of rupture plane responsible for the Sumatra earthquake are kept similar to that used by Sorensen et al. (2007) and are given in Table 5.3. The entire rupture plane of dimension 750 km×150 km has been divided into 100 sub-faults. Each sub-fault represents an earthquake of magnitude 7.0 (M_w). The seismic moment of the target earthquake is considered as 4.0×10^{29} dyne-cm (Global CMT). The velocity model in the source region of the Sumatra earthquake used in testing modified semi-empirical technique is given in Table 5.4.

Table 5.3 Parameters of the rupture model of the Sumatra earthquake

Modeling Parameter	Source
Length = 750 km	Lay et al. (2005)
Width = 150 km	Yagi (2005)
Dip = 10°	Yagi (2005)
N_L = 10, N_W = 10	Based on scaling relation by Kanamori and Anderson (1975)
V_r = 3.0 km/sec	Yagi (2005)

Table 5.4 Velocity model in source region of the Sumatra earthquake (modified after Sorensen et al. 2007)

Depth (km)	S-wave Velocity (km/sec)	Density (g/cm^3)
9.4	1.5	1.8
11	3.36	2.4
17	3.4	2.6

Software named MSEMP (Modified Semi Empirical Modeling Program) in FORTRAN language has been developed to simulate records of the great earthquake at any observation point using modified technique described in Chapter 2. This software require coordinates of recording station in a three dimensional Cartesian system in which the X -and the Y -axes are parallel to the strike and the dip direction of the rupture plane, respectively and Z-axis is positive in vertically downward direction. Acceleration records have been simulated at PSI and MDRS stations. Details of these stations are given in Table 5.5 and location of these stations and modeled rupture plane in the assumed Cartesian coordinate system has been shown in Figure 5.7. For the two dimensional model of the rupture plane, selection of nucleation point remains an important task. Final selection of nucleation point responsible for the Sumatra earthquake is based on the comparison of the observed and the simulated record obtained at PSI station from various models. In order to compare the simulated record with the observed velocity record, the simulated acceleration record has been integrated using the integration property of the Fourier transform. This simulated velocity record has been filtered with the same band-pass filter as used for the processing of the observed velocity record at PSI station. Root mean square error between observed and simulated waveform of the velocity record has been calculated for each cases using time window up to 500 seconds. Various simulated records and its comparison with observed record in terms of RMSE for different possibilities of nucleation point is shown in Figure 5.8. Root mean square error for these simulations varies from 0.004 to 0.023. It has been observed that nucleation point marked with sub-fault number 6 at depth of 38 km gives minimum RMSE and has been retained for further simulations.

Table 5.5 Site information for simulation of the Sumatra earthquake

Station Code	Latitude (In degree)	Longitude (In degree)	Hypocentral Distance (km)	Station Name	Network
PSI	02.69	98.92	355	Parapet, Indonesia	PS-OHP
MDRS	13.00	80.00	2060	Chennai, India	IMD

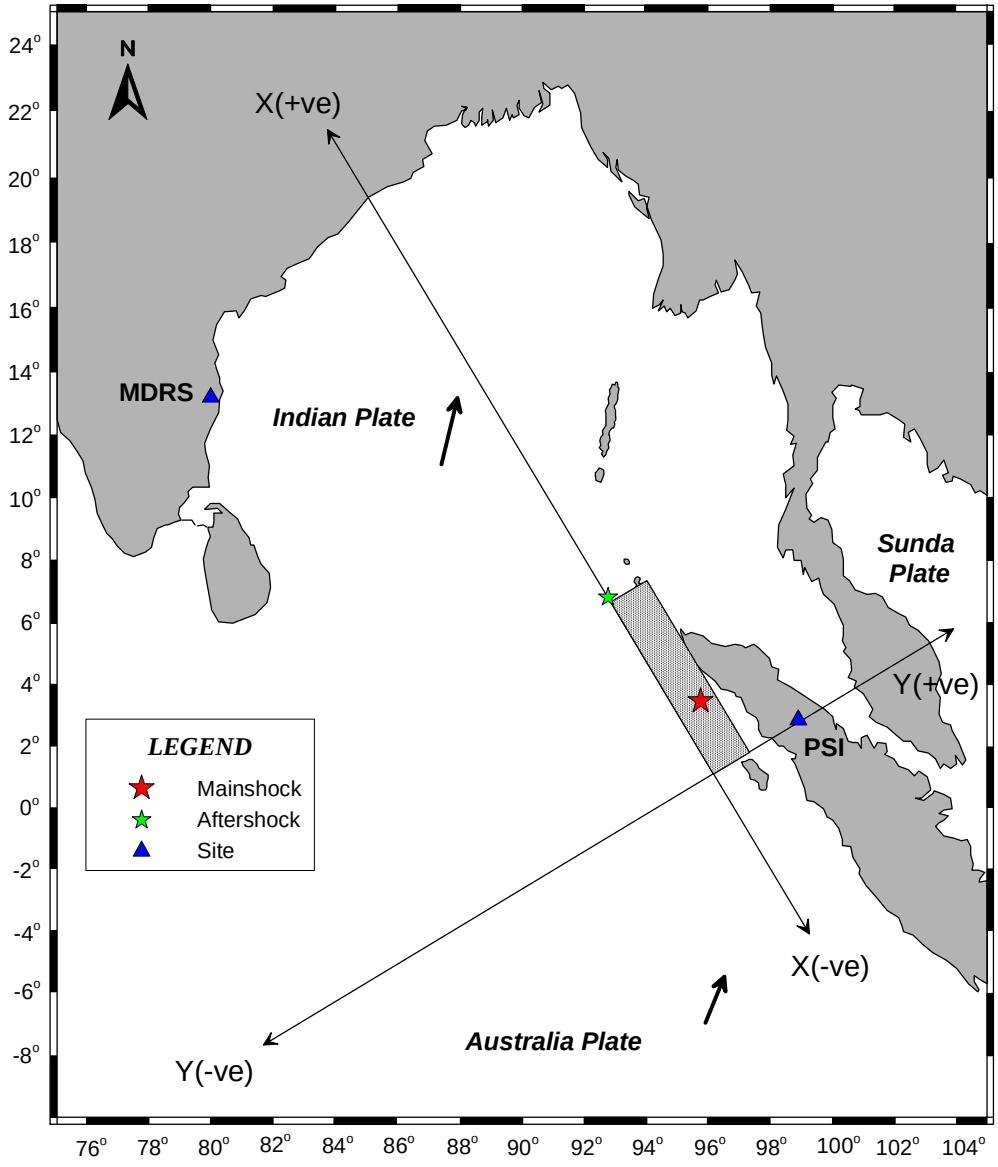

Figure 5.7 Location of assumed rupture plane responsible for the Sumatra earthquake indicated by shaded region has been placed in Cartesian coordinate system. The location of epicenters is taken from Global CMT

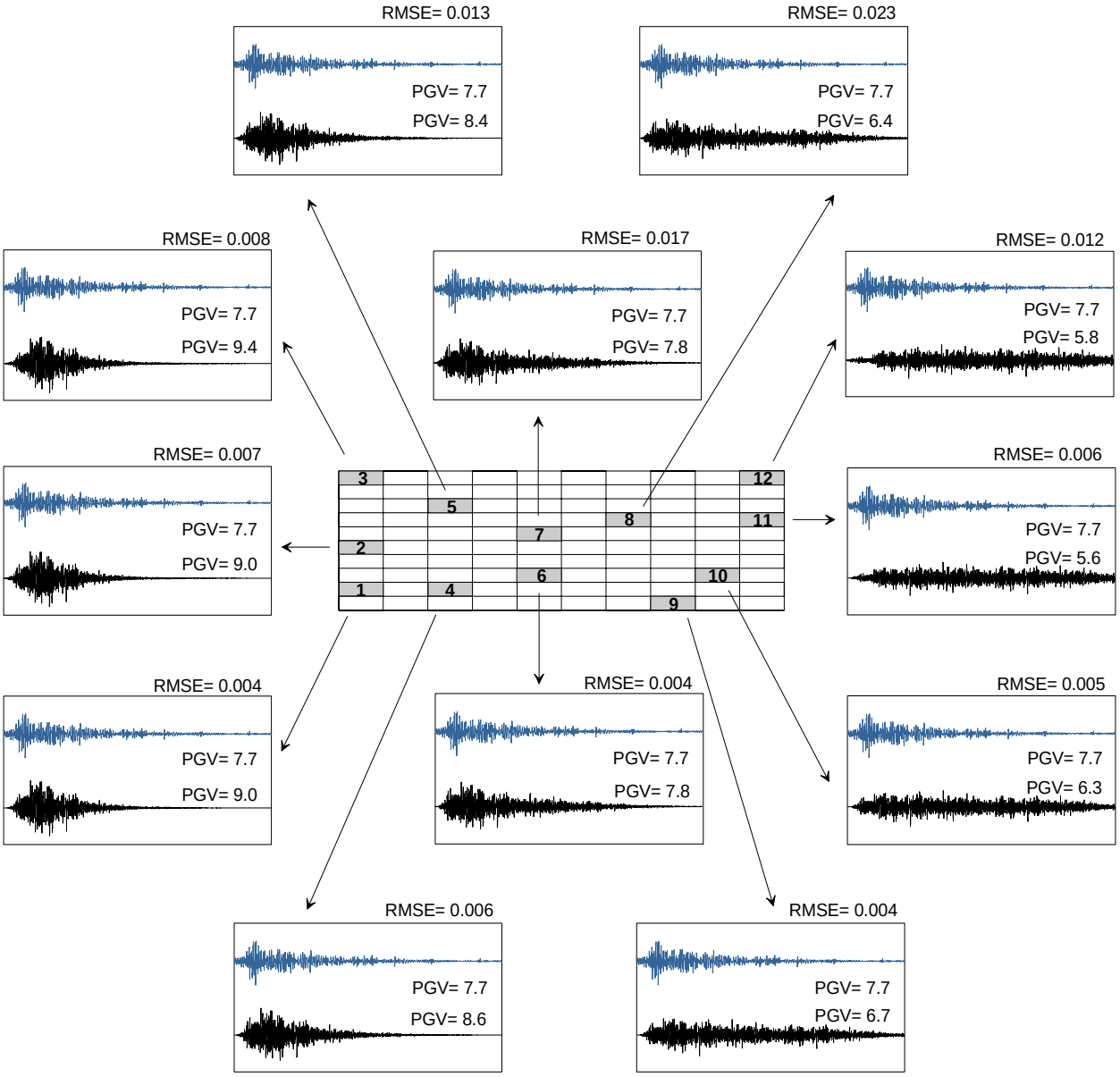

Figure 5.8 Filtered NS component of observed (in blue) and simulated (in black) record at PSI station has been shown in boxes for different possibilities of nucleation points. Nucleation points have been indicated by arrows. Both observed and simulated records filtered in a frequency range of 0.3–4.0 Hz. RMSE for each simulation has been shown at each box

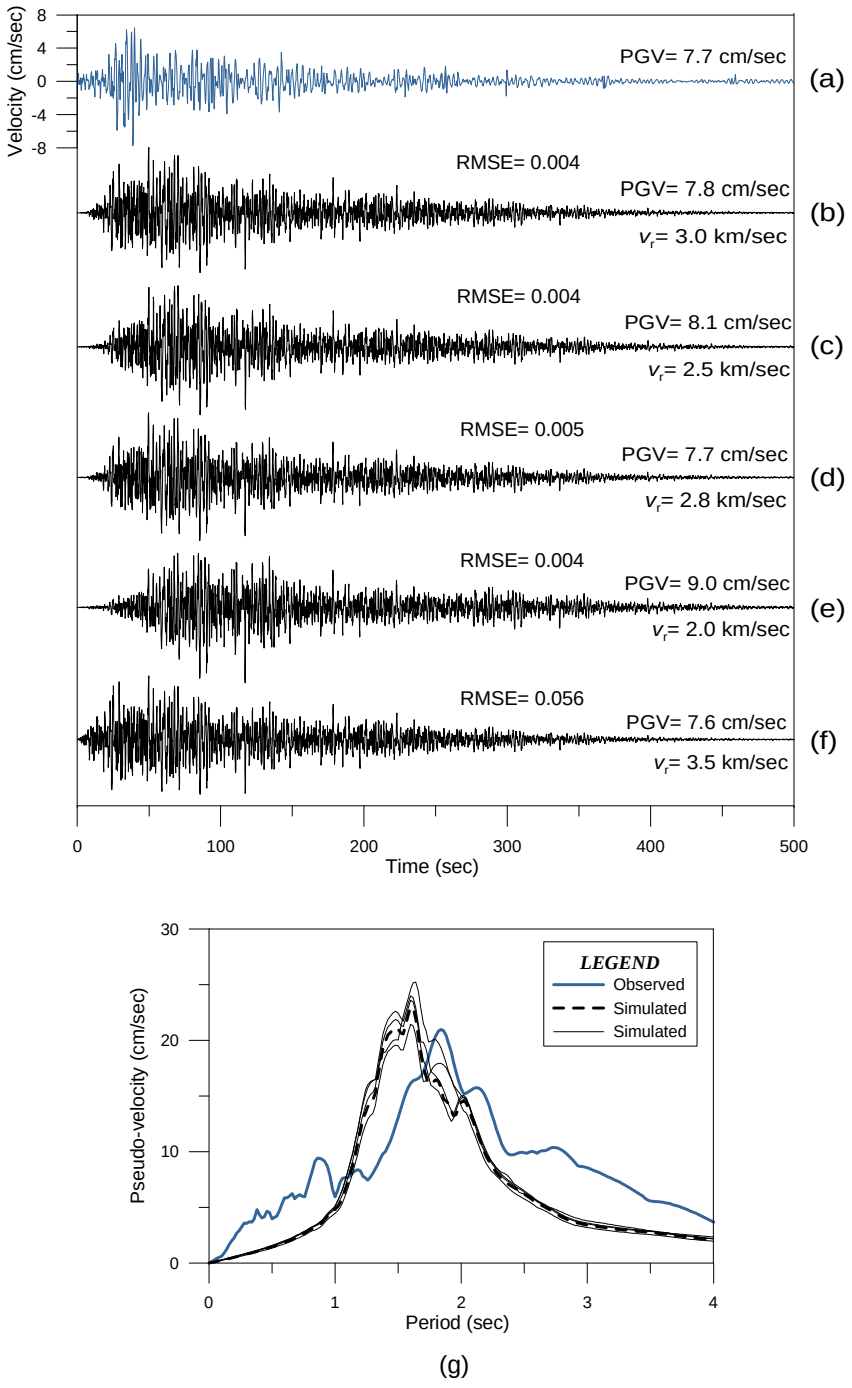

Figure 5.9 (a) Observed NS component of velocity record; simulated velocity record for rupture velocity (b) 3.0 km/sec, (c) 2.5 km/sec, (d) 2.8 km/sec, (e) 2.0 km/sec and (f) 3.5 km/sec at PSI station in the range of frequencies 0.3–4.0 Hz. (g) Comparison of pseudo-velocity response spectra with 5% damping of observed and simulated velocity record for different rupture velocity where dashed line shows the good match with the observed one

In all models used for selecting nucleation point, rupture velocity has been assumed as 3.0 km/sec (Sorensen et al. 2007). In order to select rupture velocity of the final rupture model, different records at the PSI station have been simulated using different rupture velocities within a range of 2.0 to 3.5 km/sec. The RMSE between the observed and the simulated waveforms shown in Figure 5.9 varies from 0.004 to 0.05 which reveals that minimum RMSE has been obtained for rupture velocity 3.0 km/sec. It has been observed from the comparison of response spectra obtained from observed and simulated record in Figure 5.9g that the simulated record obtained by using rupture velocity of 3.0 km/sec give a comparable match. Comparison of simulated and observed record for various range of modeling parameters confirm final rupture model shown in Figure 5.10. Simulated acceleration record at PSI station using final rupture parameters has been shown in Figure 5.11a. Comparison of observed and simulated velocity record at PSI station in Figure 5.11 shows that simulated record bears realistic shape as that of observed record and the peak ground velocity of the observed and the simulated record is also comparable. This confirms the suitability of the model and selected model parameters used for simulation of ground motion due to the Sumatra earthquake. The final model used for simulating record at PSI station is further used to simulate records at MDRS station which lies at an epicentral distance of 2060 km. The simulated record at this station has been shown in Figure 5.12.

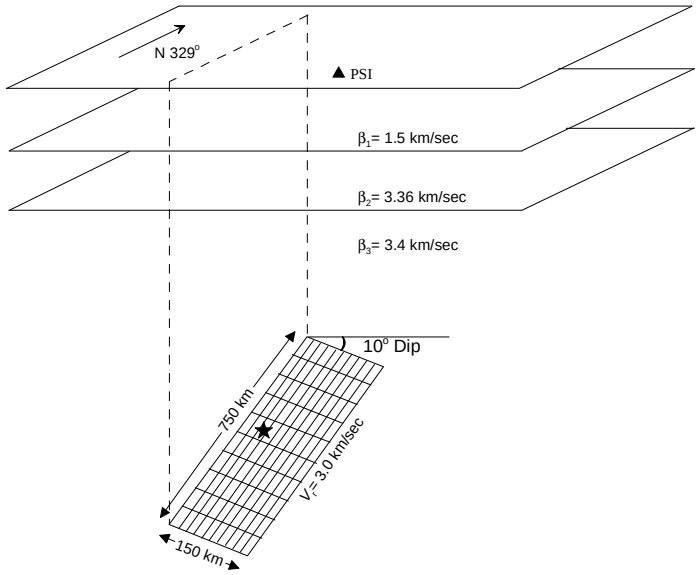

Figure 5.10 Rupture model of the Sumatra earthquake consisting of 10×10 sub-faults in a layered medium with 329°N strike direction. Solid triangle shows the location of PSI station and star shows the starting position of rupture

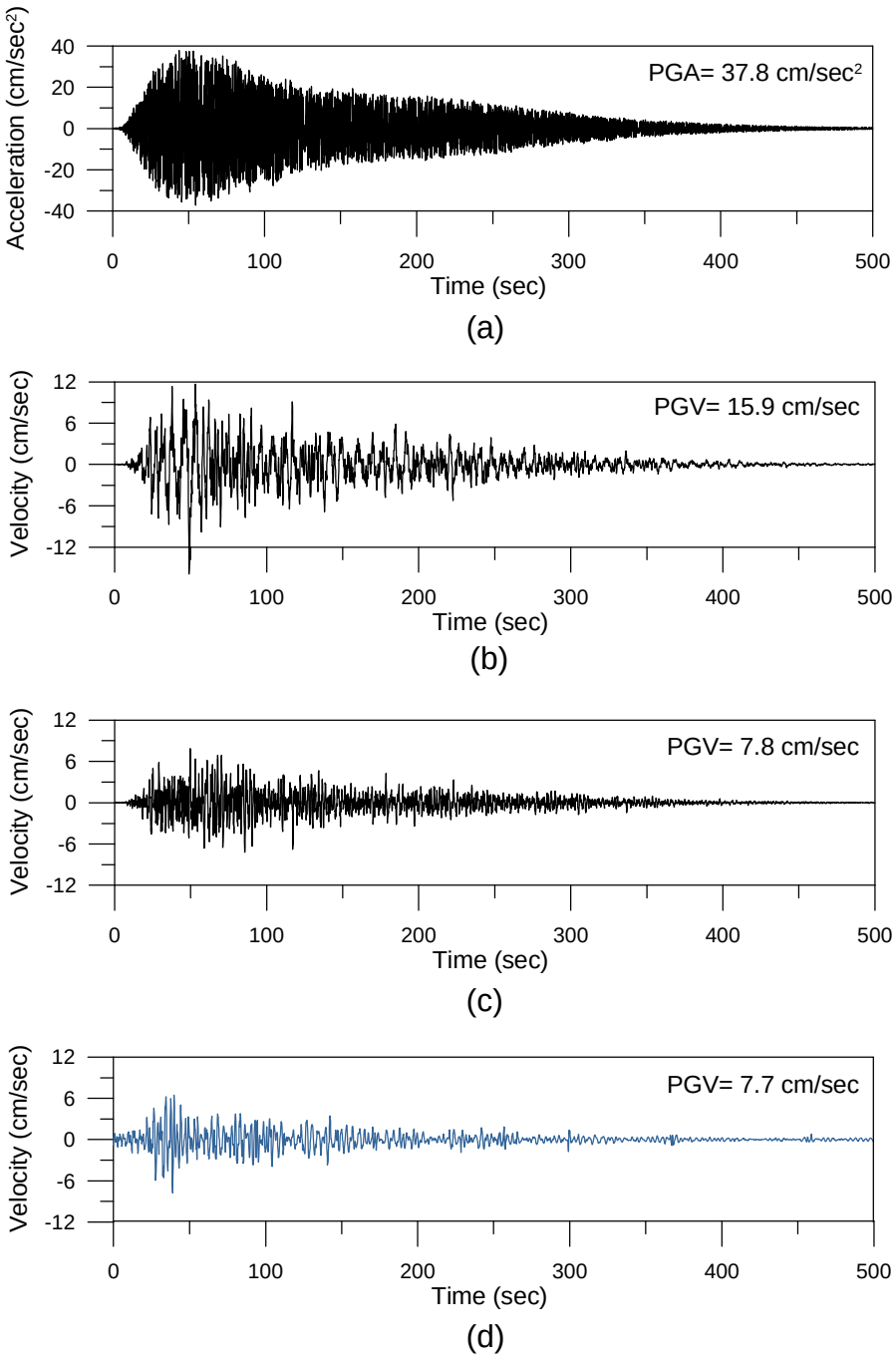

Figure 5.11 (a) Simulated acceleration record at PSI station, (b) Velocity record obtained from integration of simulated acceleration record, (c) Filtered velocity record in in a frequency range of 0.3–4.0 Hz and (d) Observed velocity record at PSI station filtered in a frequency range of 0.3–4.0 Hz

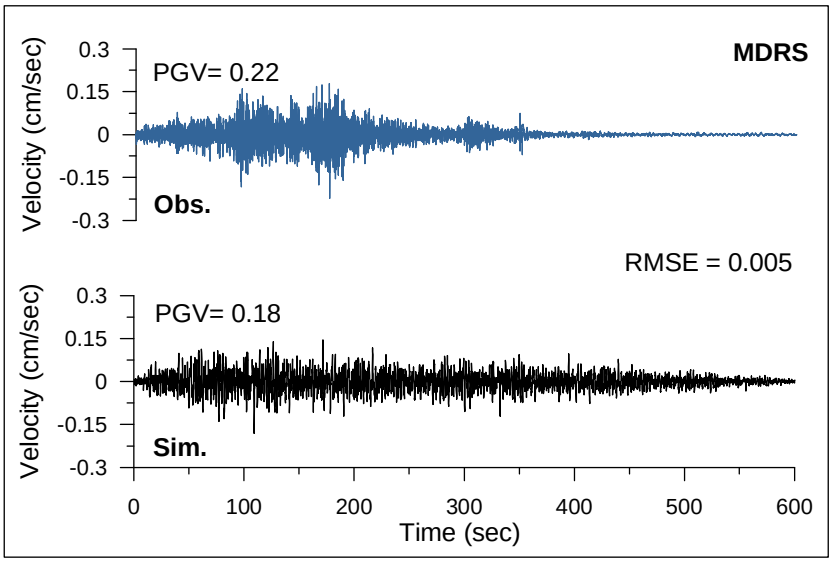

Figure 5.12 Filtered observed (in blue) and simulated (in black) velocity record at MDRS station

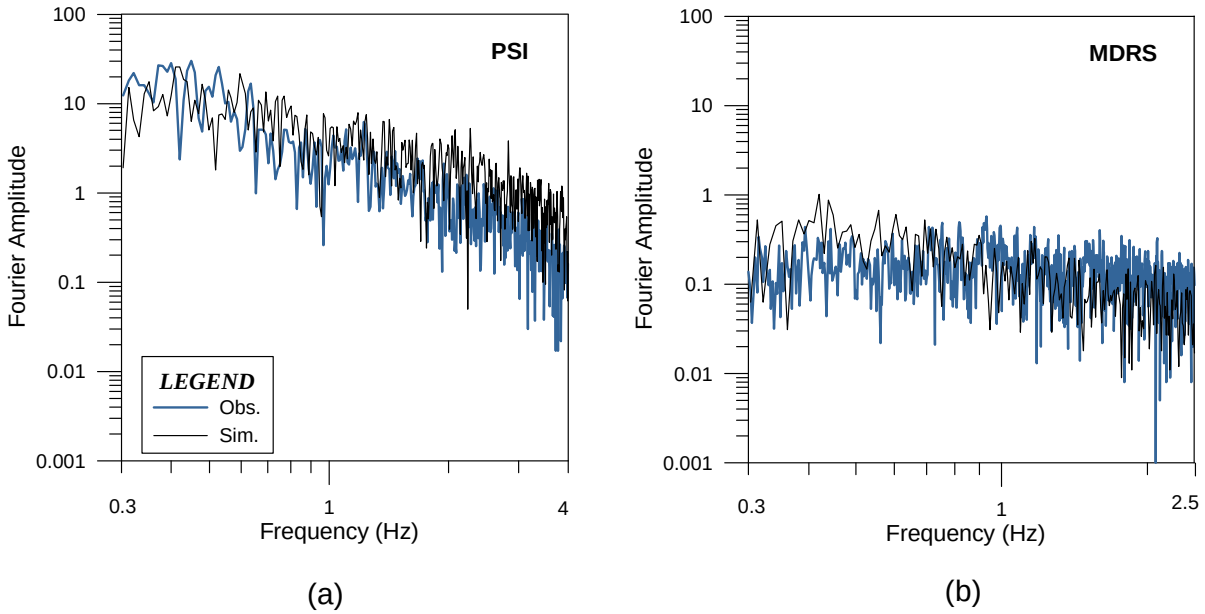

Figure 5.13 Comparison of Fourier amplitude spectrum of observed and simulated velocity record at (a) PSI and (b) MDRS stations. The observed and simulated records have been filtered in a frequency range of 0.3–4.0 Hz at PSI station, while at MDRS station it has been filtered in a frequency range of 0.3–2.5 Hz

Table 5.6 Parameters of the observed and simulated records at various stations

Station	PGV (cm/sec)		Predominant Frequency (Hz)	
	Observed	Simulated	Observed	Simulated
PSI	7.7	7.8	0.44	0.42
MDRS	0.22	0.18	0.93	0.42

The comparison of simulated records with observed records at these stations shows that the method is capable of effectively simulating ground motion. The spectral contents of simulated velocity records at these stations has been compared with the spectral contents of observed velocity record and has been shown in Figure 5.13 which clearly shows the capability of method to properly simulate frequency contents actually present in the observed records. Comparison of peak ground velocity (PGV) and predominant frequency of observed and simulated records given in Table 5.6 confirm the efficacy of modified semi-empirical approach to model a great earthquake at considerable distance.

The final rupture model responsible for the Sumatra earthquake has been used to simulate both horizontal component of ground motion. The mathematical formulation presented in Chapter 2 for component-wise simulation is further used in the modified semi-empirical technique to simulate both horizontal components of records. Records have been simulated at PSI and MDRS stations using the software MSETCS (Modified Semi-Empirical Technique for Component-wise Simulation). The comparison of the simulated and the observed record has been made in a frequency range of 0.3–4.0 Hz at PSI station that has been shown in Figure 5.14. Comparison of observed and simulated record shows that simulated record bears realistic shape as that of observed record and the PGV from observed and simulated record is also comparable. The amplitude spectrum calculated from the observed and simulated velocity record for both NS and EW component has been compared at PSI station in Figure 5.15 which shows a good comparison in the frequency range used for simulation. This confirms the suitability of the rupture model for component-wise simulation of ground motion. Horizontal components have been simulated at MDRS station in a frequency range of 0.3–2.5 Hz and have been shown in Figure 5.16. The amplitude spectrum calculated from observed and simulated velocity record for both NS and EW component has been compared at MDRS station in Figure 5.17.

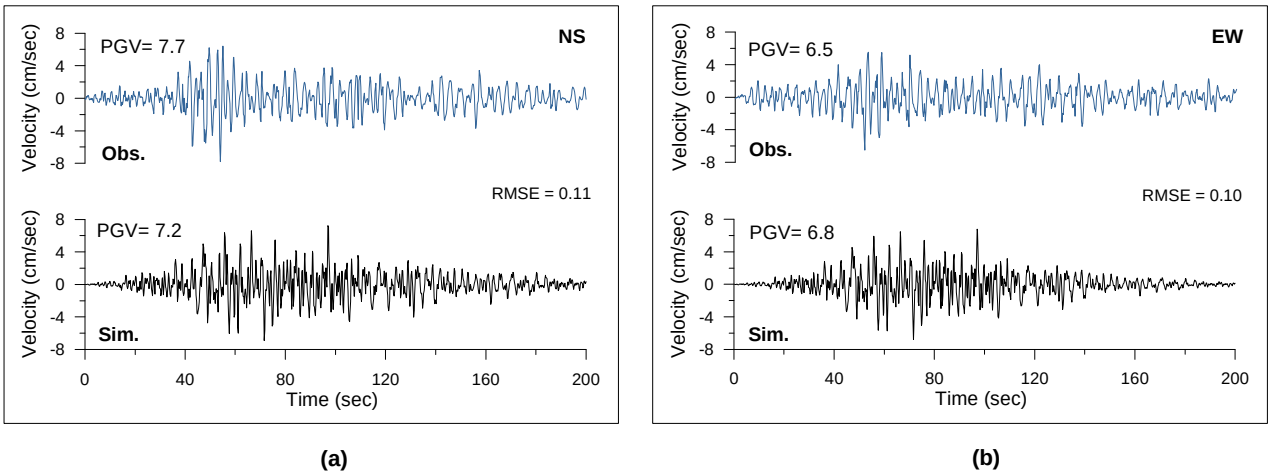

(a) (b)

Figure 5.14 Comparison of observed (in blue) and simulated (in black) velocity record calculated at (5, 3) nucleation point for (a) NS component and (b) EW component in a frequency range of 0.3–4.0 Hz at PSI station

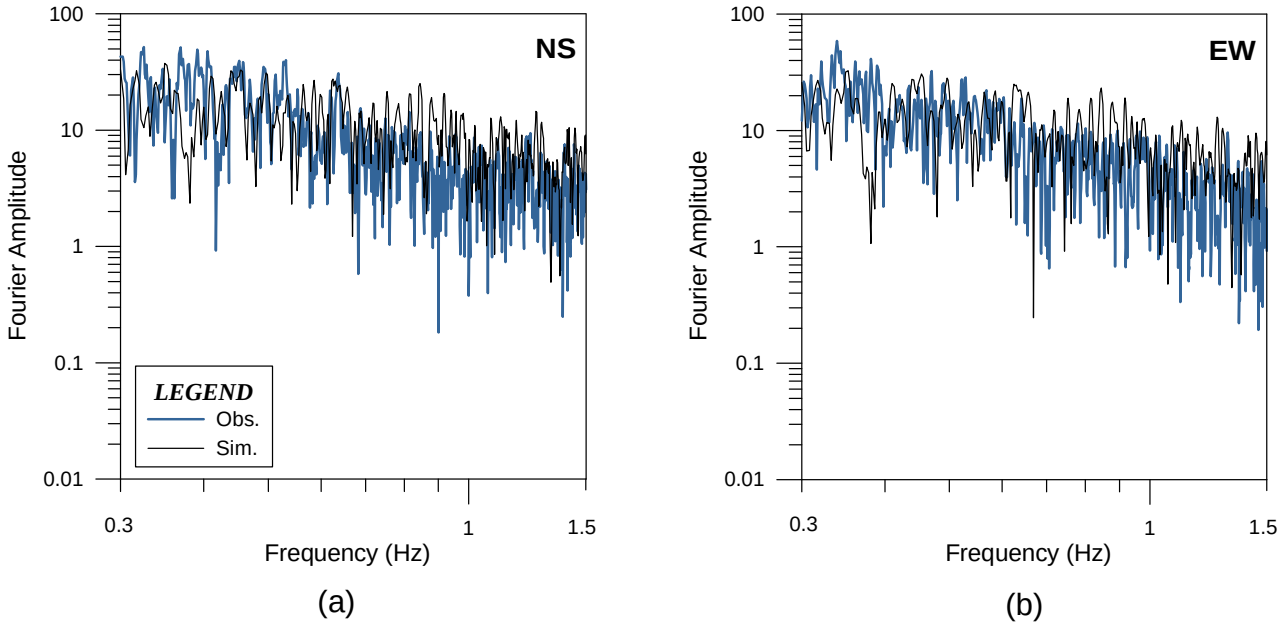

(a) (b)

Figure 5.15 Comparison of Fourier amplitude spectrum of the observed and simulated velocity record at PSI station for (a) NS component and (b) EW component

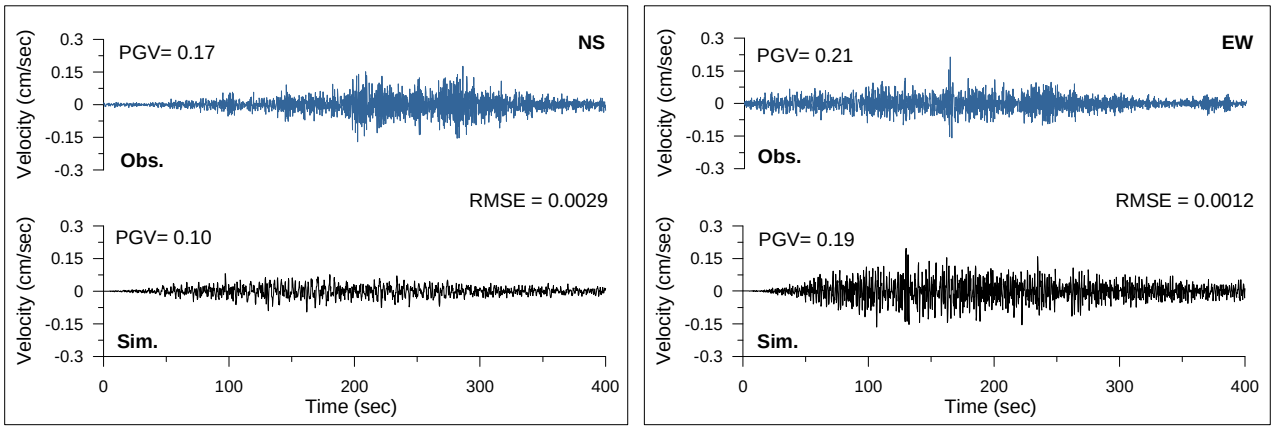

(a) (b)

Figure 5.16 Comparison of observed (in blue) and simulated (in black) velocity record calculated at (5, 3) nucleation point for (a) NS component and (b) EW component in a frequency range of 0.3–2.5 Hz at MDRS station

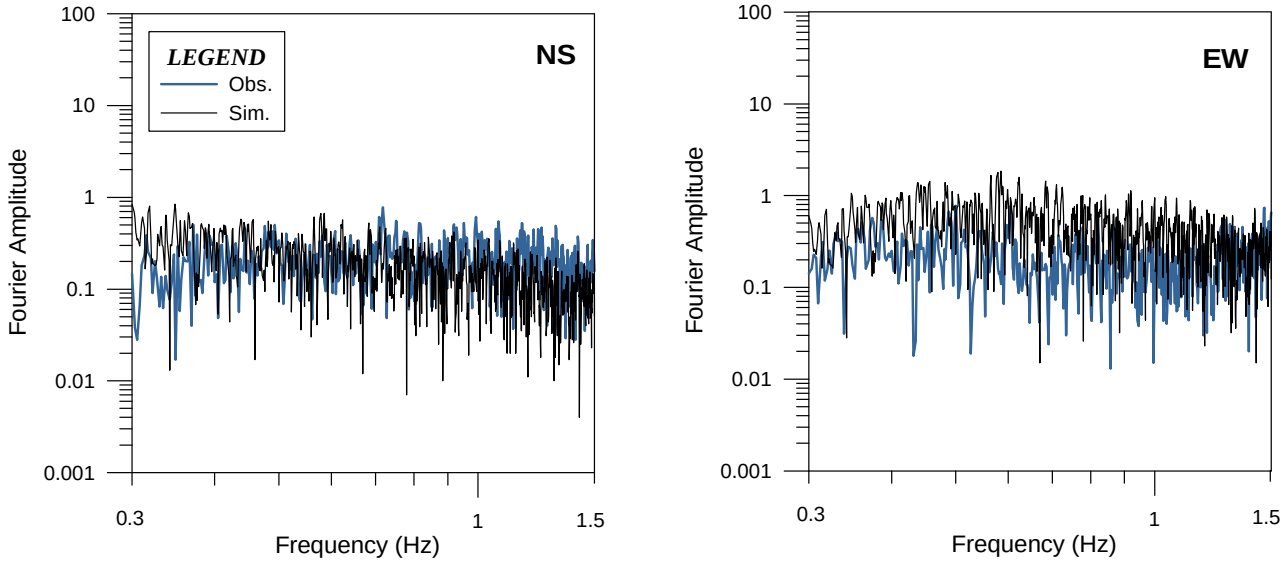

(a) (b)

Figure 5.17 Comparison of Fourier amplitude spectrum of the observed and simulated velocity record at MDRS station for (a) NS component and (b) EW component

5.3.2 Empirical Green's Function Technique

The major requirement of EGF technique is the availability of aftershock data of the target earthquake in the source region. The aftershock of the Sumatra earthquake recorded on December 26, 2004 has the fault plane solution which is similar to that of the Sumatra earthquake. This aftershock has been used as empirical Green's function in EGF technique of simulation. Parameters of this aftershock are given in Table 5.2. Self-similarity laws are used to divide the rupture plane of the Sumatra earthquake using parameters of this aftershock. The rupture plane of the target earthquake has been divided into 36 sub-faults by using self-similarity laws given by Kanamori and Anderson (1975). In the simulation process, the geometry and location of the rupture responsible for the Sumatra earthquake is kept similar to that used by Sorensen et al. (2007) and given in Table 5.7. The rupture plane has been placed in a velocity structure (Table 5.4) given by Sorensen et al. (2007) which is same as used in modified semi-empirical approach. Rupture for this earthquake has been modeled by different workers using rupture velocity that varies from 1.5 (de Groot-Hedlin 2005) to 3.0 km/sec (Yagi 2005, Ammon et al. 2005). The dip of rupture plane for this earthquake is given as 8° by Global CMT and is also estimated as large as 13° by USGS. The dip of final rupture model obtained by iterative modeling is 8.5° using EGF technique. Therefore, in order to finalize various rupture parameters like location of nucleation point, dip of rupture plane and medium velocity, the iterative forward modeling has been performed for various possibilities of these parameters. Final values of parameters have been decided on the basis of minimization of RMSE between the observed and simulated waveforms.

Table 5.7 Initial parameters of the responsible rupture plane for the Sumatra earthquake used for simulation using the EGF technique

Modeling Parameter	Source
Length = 750 km	Lay et al. (2005)
Width = 150 km	Yagi (2005)
Dip = 8°	Global CMT
$N_L = 6$, $N_W = 6$	Based on scaling relation by Kanamori and Anderson (1975)
$V_r = 3.0$ km/sec	
$\beta = 2.5$ km/sec	Yagi (2005)
$Q_\beta(f) = 100f^{0.8}$	Sorensen et al. (2007)

Software named Empirical Green's Function Technique (EGFT) in FORTRAN language has been developed for simulation of records using EGF technique, which is capable of simulating large-duration waveform caused by great earthquake. This program require coordinates of recording station in a Cartesian system in which the X- and the Y-axes are parallel to strike and dip direction of the rupture plane, respectively. The Z-axis is positive in vertically downward direction. The Cartesian system used in simulation of ground motion is same as adopted in case of modified semi-empirical method. Coordinates of stations used for simulation are given in Table 5.5 and shown in Figure 5.7. The EW component of velocity record has been simulated at PSI station for several possibilities of rupture parameters. The simulated velocity record has been generated for the same band-pass filtering range that is used for the processing of observed record at PSI station. Root mean square error between observed and simulated velocity record has been calculated for each possibility of rupture parameters.

The starting point of rupture or nucleation point is the element, which is first to emit the energy. It has been observed that the shape of record is strongly influenced by the geometry of rupture propagation, which in turn depends on starting point of rupture within the rupture plane. Rupture plane has been divided into 36 sub-faults on the bases of self-similarity laws. Each of sub-faults can be the nucleation point. All 36 possibilities of starting point of rupture within the rupture plane have been considered and the EW components of records have been simulated at PSI station. Simulated records for various possibilities of nucleation point with the observed record have been shown in Figure 5.18. It has been observed from Figure 5.18 that the shape of simulated record varies drastically for different locations of nucleation point. Comparison of waveform has been made in terms of RMSE. Minimum RMSE (in Figure 5.18b) has been obtained at (2, 3) nucleation point, which coincide with the zone of high-slip asperity as defined by Sorensen et al. (2007). Once the nucleation point is fixed various possibilities of rupture velocities have been checked. Several rupture model with different rupture velocities have been considered for this purpose. Rupture velocities in these model varies from 1.5 to 3.7 km/sec. Records have been simulated at PSI station using these models. Dependency of simulated record on the rupture velocity has been shown in Figure 5.19 where minimum RMSE has been obtained for rupture velocity of 3.0 km/sec. The obtained final rupture velocity is close to that modeled by Sorensen et al. (2007). The velocity of medium which control the arrival times of shear wave energy also changes the shape of record. Using the velocity model given by Sorensen et al. (2007), velocity in each layer has been changed

±5% of its initial value and simulated records have been compared with observed ones in terms of RMSE that has been shown in Figure 5.20. It has been observed that velocity model given in Table 5.8 gives minimum RMSE at PSI station. The dip of the rupture plane has been iteratively changed from 6.5° to 13° and records have been simulated for different cases assuming finalized rupture plane and rupture velocity. It has been observed that the shape of simulated record is not heavily dependent on the dip of the rupture plane; however, parameters like PGV in the simulated record are strongly influenced on choice of dip as observed in Figure 5.21.

The comparison of simulated record with observed record for various possibilities of dip in terms of RMSE shows that the 8.5° dip of rupture plane gives minimum RMSE between observed and simulated waveform (Figure 5.21b). The iterative modeling considering various possibilities of rupture parameters give final rupture parameters corresponding to minimum RMSE between the observed and simulated waveforms. The final modeling parameters have been given in Table 5.8 and the corresponding model has been shown in Figure 5.22.

Table 5.8 Final modeling parameters of rupture plane responsible for the Sumatra earthquake

Modeling Parameters
Length = 750 km
Width = 150 km
Dip = 8.5°
N_L = 6
N_W = 6
V_r = 3.0 km/sec
Nucleation point = (2, 3)

S-wave velocity of medium	
Depth (km)	**Velocity (km/sec)**
9.4	2.25
11	3.41
17	5.50

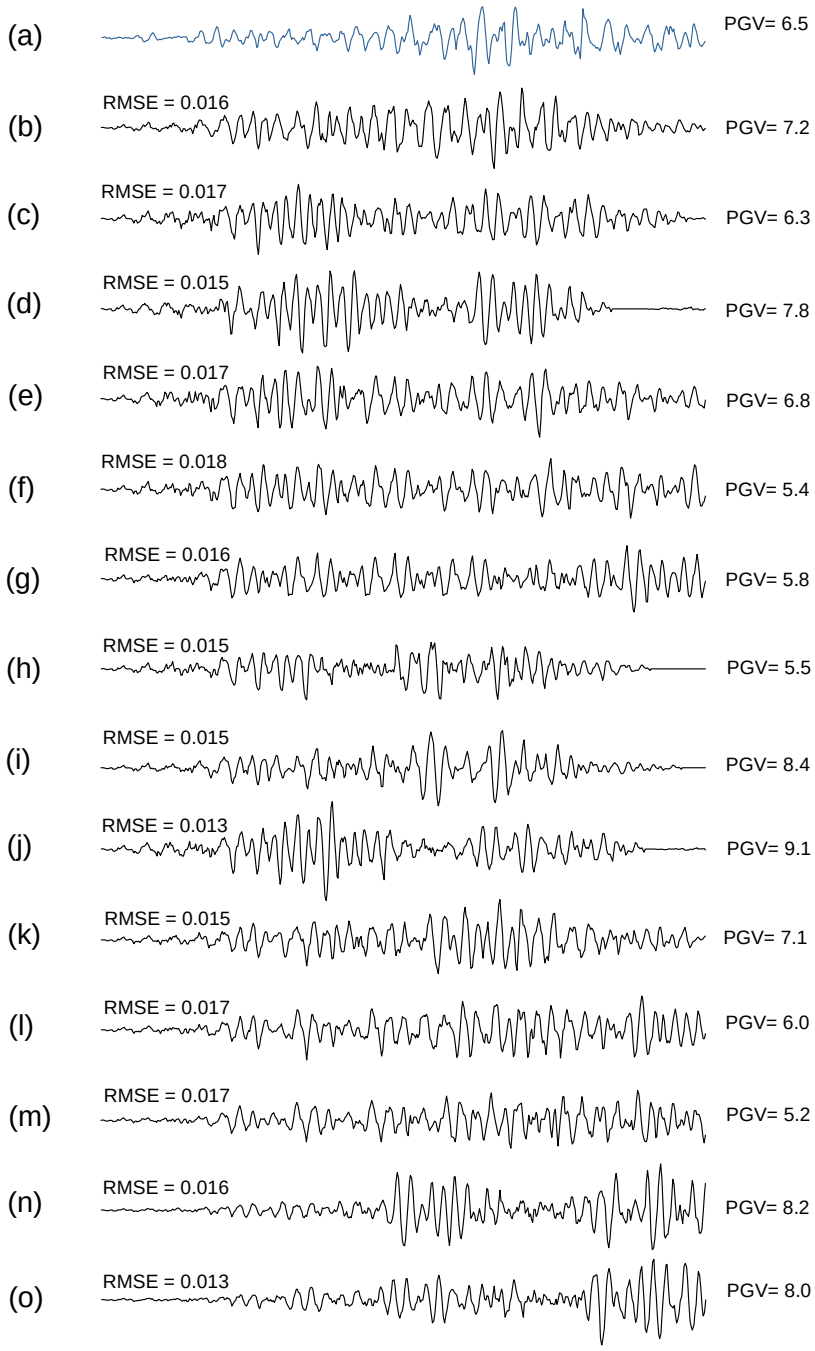

Figure 5.18 Comparison of filtered (a) observed and (b) to (o) simulated EW component of velocity record at PSI station for different locations of nucleation point. The simulations have made for rupture dipping at an angle 8.5° in final velocity model with rupture velocity of 3.0 km/sec. The simulated record corresponding to minimum RMSE has shown in (b)

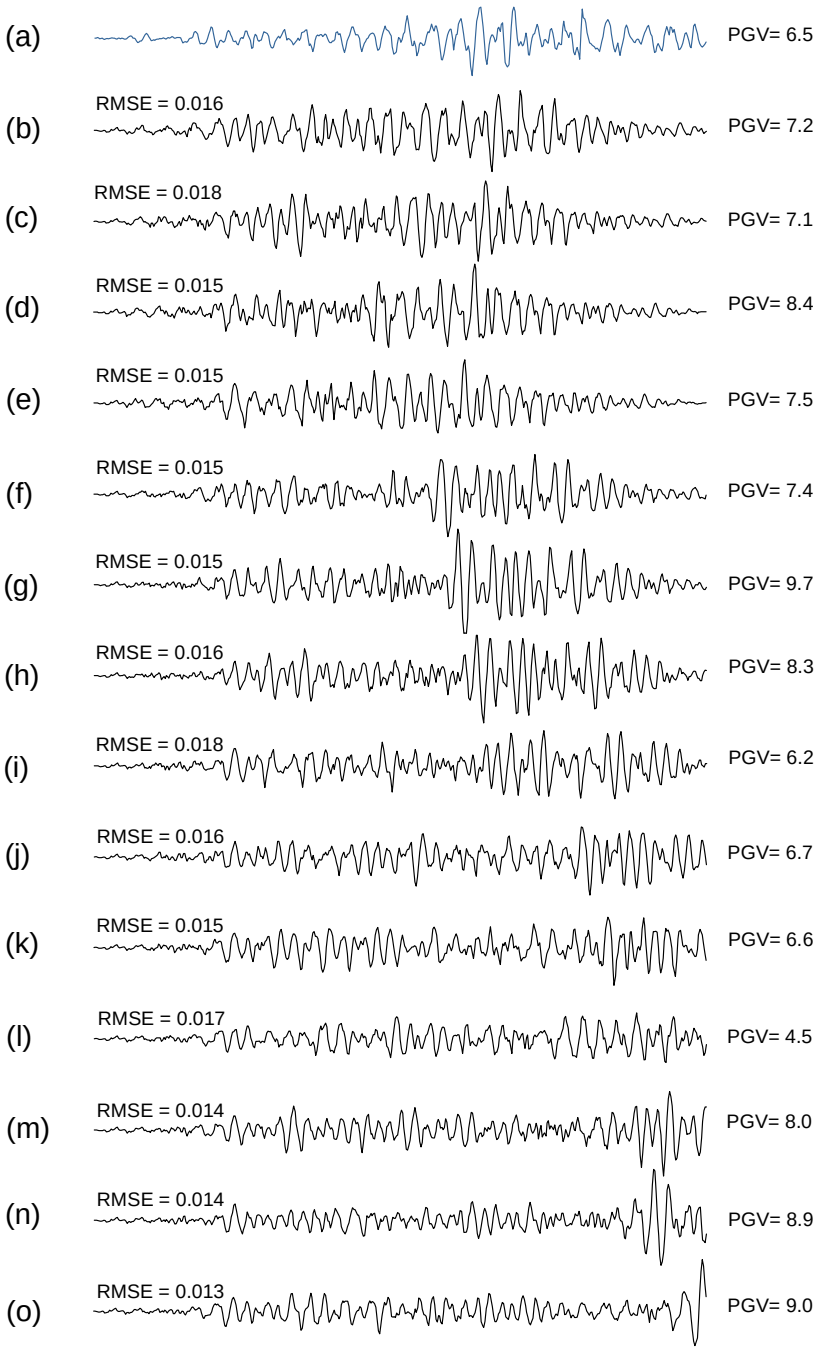

Figure 5.19 Comparison of filtered (a) observed and (b) to (o) simulated EW component of velocity record at PSI station for different rupture velocity. The dip of rupture plane has assumed as 8.5° in a velocity model selected as final model and nucleation point at (2, 3). The simulated record corresponding to minimum RMSE has shown in (b)

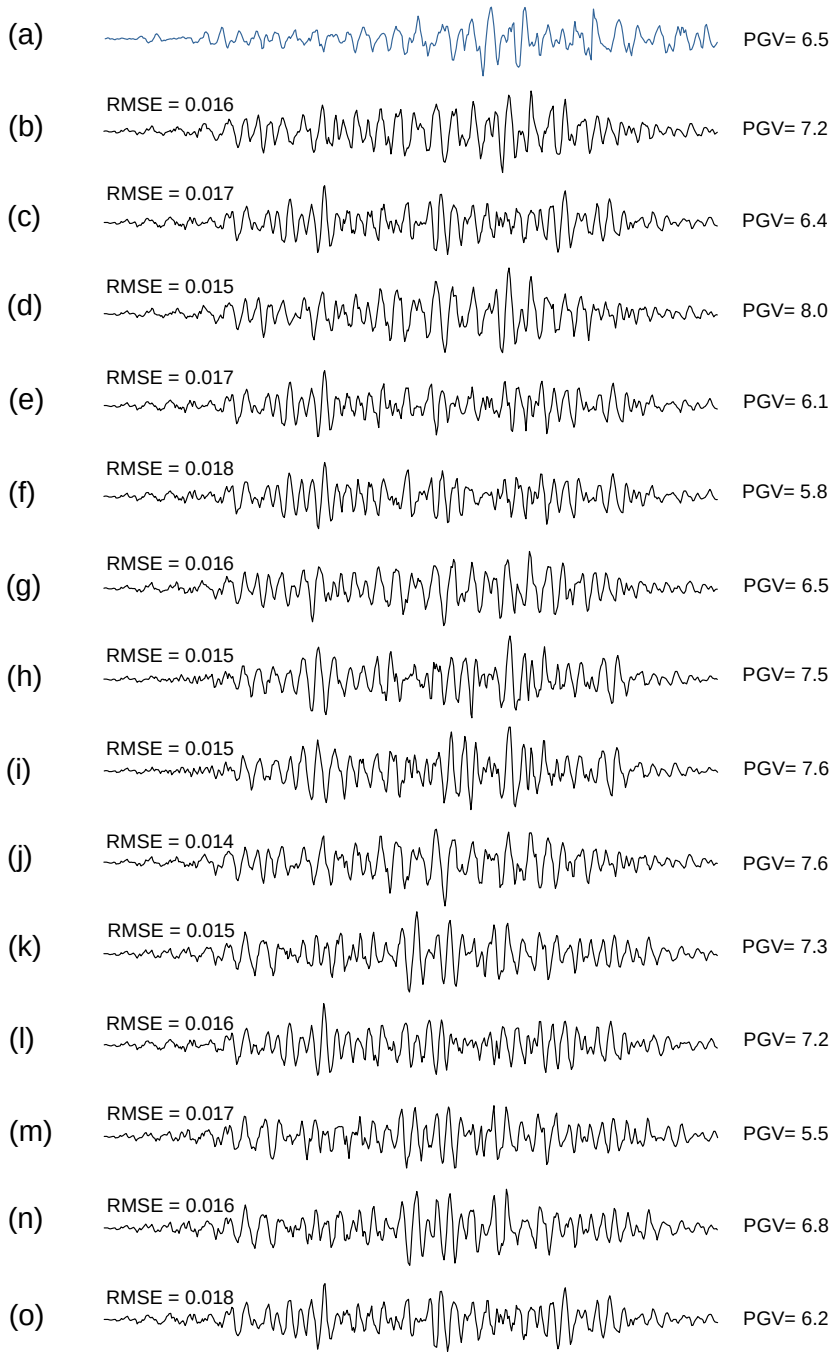

Figure 5.20 Comparison of filtered (a) observed and (b) to (o) simulated EW component of velocity record at PSI station for different velocity structure. The dip of rupture plane has assumed as 8.5°, rupture velocity as 3.0 km/sec and nucleation point at (2, 3) grid point. The simulated record corresponding to minimum RMSE has shown in (b)

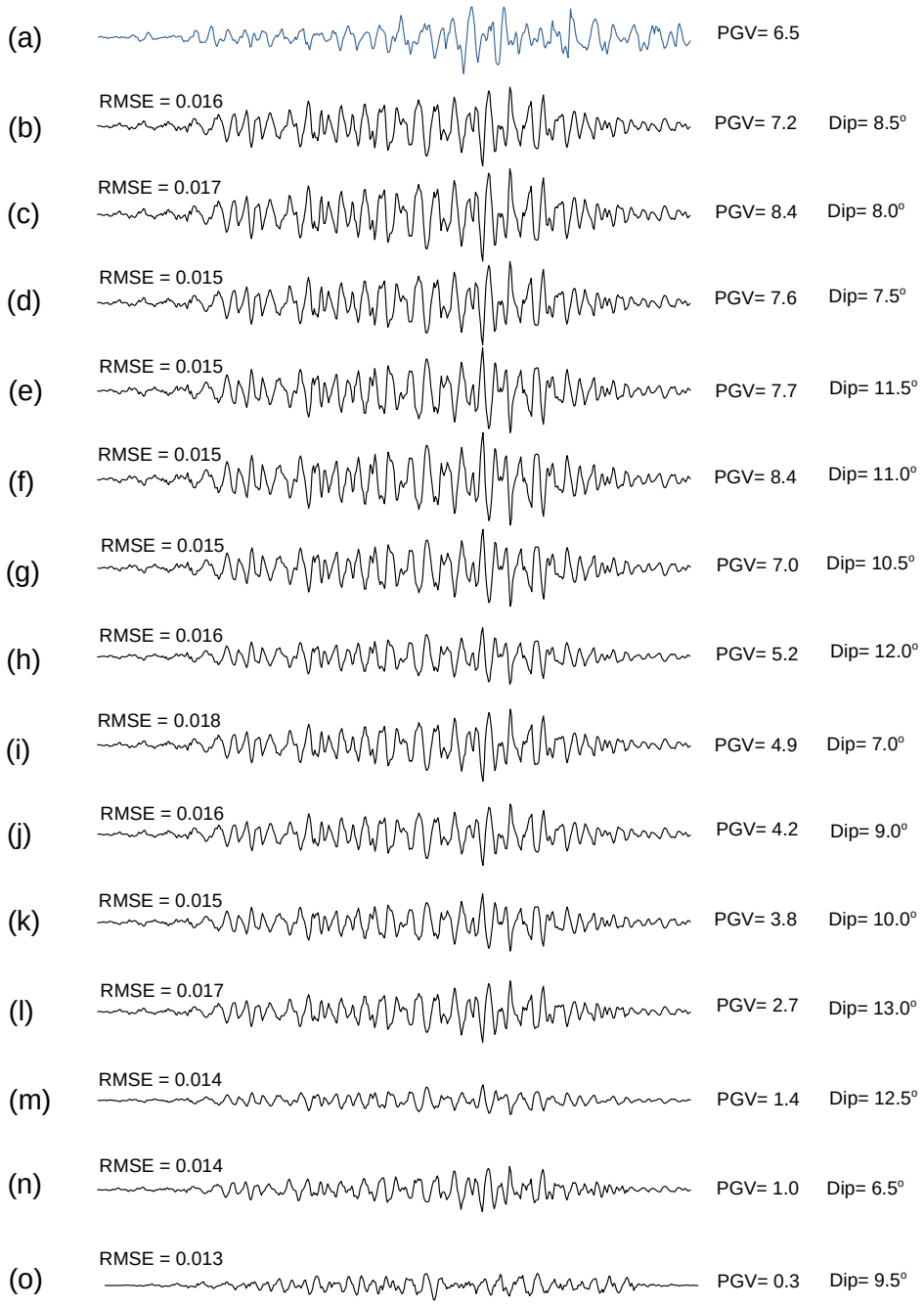

Figure 5.21 Comparison of filtered (a) observed and (b) to (o) simulated EW component of velocity record at PSI station for different dip of rupture plane. The rupture velocity has assumed as 3.0 km/sec, velocity model selected as final model, nucleation point at (2, 3). The simulated record corresponding to minimum RMSE has shown in (b)

The NS component of velocity record has been simulated at PSI station using the final rupture model shown in Figure 5.22. The comparison between the observed and simulated velocity records at PSI station for NS and EW component has been shown in Figure 5.23. Comparison shows that simulated record bears realistic shape as that of observed record, and the PGV parameter from the observed and simulated record is also comparable. The Fourier spectrum of filtered observed and simulated NS and EW component of velocity record has been shown in Figure 5.24 and it shows a good comparison in a range of frequency used for simulation. This confirms the suitability of the model and its selected parameters. Using same model as given in Figure 5.22, records have been simulated at MDRS station, which is at an epicentral distance of 2060 km. Since velocity model for MDRS station will be different than that used for PSI station; again iterative search for final velocity model at MDRS station have been performed. For this selection, records have been simulated at MDRS station and compared with the horizontal component of velocity record in terms of RMSE.

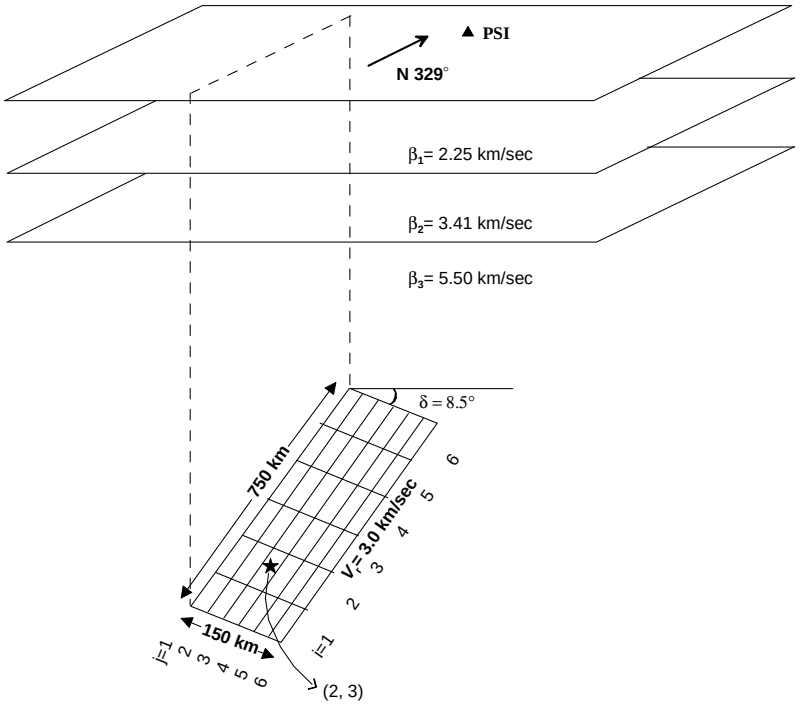

Figure 5.22 Final rupture model of the Sumatra earthquake consisting of 6×6 sub-faults in a layered medium with 329°N strike direction. Star on the rupture plane indicates the position of nucleation point of the target earthquake

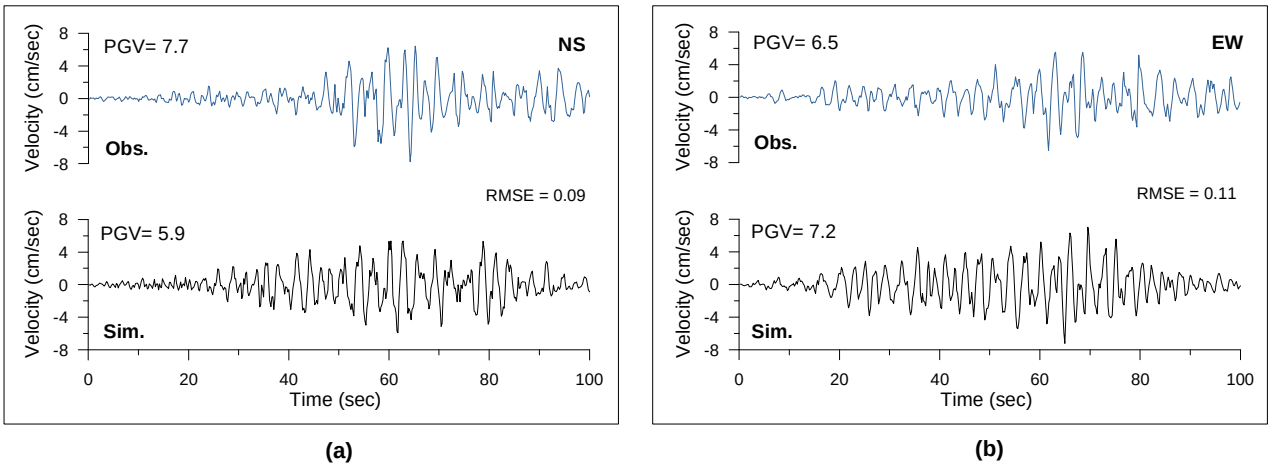

(a) (b)

Figure 5.23 Comparison of observed (in blue) and simulated (in black) velocity record for (a) NS component and (b) EW component in a frequency range of 0.3–2.0 Hz at PSI station due to shear wave propagation

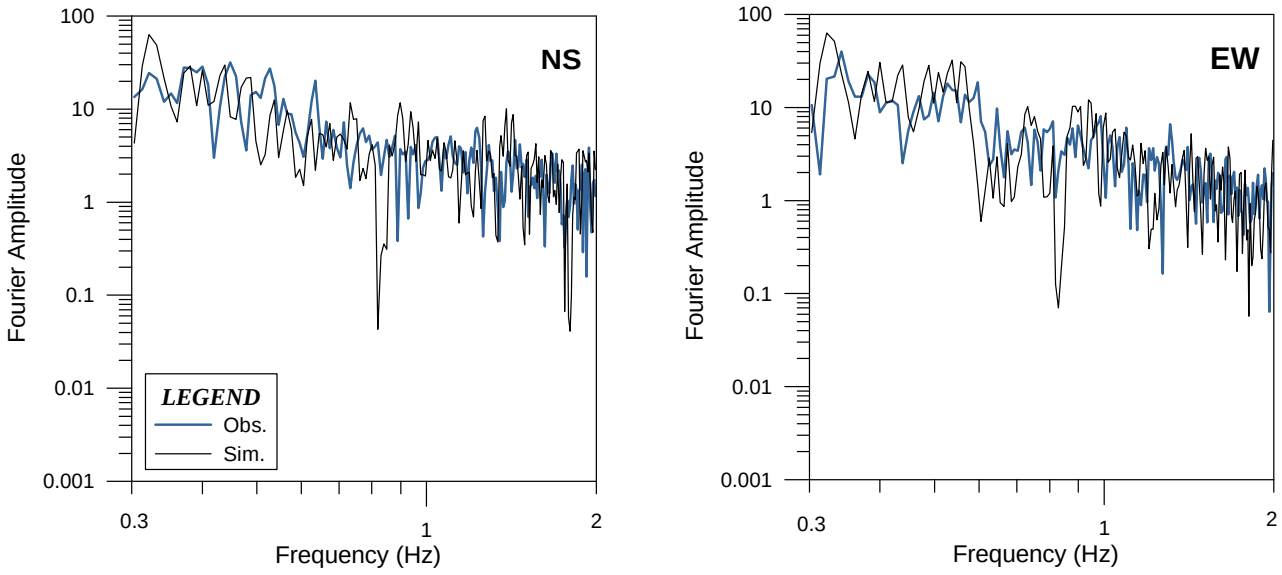

(a) (b)

Figure 5.24 Comparison of Fourier amplitude spectrum of the observed and simulated velocity record at PSI station for (a) NS component and (b) EW component

Table 5.9 Final velocity model used for simulation of record at MDRS station

Depth (km)	S-wave Velocity (km/sec)
9.4	1.75
11	3.38
17	4.75

The final velocity model for MDRS station, which gives minimum RMSE has been given in Table 5.9. Using this final velocity model and finalized rupture parameters given in Table 5.8, horizontal components of velocity record have been simulated. The comparison of filtered observed and simulated waveform due to S-wave has been shown in Figure 5.25 at MDRS station. A comparison of Fourier spectrum of the velocity records at this station has been shown in Figure 5.26. The comparison of ground motion parameters estimated from the observed and simulated horizontal velocity record of the Sumatra earthquake recorded at PSI and MDRS station has been given in Table 5.10.

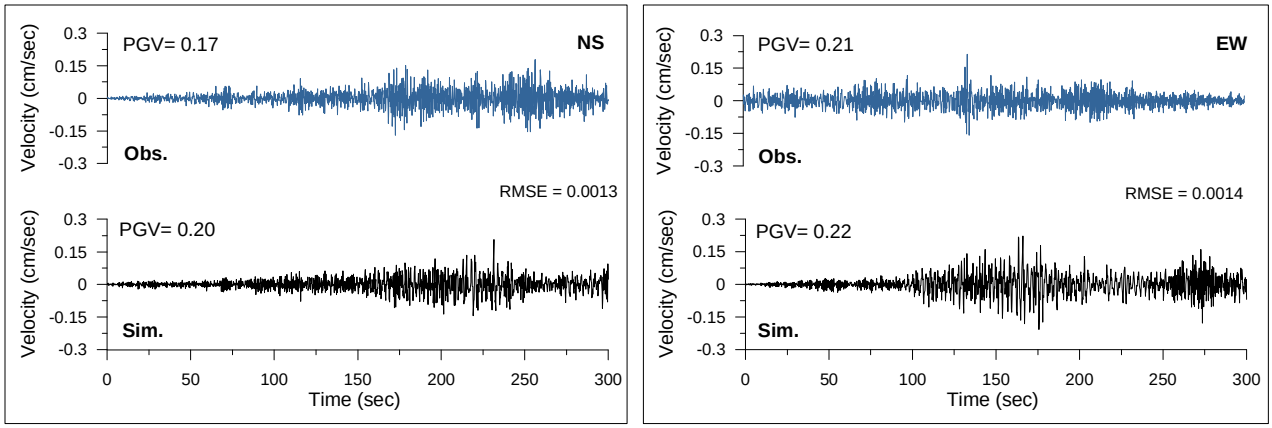

Figure 5.25 Comparison of observed (in blue) and simulated (in black) velocity record for (a) NS component and (b) EW component in a frequency range of 0.3–2.0 Hz at MDRS station due to shear wave propagation

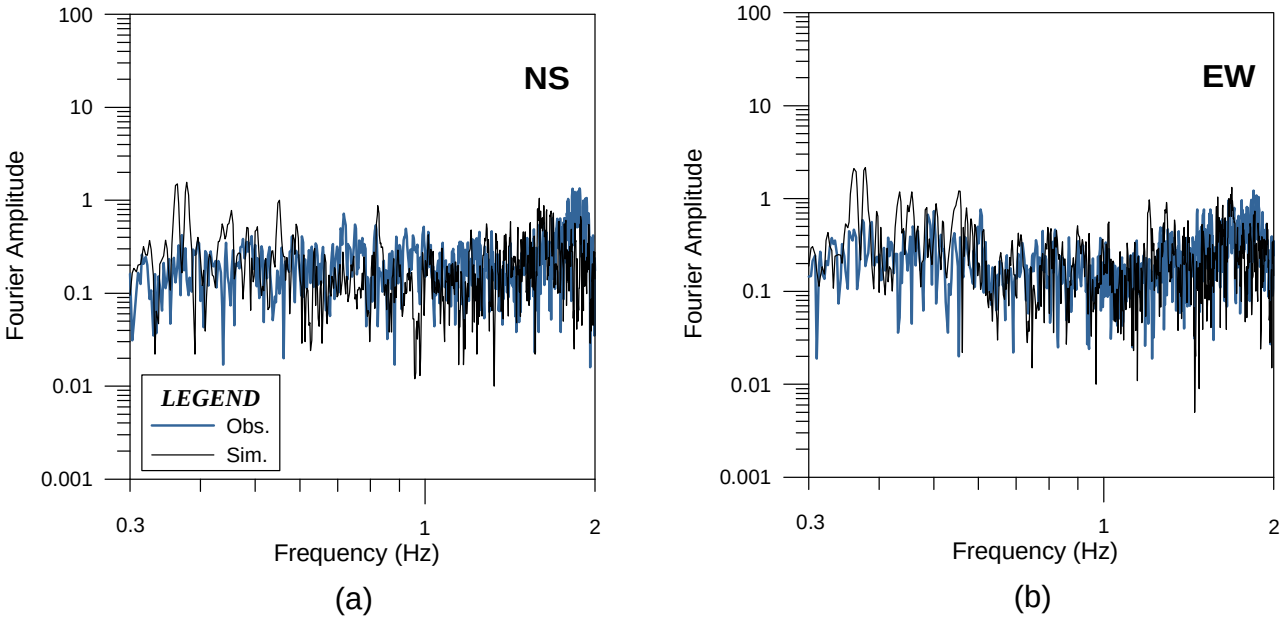

Figure 5.26 Comparison of Fourier amplitude spectrum of the observed and simulated velocity record at MDRS station for (a) NS component and (b) EW component

Table 5.10 Estimated parameters from observed and simulated records of the Sumatra earthquake recorded at PSI and MDRS station

Station	PGV (cm/sec)				Predominant Period (Hz)			
	Observed		Simulated		Observed		Simulated	
	NS	EW	NS	EW	NS	EW	NS	EW
PSI	7.7	6.5	5.9	7.2	2.72	1.76	3.02	3.02
MDRS	0.17	0.21	0.20	0.22	0.52	0.56	2.68	2.68

The comparison of simulated record with observed records shows that the parameters of the Sumatra earthquake are effective in modeling the rupture source of this earthquake. The study also confirms the suitability of the final rupture model obtained from modified semi-empirical approach. It has been observed that the final rupture models obtained by using two different techniques are nearly same.

5.4 Simulation of Strong Ground Motion due to the Sumatra Earthquake at different Hypothetical Stations

Simulations obtained from the modified semi-empirical and empirical Green's function technique for the Sumatra earthquake confirm the efficacy of these techniques for simulating ground motions for real earthquake scenario. One of the advantage of the modified semi-empirical technique is that it can be used to simulate record at any location. The modified semi-empirical technique does not require aftershock record at the point of simulation as in the case of EGF technique. This has motivated to simulate distribution of PGA from resultant record due to the final rupture model of the Sumatra earthquake.

A total of 1570 stations surrounding the rupture model of the Sumatra earthquake have been considered for simulation using modified semi-empirical technique. Among these stations 1125 stations have been located within the surface projection of rupture and are closely spaced at 10 km spacing while other 234 and 211 stations away from the source have been spaced at 30 and 50 km, respectively. Distribution of stations has been shown in Figure 5.27a. The parameters of rupture model are kept same as that shown in Figure 5.10. Strong motion records at all 1570 stations have been simulated and the PGA value from the simulated record has been used for the preparation of isoacceleration contours.

The distribution of isoacceleration contour obtained from several strong motion records has been shown in Figure 5.27b. The isoacceleration contours shows that high peak acceleration zones of value more than 2g have observed in the source zone of this earthquake which gradually decreases with distance. Strong motion record has also been simulated at a hypothetical station of coordinate 5.5°N and 95.3°E which lies at an epicenteral distance of 291 km from the epicenter of the Sumatra earthquake and the simulated record has been shown in Figure 5.28. It has been observed that the simulated record is highly energetic with PGA of 526 gal at this hypothetical station. Peak displacement of the order of 1.28 m has been obtained at this station from the displacement record. The response spectra obtained from this simulated record in Figure 5.28d show that high ground acceleration has been observed for 0.4 sec period.

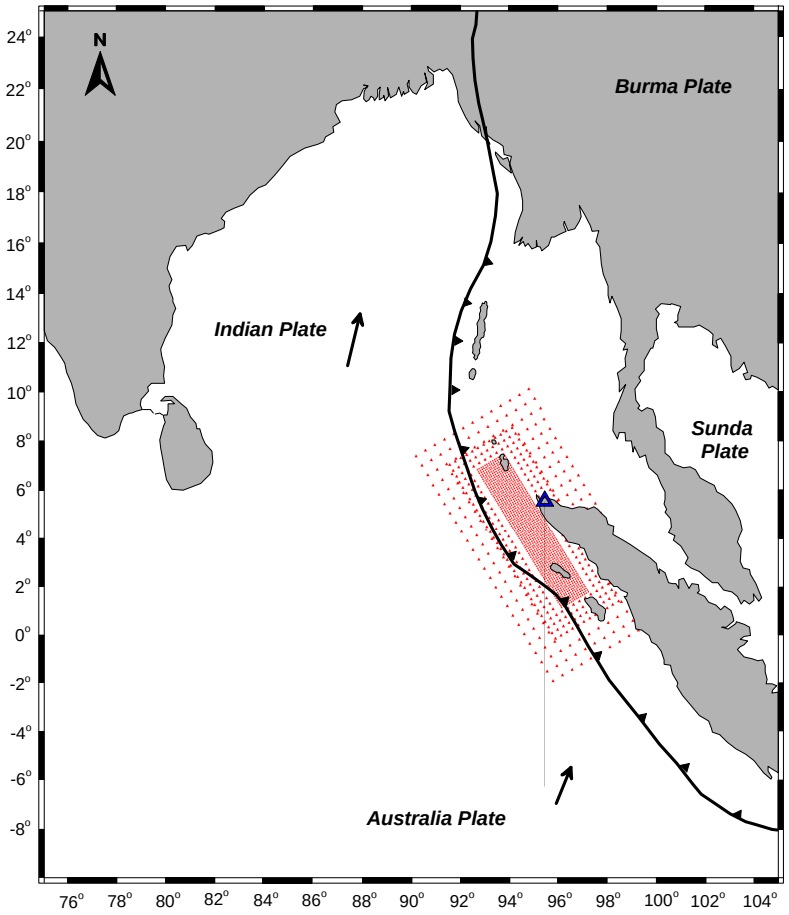

(a)

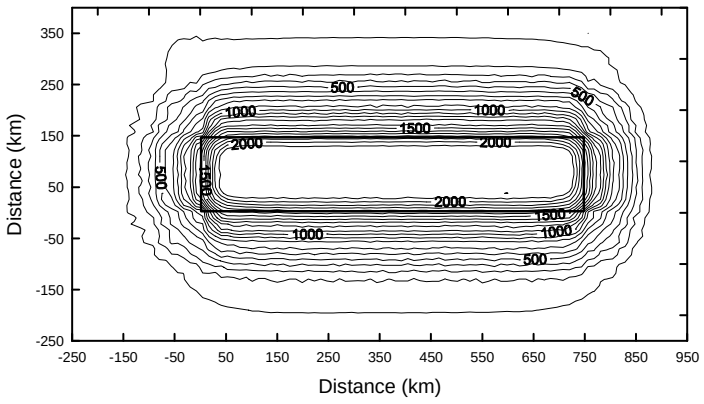

(b)

Figure 5.27 (a) Distribution of hypothetical stations surrounding the source of the Sumatra earthquake used for simulation of strong ground motion. The station locations have shown by red triangle together with a hypothetical station by hollow triangle. (b) Contours of PGA calculated from simulated records at stations surrounding the source of the Sumatra earthquake. The rectangle with solid line shows the rupture model of the Sumatra earthquake as shown in (a)

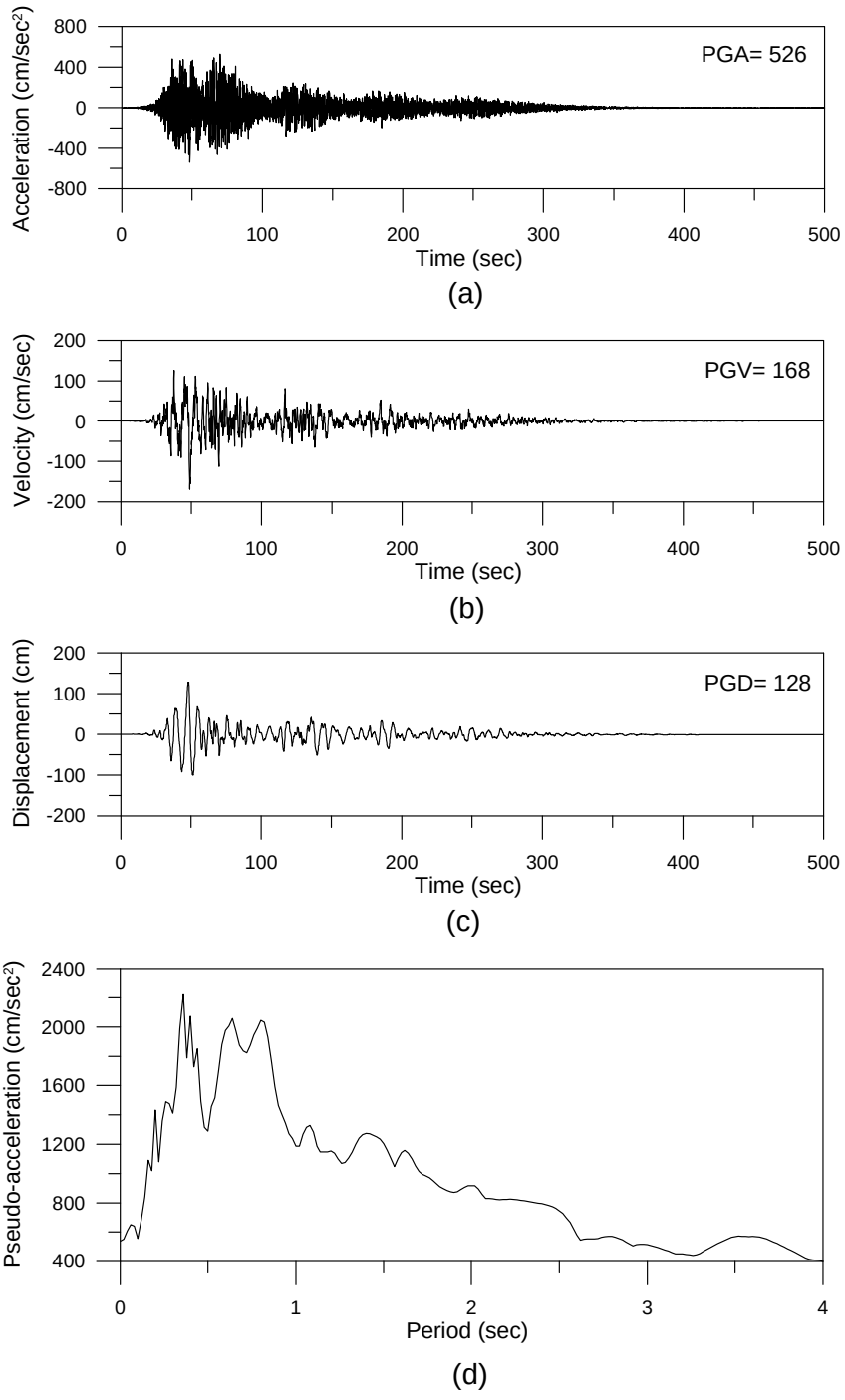

Figure 5.28 Simulated (a) Acceleration record, (b) Velocity record, (c) Displacement record and (d) Pseudo-acceleration response spectra with 5% damping determined at one of the assumed near-field station (shown in Figure 5.27a) from the final rupture model of the Sumatra earthquake

5.5 Simulation for Hypothetical Earthquake in the Andaman Region

The Andaman Islands lie in the Zone V of Seismic Zoning Map of India which is seismically highly hazardous zone (IS 1893: 2002). The entire island is also susceptible to tsunamis both from large local earthquakes and also from massive distant earthquakes. The Andaman and Nicobar Islands are located near the boundary of the Indian plate and the Burmese microplate. The Andaman arc marks this boundary and lies in the Bay of Bengal to the west of the archipelago. Another prominent feature is the north–south West Andaman fault (WAF), which is strike-slip in nature and lies in the Andaman Sea to the east of this island chain. The Indian plate is diving beneath the Burmese microplate along the Andaman arc in a process known as subduction. Bhatia et al. (1999) have suggested that the Indo-Burma border region in the north-east is the severe hazard zone. The Indian plate boundary is characterized by a complex to an oblique subduction along the Burma-Andaman arc in the east (Bhatia et al. 1999). The Sumatran fault system in the southeast, the WAF and the Sagaing fault further east, are the features supporting major lateral movements in the region (Bhatia et al. 1999). Curray (2005), Fitch (1972) and Curray et al. (1979) have suggested that the Burma-Andaman arc marks the eastern margin of the Indian plate, along which an oblique convergence between the Indian and the Burmese plate taken places.

The earthquake database in India is still incomplete, especially with regards to earthquakes prior to the historical period (before 1800 AD), Andaman Nicobar zone offer a rough guide of the earthquake hazard in any particular region (Bilham et al. 2005). Large thrust earthquakes in 1847 ($M_w > 7.5$), 1881 ($M_w = 7.9$) and 1941 ($M_w = 7.7$) appear to have occurred on intermediate regions of the down-dip boundary areas that have been surrounded and probably incorporated into the December 26, 2004 rupture (Bilham et al. 2005). Bilham et al. (2005) has estimated a shorter recurrence interval of 400 years for the epicentral region where convergence rates are higher. The rupture areas of these early earthquakes represent less than one-third of the down-dip width of the Sumatra earthquake (Bilham et al. 2005). The Andaman and Nicobar Island falls in source zone 81 and 83 marked by Bhatia et al. (1999), which has potential to generate earthquake of maximum magnitude 8.5 and 7.5, respectively (Bhatia et al. 1999). These source zones are shown in Figure 5.29 with the rupture areas of early earthquakes. In this section, a hypothetical earthquake of magnitude 8.5 has been modeled and the causative rupture for this earthquake is placed in the source zone 81 marked by Bhatia et al. (1999). Bilham et al. (2005) has also placed the rupture of 1941 ($M_w = 7.7$) earthquake in the same source zone. Position of modeled rupture plane of

hypothetical earthquake has been shown in Figure 5.30. This rupture plane has been modeled to simulate strong motion records using both the empirical Green's function technique and modified semi-empirical technique for component-wise simulation.

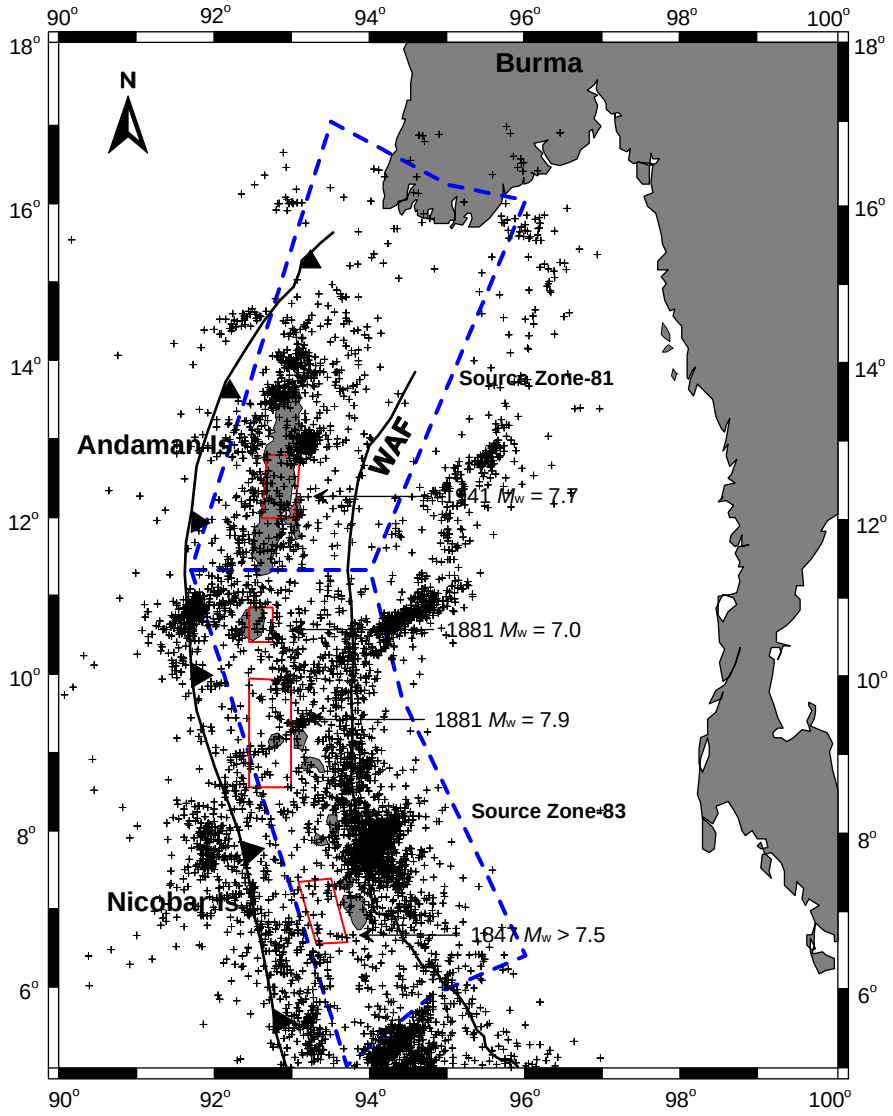

Figure 5.29 Probable, source zone 81 with maximum magnitude 8.5 and source zone 83 with maximum magnitude 7.5 (Bhatia et al. 1999) located with blue dashed lines by GSHAP (Global Seismic Hazard Assessment Program) and few historical rupture position with their magnitude in Andaman and Nicobar region (Bilham et al. 2005) are located with red rectangles. Seismicity in Andaman and Nicobar region from 1973 to 2010 has been plotted by scatters using USGS database

It has been observed that the region itself has experienced earthquakes of both the reverse and the oblique strike-slip fault mechanism (Ortiz and Bilham 2003; Chatherine et al. 2009). Synthetic acceleration record has been simulated due to both types of rupture mechanism. The rupture length and its downward extension for 8.5 (M_w) magnitude earthquake are calculated as 324 and 75 km, respectively using the empirical relation given by Wells and Coppersmith (1994) for the thrust mechanism. The rupture length and its downward extension for 8.5 (M_w) magnitude earthquake are calculated as 501 and 34 km, respectively using the empirical relation given by Wells and Coppersmith (1994) for strike-slip mechanism. The fault plane solution for thrust mechanism is used as that defined for the Sumatra earthquake and is given in Table 5.1. However, the fault plane solution for the strike-slip mechanism is kept similar to the fault plane solution of the earthquake defined in Table 5.11. The velocity structure for the Andaman region has been used as that given by Parvez et al. (2003). The rupture velocity has been kept as 3.0 km/sec which is similar to that obtained from final rupture parameters of the Sumatra earthquake. Based on depth of subduction zone in this region, the rupture plane for this hypothetical earthquake has been placed at a depth of 15 km. Acceleration records for EW and NS components of ground acceleration for both the thrust and the strike-slip mechanism have been simulated at POR station which lies at an epicentral distance of 109 km in the Andaman region.

The rectangular hypothetical rupture plane has been placed in the Cartesian coordinate system that follows the trend of source zone as shown in Figure 5.30. The rupture plane of the target earthquake has been divided into 10×10 sub-faults using the self-similarity laws given by Kanamori and Anderson (1975). Other modeling parameters are similar to that used for modeling of the rupture plane due to the thrust mechanism. Records have been simulated at POR station for different possibilities of nucleation point within the rupture plane using the modified semi-empirical technique. The simulated EW and NS component of acceleration records for thrust and strike-slip mechanism have been shown in Figure 5.31 and Figure 5.32, respectively. Simulated record shows that any great earthquake in the Andaman region can generate PGA of the order of 2 g in the near source region.

Table 5.11 Parameters of the aftershock August 10, 2008 of the Sumatra earthquake recorded at Port Blair (POR) station used for hypothetical earthquake

Hypocenter	Size	Fault Plane Solution	Reference
08:20:37 GMT 10.96°N, 91.83°E 15.8 km	M_o = 2.12×10^{25} dyne-cm M_w = 6.2	NP1 φ = 48°, δ = 76°, λ = -7° NP2 φ = 140°, δ = 83°, λ = -166°	Global CMT

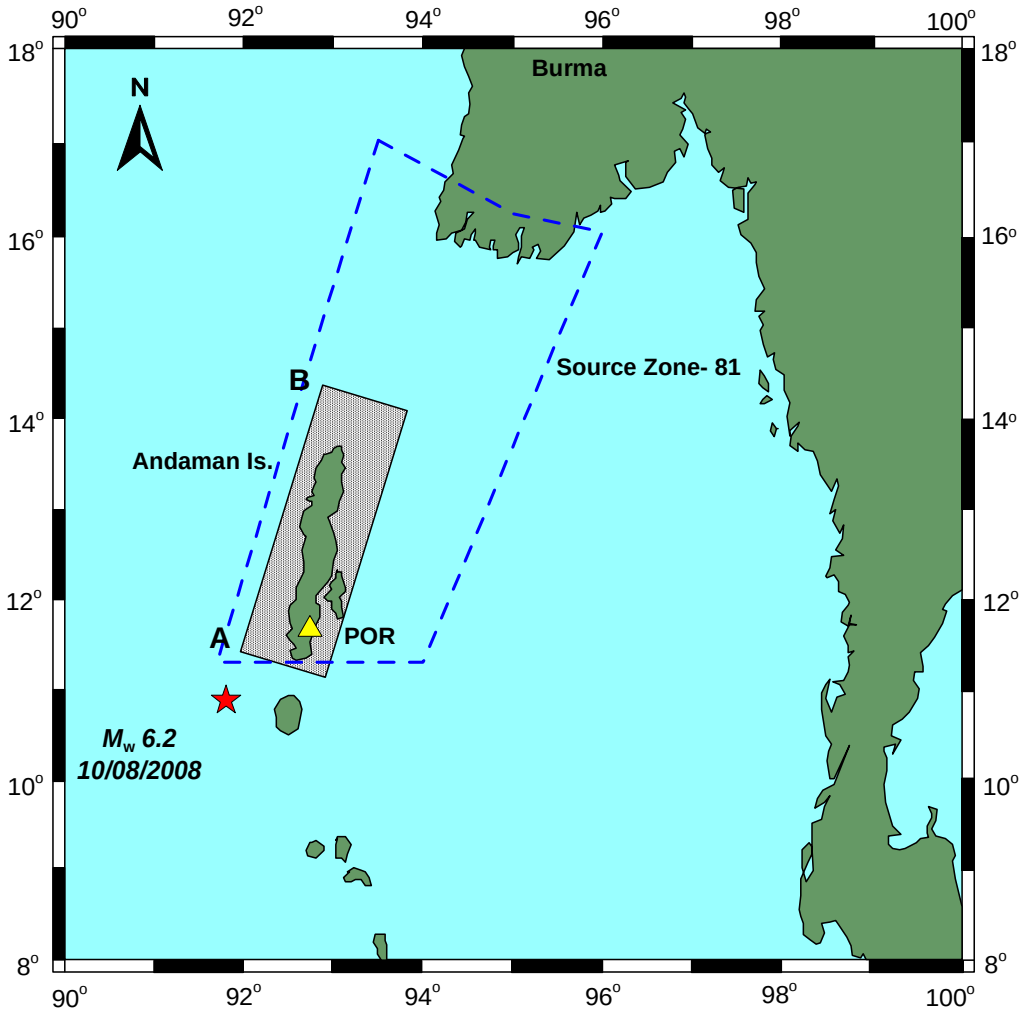

Figure 5.30 Location of the rupture modeled for hypothetical earthquake in Andaman region, which lies in the source zone 81 (blue dashed lines). For simulation, selected aftershock of the Sumatra earthquake is shown by red star and POR station at which simulation has been made is shown with yellow triangle. A and B shows the end points of the rupture plane along length

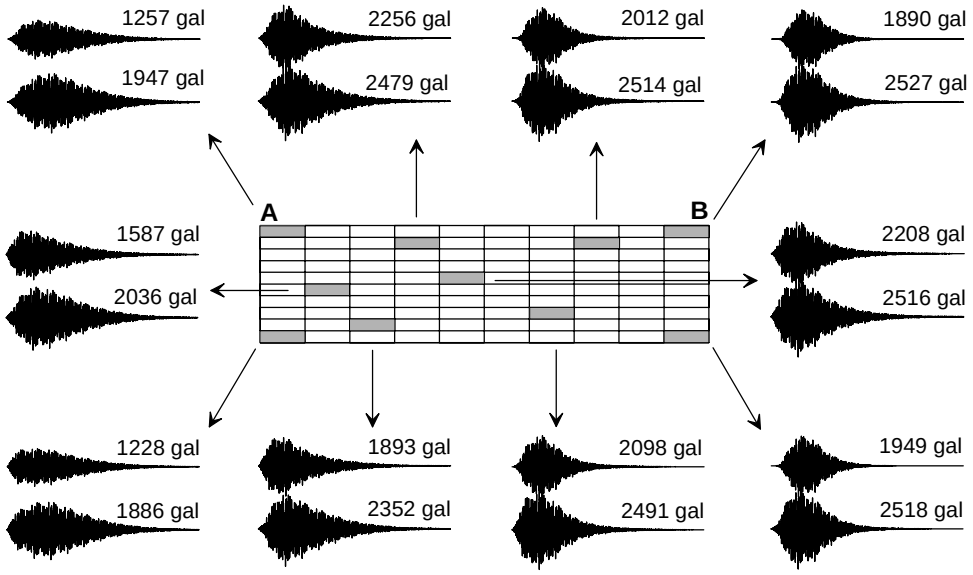

Figure 5.31 Simulated EW and NS acceleration record at different nucleation point of the rupture plane of length 324 km and width 75 km for the reverse mechanism same as for the Sumatra earthquake. Simulated acceleration record have been generated at POR station for a hypothetical earthquake of magnitude 8.5 using modified semi-empirical technique

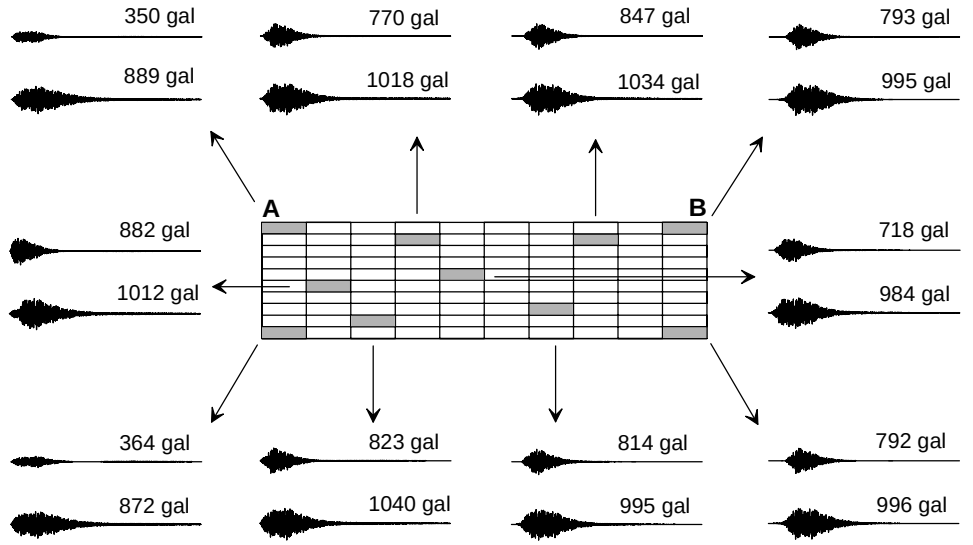

Figure 5.32 Simulated EW and NS acceleration record at different nucleation point of the rupture plane of length 501 km and width 34 km for the strike-slip mechanism of August 10, 2008 aftershock of the Sumatra earthquake. Simulated acceleration record have been generated at POR station for a hypothetical earthquake of magnitude 8.5 using modified semi-empirical technique

The simulations obtained from hypothetical earthquake in the Andaman region using modified semi-empirical technique has been further confirmed with the simulations obtained from well-established EGF technique. The same scenario earthquake has also been modeled by using EGF technique. The aftershock record at the point of simulation of the target earthquake is among major input required for the EGF technique. Department of Earthquake Engineering, Indian Institute of Technology Roorkee, India is maintaining 284 strong motion stations under a major MoES (Ministry of Earth Sciences) sponsored project. A strong motion accelerograph is installed at Port Blair under this project. An earthquake occurred on August 10, 2008 of magnitude 6.2 (M_w) was recorded at Port Blair (POR) station. The epicenter of this earthquake is close to the proximity of zone 81 and hence is used as empirical Green's function for simulation of hypothetical earthquake in this region. Parameter of the earthquake used as EGF is given in Table 5.11.

The rupture plane of the target earthquake has been divided into 14×14 sub-faults using the self-similarity laws given by Kanamori and Anderson (1975). Records have been simulated at POR station for different possibilities of nucleation point within the rupture plane using the EGF technique. Earthquake of thrust mechanism similar to that observed for the Sumatra earthquake has been considered for this simulation. Peak ground acceleration in the range of 0.6 g to 2.0 g has been observed from simulated EW and NS components of acceleration records at POR station. Simulated records have been shown in Figure 5.33. Pseudo-acceleration response spectra (PSA) computed from the simulated EW and NS component for different nucleation point has been shown in Figure 5.34. The fault plane solution similar to the oblique strike-slip mechanism of the aftershock event given in Table 5.11 has been used to model an earthquake having strike-slip mechanism. The simulated record and its response spectra have been shown in Figure 5.35 and 5.36, respectively. Simulated EW and NS component of the acceleration record for several possibilities of nucleation point indicate that PGA can vary from 0.1 to 0.7 g.

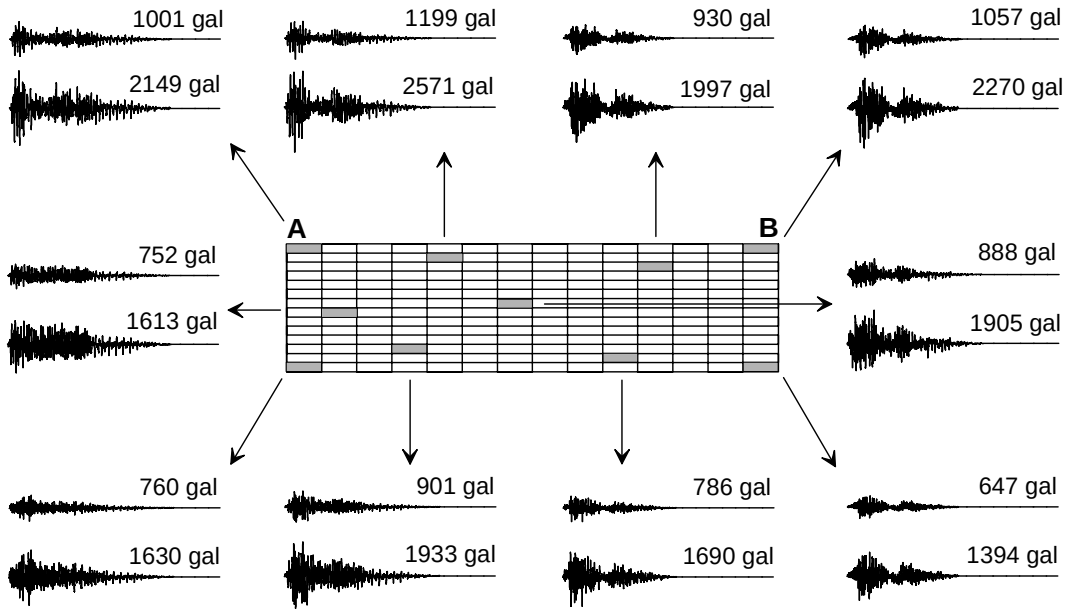

Figure 5.33 Simulated EW and NS acceleration record at different nucleation point of the rupture plane of length 324 km and width 75 km for the reverse mechanism same as for the Sumatra earthquake using EGF technique

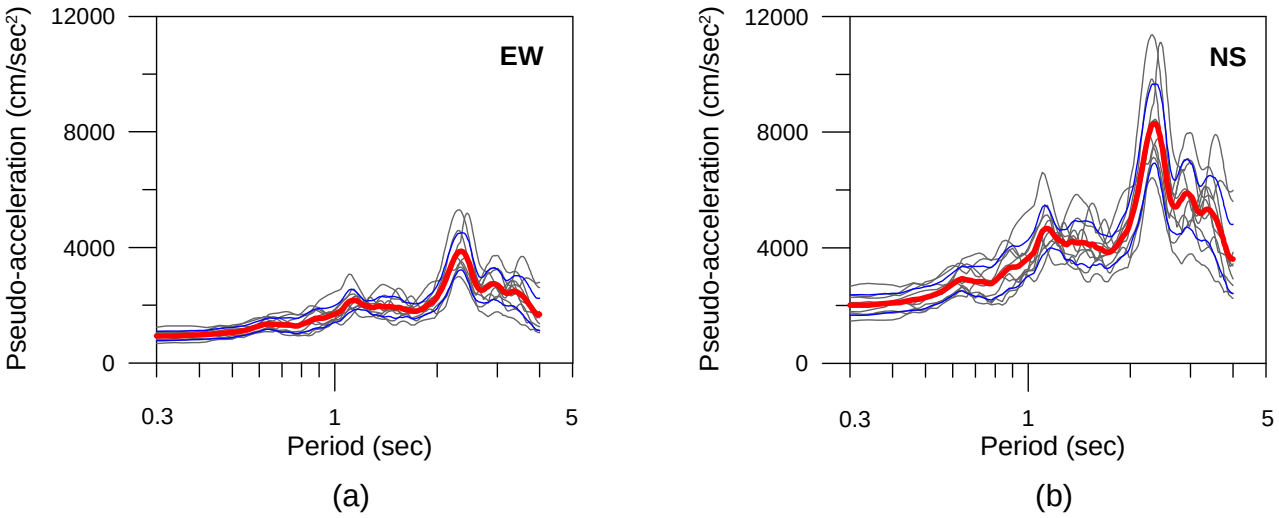

Figure 5.34 Pseudo-acceleration (PSA) response spectrums with 5% damping determined from simulated acceleration record for (a) EW and (b) NS component at different nucleation point. Red thick line indicates the mean of all responses and blue line indicates standard deviation

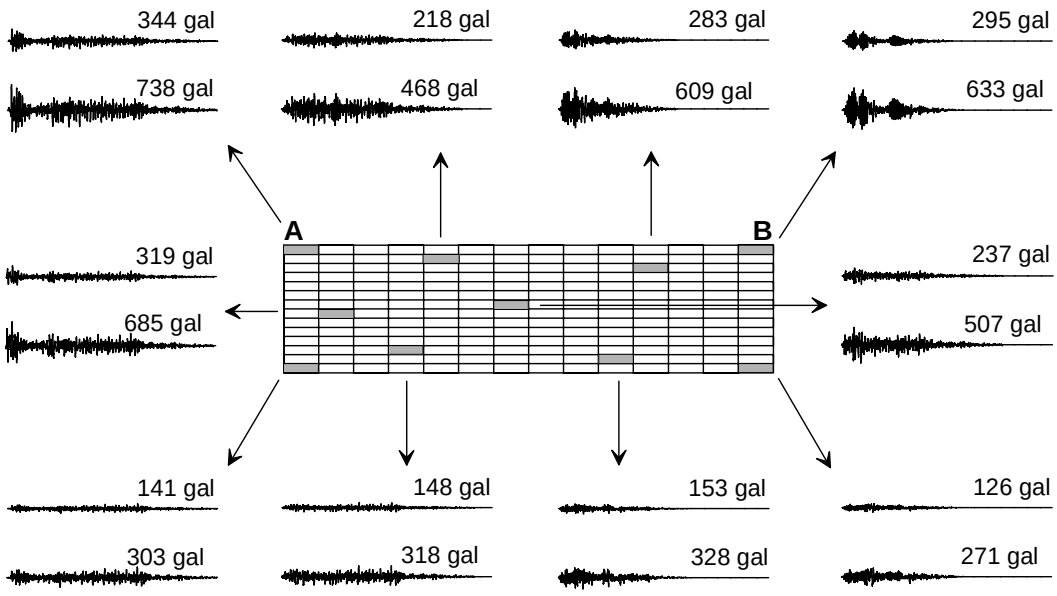

Figure 5.35 Simulated EW and NS acceleration record at different nucleation point of the rupture plane of length 501 km and width 34 km for the strike-slip mechanism of August 10, 2008 aftershock of the Sumatra earthquake using EGF technique

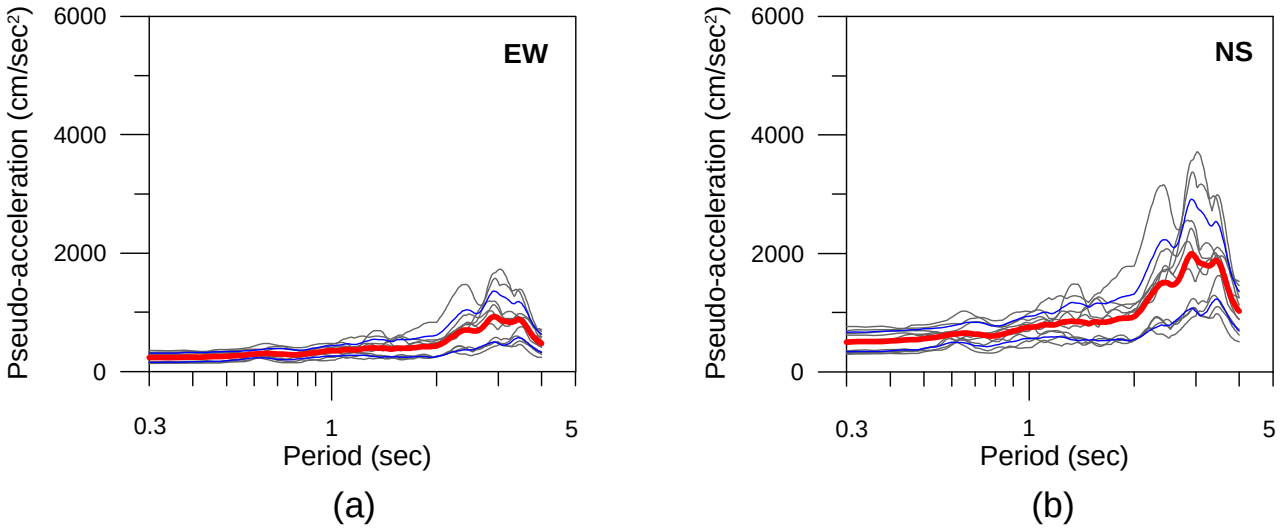

Figure 5.36 Pseudo-acceleration (PSA) response spectrums with 5% damping determined from simulated acceleration record for (a) EW and (b) NS component at different nucleation point. Red thick line indicates the mean of all responses and blue line indicates standard deviation

It has been observed that simulations from modified semi-empirical technique and EGF technique for both type of rupture mechanism are giving high values of peak ground accelerations at POR station. The order of PGA obtained for this hypothetical earthquake indicates that the seismic hazard potential of any probable great earthquake of magnitude 8.5 in the near source region is very high.

5.6 Conclusion

The Sumatra earthquake has been studied using both modified semi-empirical technique and empirical Green's function technique. The parameters of rupture model have been confirmed from several simulations. The comparison of simulated and observed record using modified semi-empirical technique and empirical Green's function technique confirm almost similar rupture model responsible for the Sumatra earthquake. It has been further observed that due to dependency of empirical Green's function technique on aftershock record, simulations at a far-field station has been compared in the frequency range of 0.3–2.0 Hz; whereas modified semi-empirical technique simulations have been compared in the frequency range of 0.3–4.0 Hz. The records simulated using technique depends on the phase, thus, in the present work S-phase has been used for simulation, therefore simulated record using empirical Green's function technique simulates only S-phase. The modified semi-empirical technique makes use of complete phase or envelope of record starting from onset of S-phase and hence gives complete record after comparison.

To verify the modified semi-empirical and empirical Green's function technique, strong motion records have been simulated for the Sumatra earthquake of December 26, 2004. The obtained source model is valid to explain the main features of the observed ground motion by comparing simulated and observed velocity records.

Chapter – 6

SUMMARY AND CONCLUSIONS

6.1 Summary

Modifications in the semi-empirical method have been made in the present thesis to incorporate the effect of radiation pattern and seismic moment of the target earthquake in this technique to include faulting mechanism associated with great earthquakes. These modifications have removed the dependency of semi-empirical method on attenuation relation. The semi-empirical method has been also modified to resolve the obtained record into two horizontal components. The modified technique has been studied in detail to check the presence of various strong motion properties like directivity effect and variation of PGA with respect to surface projection of the rupture plane. Strong motion records have been simulated for the Niigata, Japan earthquake (M_w = 6.6) to validate the modified technique. Based on satisfactory results obtained from simulation of this well recorded and well-studied earthquake, data of two earthquakes in Indian subcontinent viz., the Sikkim earthquake (M_w = 6.9) and the Sumatra earthquake (M_w = 9.0) have been used to test the applicability of the modified technique. This technique is further applied to present a ground motion scenario due to a great earthquake in the Andaman Island, India. The rupture due to hypothetical earthquake is placed at seismically active zone identified by Bhatia et al. (1999) in the Andaman region. Records have been simulated using the modified semi-empirical technique. Same model has been used to simulate strong ground motion using well established empirical Green's function (EGF) technique.

Seismic moment has been considered as major input parameter in the modified simulation technique. Seismic moment, corner frequency, and stress drop have been calculated using source displacement spectra. The scaling of envelope of accelerograms has been done using duration parameter. Duration parameter has been calculated using regression relation dependent on seismic moment and hypocentral distance. The coefficient of regression relation of the duration parameter for the Niigata, Sikkim and Sumatra earthquake have been determined by using 23, 13 and 23

observed records, respectively. Modified semi-empirical technique presents a forward problem approach of calculating source parameters of earthquake having strong motion data. Several possibilities of modeling parameters like position of nucleation point, rupture velocity and dip of the rupture plane have been considered before arriving to final parameters of source model. The selection of final model is based on RMSE calculated between simulated and observed waveform. Strong motion parameters obtained from simulated records such as peak ground acceleration (PGA) and peak ground velocity (PGV) are compared with that obtained from observed data. Response spectrum at 5% damping has been calculated at each station and compared with the observed response spectrum. The comparison is quantified in terms of RMSE.

Directivity effects are considered to be one of the most important properties that are present in strong motion data. Presence of directivity effect in the modified semi-empirical technique has been numerically experimented in the present work. In this numerical experiment, rupture plane of length 750 km and downward extension 150 km has been considered. This numerical experiment has been performed for rupture source having both reverse and strike-slip mechanism. Strong motion records have been simulated at several stations surrounding the horizontal projection of the rupture plane for both bilateral and unilateral rupture propagations. Variation of PGA on both sides of the rupture plane in strike direction for unilateral and bilateral rupture propagation reveals that, in case of unilateral rupture propagation, PGA values are relatively higher in the direction of rupture propagation as compared to PGA in opposite direction of the rupture propagation. In case of bilateral rupture propagation, similar value of PGA has been obtained in both sides of rupture propagation. This confirms the presence of directivity effect in the simulated strong motion data using modified semi-empirical technique.

To validate the developed technique, synthetic ground motions have been generated for the Niigata-ken Chuetsu, Japan earthquake of magnitude 6.6 (M_w). This earthquake was recorded on a dense network of strong motion recorders installed within entire Japan at 286 strong motion stations of Kiban-Kyoshin network (KiK-net) and 327 stations of Kyoshin network (K-NET). Records from the borehole sensor of KiK-net have been used for the purpose of comparison to avoid site amplifications which are present in sensor at the surface. Therefore, acceleration data recorded at three borehole stations (NIGH01, NIGH13 and NIGH19) of KiK-net are used in the present study. The rupture model for this earthquake has been assumed to be same as used by Joshi

and Mohan (2008). The strong motion records have been simulated at several stations using modified semi-empirical technique. Iterative modeling suggests that rupture propagate bilaterally in northwestern direction at a depth of 13 km with rupture velocity 3.1 km/sec. The same rupture model has been used to simulate strong ground motion using EGF technique to confirm the efficacy of the modified technique. This modified technique has been applied for simulating strong ground motion due to two Indian earthquakes. Applicability of the present modified technique for simulating strong ground motion due to earthquakes in the Indian subcontinent has been considered by simulating records of the Sikkim earthquake (M_w = 6.9) of September 18, 2011, and the great Sumatra earthquake (M_w = 9.0) of December 26, 2004.

The state of Sikkim in north-eastern part of India was struck by a strong earthquake of magnitude 6.9 (M_w) near the boundary between the Indian and the Eurasian tectonic plates on September 18, 2011. The rupture responsible for this earthquake has been placed at a depth of 44 km between Tista and Gangtok lineaments. The length and width of the rupture responsible for the Sikkim earthquake has been calculated using the empirical relation given by Wells and Coppersmith (1994). The length and width of the rupture plane is obtained as 51 and 13 km, respectively using empirical relation of Wells and Coppersmith (1994). This rupture plane has been divided into 49 sub-faults using self-similarity laws. The strike of the rupture plane is assumed to be parallel to the Tista lineament and is 328°N which is close to that obtained from fault plane solution of this earthquake given by Global CMT. Simulated records have been compared in the range of 0.01–20.0 Hz with the observed record in terms of RMSE of waveform comparison. Root mean square error between observed and simulated accelerograms varies from 0.46 to 0.56 at the near-field stations and from 0.32 to 0.62 at the far-field stations, respectively. Based on iterative modeling, simulation result shows that the rupture responsible for the Sikkim earthquake started from the extreme north-west corner of the rupture plane at a depth of 47 km and propagated in the southeastern direction.

Sumatra earthquake has released energy of about 4.3×10^{18} J (Ammon et al. 2005; Bilham 2005; Lay et al. 2005). It ruptured along the boundary between the Indo-Australian plate and the Eurasian plate along the northwestern Sumatra, Nicobar Island and Andaman Island (Sorensen et al. 2007). The closest broadband station which has recorded this earthquake is PSI station which lies at an epicentral distance of 355 km. In the present work the modified semi-empirical and EGF

techniques have been used to model the source of the Sumatra earthquake. The final rupture model obtained after iterative modeling has been used to simulate both horizontal component of ground motion at PSI and MDRS stations which lies at an epicentral distances of 355 and 2060 km, respectively. The simulated acceleration records have been integrated to obtain velocity records for comparison with observed velocity records at PSI and MDRS stations.

The simulation technique developed in this work has been further used to model a hypothetical earthquake of magnitude 8.5 (M_w) in the Andaman region of Indian subcontinent. This region lies close to the epicenter of the Sumatra earthquake. The causative rupture for this hypothetical earthquake has been placed in the source zone 81 marked by Bhatia et al. (1999). This source zone has potential of generating 8.5 magnitude earthquake (Bhatia et al. 1999). Simulated strong motion records using modified semi-empirical technique are further confirmed by simulating strong ground motion for same rupture model using EGF technique. An aftershock record available at POR station has been used for simulation of strong ground motion using EGF technique. The Andaman region itself has experienced earthquakes of both reverse and oblique strike-slip fault mechanism (Ortiz and Bilham 2003; Chatherine et al. 2009). Synthetic acceleration records have been simulated due to both types of rupture mechanism using both simulation techniques. The rupture length and its downward extension for 8.5 (M_w) magnitude earthquake having reverse and strike-slip mechanism are calculated by Wells and Coppersmith (1994) relation. This gives a rupture plane of dimension 324 km×75 km and 501 km×34 km for reverse and strike-slip mechanism, respectively. Several possibilities of rupture have been considered by changing position of the nucleation point within the rupture plane. Both NS and EW component of horizontal record have been simulated for reverse and oblique strike-slip type of earthquake source mechanism in this region. It has been observed that PGA obtained from several records using both methods with different possibility of nucleation point lies within a range of 0.3 to 2.0 g for reverse source mechanism and within a range of 0.1 to 2.0 g for oblique strike-slip source mechanism at POR station.

6.2 Conclusions

The work presented in this thesis shows that modified semi-empirical technique provide a basic tool to simulate strong ground motion due to any earthquake using finite rupture model.

Efficacy of this technique has been established by comparing simulated records with observed records of the Niigata, the Sikkim and the Sumatra earthquakes. The objectives identified for the present work have been fulfilled by synthesizing component-wise strong ground motion using semi-empirical modeling technique in a broad frequency range and use of simple and easily accessible parameters from earthquakes of wide ranging magnitude. Further, validation of developed technique with case studies of known earthquakes and with well-established technique of simulation of strong ground motion has been successfully done. The strong ground motion has been generated for scenario earthquake for various techno economically important locations in Indian subcontinent using modified technique and compared its obtained results with well-established simulation technique.

Major conclusions drawn on the research work carried out in present thesis is listed as follow:

1. Comparison of observed records with the simulated records obtained using modified semi-empirical technique indicate that this technique is capable of producing records that has realistic appearance and correct statistical properties closure to the observed records.
2. Simulations at several stations surrounding the projection of rupture plane indicate that directivity effects are well preserved in the modified semi-empirical approach.
3. Several simulations at same stations due to finite rupture of same dimension having different sub-fault geometry indicates that similar simulated records are obtained from same rupture source at same station as long as self-similarity of source geometry is maintained. This confirms the stability of modified technique.
4. The modified semi-empirical technique makes use of envelope of acceleration record starting from onset of S-phase and hence simulation technique presented in this work gives complete record after arrival of S-phase. Such representation is absent in other simulation techniques which are capable of simulating only individual phases.
5. The comparison of simulated waveform obtained from modified semi-empirical and empirical Green's function technique with the observed record in terms of RMSE indicate that the modified method gives comparable RMSE with that obtained from empirical Green's function technique and that too from a model based on simple and easily accessible parameters.

6. Comparison of simulated records with observed records obtained from three earthquakes having magnitude ranging from 6.6 to 9.0 (M_w) at an epicentral distance ranging from 19 to 2060 km, confirm the efficacy of the modified technique to model finite ruptures resulting from earthquakes of wide ranging magnitude at wide ranging epicentral distances.
7. Several simulations from iterative forward modeling confirm that rupture responsible for the Niigata earthquake have propagated bilaterally in northwestern direction with rupture velocity of 3.1 km/sec.
8. Several simulations from different source models and their comparisons with observed records indicate that the Sikkim earthquake was generated by a rupture originating at a depth of 47 km and propagating in southward direction with rupture velocity of 2.9 km/sec.
9. Iterative modeling of source of the Sumatra earthquake with several rupture parameters indicate that this earthquake was originated at 38 km depth and started propagating in northwest direction with rupture velocity of 3.0 km/sec.
10. The well-established EGF technique depends on the aftershock record. Therefore, simulations at far-field stations due to EGF technique are comparable in the frequency range of 0.3–2.0 Hz. However; the simulations using modified semi-empirical technique give good match in the frequency range of 0.3–4.0 Hz for the great Sumatra earthquake.
11. Simulations due to hypothetical earthquake in the Andaman region indicate possibilities of PGAs in range of 0.1 to 2.0 g from various models of rupture plane at POR station. Several simulations using both modified semi-empirical and empirical Green's function technique reveal that the order of PGA is high for reverse faulting mechanism as compared to oblique strike-slip mechanism.

LIST OF PUBLICATIONS FROM THE RESEARCH WORK

1. Joshi A, **Pushpa Kumari**, Sandeep Singh, Sharma ML (2012) Near-field and far-field simulation of accelerograms of Sikkim earthquake of September 18, 2011 using modified semi-empirical approach. Nat Hazards, vol. 64, 1029–1054.

2. Joshi A, **Pushpa Kumari**, Sharma ML, Ghosh AK, Agarwal MK, Ravikiran A (2012) A strong motion model of the 2004 great Sumatra earthquake: simulation using a modified semi empirical method. Journal of Earthquake and Tsunami, vol. 6, No. 4, 1250023-1–1250023-29.

3. Joshi A, **Pushpa Kumari**, Sushil Kumar, Sharma ML, Ghosh AK, Agarwal MK, Ravikiran A (2012) Estimation of model parameter of Sumatra earthquake using empirical Green's function technique and generation of hypothetical earthquake scenario for Andaman Island, India. Nat Hazards, vol. 62, 1081–1108.

4. Joshi A, **Pushpa Kumari**, Sharma ML (2012) Synthesis of strong ground motion using modified semi-empirical technique. International Journal of Engineering and Technology, vol. 4, No. 4, 424–426.

5. **Pushpa Kumari**, Joshi A, Sharma ML (2012) Modification in semi-empirical technique for component wise simulation of strong ground motion: A case study of the Sumatra earthquake. Proceedings, GEOS 2012, Singapore, 3–4 December 2012, 141–145.

6. Joshi A, **Pushpa Kumari**, Sharma ML, Ghosh AK, Agarwal MK, Ravikiran A (2011) A modified technique for simulation of great earthquake: A case study of Sumatra earthquake. Transaction, SMiRT 21, New Delhi, 6–11 November 2011 (Paper ID 835).

REFERENCES

1. Abrahamson NA, Litehiser JJ (1989) Attenuation of vertical peak acceleration. Bull Seismol Soc Am 79:549–580
2. Aki K (1967) Scaling law of seismic spectrums. J Geophys Res 72:1217–1231
3. Aki K (1968) Seismic displacements near a fault. J Geophys Res 73:5359–5376
4. Aki K, Richards PG (1980) Quantitative Seismology. Theory and Methods, WH Freeman and Company, San Francisco
5. Aki K, Richards PG (2002) Quantitative Seismology. University Science Books, Sausalito, California, USA
6. Ammon CJ, Ji C, Thio HK, Robinson D, Ni S, Hjorleifsdottir V, Kanamori H, Lay T, Das S, Helmberger D, Ichinose G, Polet J, Wald D (2005) Rupture process of the 2004 Sumatra-Andaman earthquake. Science 308:1133–1139
7. Andrews DJ (1980) A stochastic fault model. I. Static case. J Geophys Res 85:3867–3877
8. Arias A (1970) A measure of earthquake intensity. In: Hansen RJ (ed) Seismic Design for Nuclear Power Plants, MIT Press, Cambridge, Massachusetts, pp 438–483
9. Arroyo D, García D, Ordaz M, Mora MA, Singh SK (2010) Strong ground-motion relations for Mexican interplate earthquakes. J Seismol 14:769–785
10. Atkinson GM, Boore DM (1995) Ground motion relations for Eastern North America. Bull Seismol Soc Am 85:17–30
11. Atkinson GM, Boore DM (1997) Stochastic point-source modeling of ground motions in the Cascadia region. Seism Res Lett 68:74–85
12. Atkinson GM, Boore DM (2006) Earthquake ground-motion prediction equations for Eastern North America. Bull Seismol Soc Am 96(6):2181–2205
13. Atkinson GM, Silva W (2000) Stochastic modeling of California ground motions. Bull Seismol Soc Am 90:255–274
14. Bard PY (1998) Microtremor measurement: a tool for site effect estimation? Proc. of the 2nd Int. Symp. on Effects of Surface Geology on Seismic Motion, Yokohama, Japan, pp 1251–1282

15. Bard PY (1999) Microtremor measurement: a tool for site effect estimation? In: Irikura K, Kudo K, Okada H, Sasatami T (eds) The Effects of Surface Geology on Seismic Motion, Balkema, Rotterdam, pp 1251–1279
16. Bardet JP (2004) Preliminary observations of the Niigata-ken Chuetsu, Japan, earthquake of October 23, 2004. A preliminary report for the EERI-GEER Earthquake Engineering Reconnaissance Team
17. Benjamin JR and Associates (1988) A criterion for determining exceedance of the Operating Basis Earthquake. EPRI Report NP-5930, Electric Power Research Institute, Palo Alto, California
18. Beresnev IA, Atkinson GM (1997) Modeling finite-fault radiation from the ω^n spectrum. Bull Seismol Soc Am 87:67–84
19. Beresnev IA, Atkinson GM (1998) Stochastic finite-fault modeling of ground motions from the 1994 Northridge, California, earthquake. I. Validation on Rock Sites. Bull Seismol Soc Am 88:1392–1401
20. Beresnev IA, Atkinson GM (2001) Subevent structure of large earthquakes: A ground motion perspective. Geophys Res Lett 28:53–56
21. Bhatia SC, Kumar MR, Gupta HK (1999) A probabilistic seismic hazard map of India and adjoining regions. Ann Geophys 42:1153–1164
22. Bilham R (2005) A flying start, then a slow slip. Science 308:1126–1127
23. Bilham R, Engdahl ER, Feldl N, Satyabala SP (2005) Partial and complete rupture of the Indo-Andaman plate boundary 1847-2004. Seism Res Lett 76:299–311
24. Boatwright J (1982) A dynamic model for far-field acceleration. Bull Seismol Soc Am 72:1049–1068
25. Boatwright J (1988) The seismic radiation from computer models of faulting. Bull Seismol Soc Am 78:489–508
26. Bolt BA (1969) Duration of strong motion. Proc. of the 4th World Conference on Earthquake Engineering, Santiago, Chile, pp 1304–1315
27. Bonnefoy-Claudet S, Cornou C, Bard PY, Cotton F, Moczo P, Kristek J, Fah D (2006) H/V ratio: a tool for site effects evaluation: results from 1D noise simulations. Geophys J Int 167(2):827–837

28. Boore DM (1983) Stochastic simulation of high-frequency ground motions based on seismological models of the radiated Spectra. Bull Seismol Soc Am 73:1865–1894
29. Boore DM (2003) Simulation of ground motion using the stochastic method. Pure Appl Geophys 160:635–676
30. Boore DM, Atkinson GM (1987) Stochastic prediction of ground motion and spectral response parameters at hard-rock sites in eastern North America. Bull Seismol Soc Am 77:440–467
31. Boore DM, Bommer JJ (2005) Processing of strong-motion accelerograms: needs, options and consequences. Soil Dyn Earthquake Eng 25:93–115
32. Boore DM, Campbell KW, Atkinson GM (2010) Determination of stress parameters for eight well-recorded earthquakes in Eastern North America. Bull Seismol Soc Am 100:1632–1645
33. Boore DM, Joyner WB (1991) Estimation of ground motion at deep soil sites in eastern North America. Bull Seismol Soc Am 81:2167–2185
34. Boore DM, Joyner WB, Oliver AA, Page RA (1980) Peak acceleration, velocity and displacement from strong motion records. Bull Seismol Soc Am 70:305–321
35. Brocher TM (2005) Empirical relations between elastic wave speeds and density in the Earth's crust. Bull Seismol Soc Am 95:2081–2092
36. Brune JN (1970) Tectonic stress and the spectra of seismic shear waves from earthquakes. J Geophys Res 75:4997–5009
37. Brune JN (1971) Correction. J Geophys Res 76:5002
38. Campbell KW (1981) Near source attenuation of peak horizontal acceleration. Bull Seismol Soc Am 71(6):2039–2070
39. Campbell KW (1985) Strong motion attenuation relations: A ten-year perspective. Earthquake Spectra 1(4):759–804
40. Campbell KW (1997) Empirical near-source attenuation relationships for horizontal and vertical components of peak ground acceleration, peak ground velocity, and pseudo-absolute acceleration response spectra. Seism Res Lett 68(1):154–179
41. Campbell KW (2001) Hybrid empirical model for estimating strong ground motion in regions of limited strong-motion recordings. Proc. of the OECD/NEA Workshop on the

Engineering Characterization of Seismic Input, NEA/CSNI/R(2000)2, Nuclear Energy Agency, Paris, 1:315–332

42. Catherine JK, Gahalaut VK, Ambikapathy A, Kundu B, Subrahmanyam C, Jade S, Amit Bansal, Chadha RK, Narsaiah M, Premkishore L, Gupta DC (2009) 2008 Little Andaman aftershock: Genetic linkages with the subducting 90°E ridge and 2004 Sumatra–Andaman earthquake. Tectonophysics 479:271–276
43. Chadha RK, Latha G, Yeh H, Peterson C, Katada T (2005) The tsunami of the great Sumatra earthquake of M 9.0 on 26 December 2004 – Impact on the east coast of India. Curr Sci 88(8):1297–1301
44. Coats DA, Kanamori H, Houston H (1984) Simulation of strong ground motion from the 1964 Alaskan earthquake (Abs). Earthquake Notes 55:18
45. Cotte N, Pedersen H, Campillo M, Mars J, Ni J, Kind R, Sandvol E, Zhao W (1999) Determination of the crustal structure in Southern Tibet by dispersion and amplitude analysis of Rayleigh waves. Geophys J Int 138:809–819
46. Curray JR (2005) Tectonics and history of the Andaman Sea region. J Asian Earth Sci 25:187–232
47. Curray JR, Moore DG, Lawver LA, Emmel FJ, Raitt RW, Henry M, Kieckhefer R (1979) Tectonics of the Andaman Sea and Burma. In: Watkins JS, Montaderi L, Dickenson PW (eds) Geological and Geophysical Investigations of Continental Margins, pp 189–198
48. Dasgupta S, Ganguly J, Neogi S (2004) Inverted metamorphic sequence in the Sikkim Himalayas: Crystalline history, P-T gradient and implications. J Metamorph Geol 22:395–412
49. De Groot-Hedlin CD (2005) Estimation of the rupture length and velocity of the great Sumatra earthquake of Dec 26, 2004 using hydroacoustic signals. Geophys Res Lett 32:L11303
50. Dimri VP, Srivastava K (2007) Tsunami propagation of the 2004 Sumatra earthquake and the fractal analysis of the aftershock activity. Indian J Marine Sci 36(2):128–135
51. Douglas J (2011) Ground-motion prediction equations 1964-2010. PEER Report 2011/102, Pacific Earthquake Engineering Research Center, UC Berkeley
52. Field E, Jacob K (1993) The theoretical response of sedimentary layers to ambient seismic noise. Geophys Res Lett 20(24):2925–2928

53. Fitch TJ (1972) Plate convergence, transcurrent faults and internal deformation adjacent to Southeast Asia and the western Pacific. J Geophys Res 77:4432–4460
54. Frankel A (1991) High-frequency spectral falloff of earthquakes, fractal dimension of complex rupture, b value, and scaling of strength on faults. J Geophys Res 96:6291–6302
55. Frankel A (1995) Simulating strong motion of large earthquakes using recordings of small earthquakes: the Loma Prieta mainshock as a test case. Bull Seismol Soc Am 85:1144–1160
56. Fukuyama E, Irikura K (1986) Rupture process of the 1983 Japan sea (Akita-Oki) earthquake using a waveform inversion method. Bull Seismol Soc Am 76:1623–1640
57. Ghasemi H, Fukushima Y, Koketsu K, Miyake H, Wang Z, Anderson JG (2010) Ground-motion simulation for the 2008 Wenchuan, China, earthquake using the stochastic finite-fault method. Bull Seismol Soc Am 100:2476–2490. doi:10.1785/0120090258
58. GSI (2000) Seismotectonic atlas of India and its environs. In: Dasgupta S, Pande P, Ganguly D, Iqbal Z, Sanyal E, Venkatraman NV, Dasgupta S, Sural B, Harendranath L, Mazumdar K, Sanyal S, Roy A, Das LK, Mishra PS, Gupta HK (eds) Geol Soc India, 43
59. Hadley DM, Helmberger DV (1980) Simulation of strong ground motions. Bull Seismol Soc Am 70:617–630
60. Hadley DM, Helmberger DV, Orcutt JA (1982) Peak acceleration scaling studies. Bull Seismol Soc Am 72:959–979
61. Hanks TC (1979) *b* values and $\omega^{-\gamma}$ seismic source models: Implications for tectonic stress variations along active crustal fault zones and the estimation of high-frequency strong ground motion. J Geophys Res 84(B5):2235–2242
62. Hanks TC, McGuire RK (1981) The Character of high frequency strong ground motion. Bull Seismol Soc Am 71:2071–2095
63. Hartzell SH (1978) Earthquake aftershocks as Green's functions. Geophys Res Lett 5:1–4
64. Hartzell SH (1982) Simulation of ground accelerations for May 1980 Mammoth Lakes, California, earthquakes. Bull Seismol Soc Am 72:2381–2387
65. Hazarika P, Kumar MR, Srijayanthi G, Raju PS, Rao NP, Srinagesh D (2010) Transverse tectonics in the Sikkim Himalaya: evidence from seismicity and focal-mechanism data. Bull Seismol Soc Am 100(4):1816–1822

66. Heaton TH, Hartzell SH (1989) Estimation of strong ground motions from hypothetical earthquakes on the Cascadia subduction zone, Pacific Northwest. Pure Appl Geophys 129:131–201
67. Heaton TH, Helmberger DV (1977) A study of the strong ground motion of the Borrego Mountain, California, earthquake. Bull Seismol Soc Am 67:315–330
68. Honda R, Aoi S, Morikawa N, Sekiguchi H, Kunugi T, Fujiwara H (2005) Ground motion and rupture process of the 2004 Mid Niigata Prefecture earthquake obtained from strong motion data of K-NET and KiK-net. Earth Planets Space 57:527–532
69. Housner GW, Jennings PC (1964) Generation of artificial earthquakes. Proc. ASCE, J Eng Mech Div 90:113–150
70. Houston H, Kanamori H (1984) The effect of asperities on short period seismic radiation with application on rupture process and strong motion. Bull Seismol Soc Am 76:19–42
71. Houston H, Kanamori H (1986) Source characteristics of the 1985 Michoacan, Mexico, earthquake at periods of 1 to 30 seconds. Geophys Res Lett 13:597–600
72. Hutchings L (1985) Modeling earthquakes with empirical Green's functions (Abs). Earthquake Notes 56:14
73. Imagawa K, Mikami N, Mikumo T (1984) Analytical and semi empirical synthesis of near field seismic waveforms for investigating the rupture mechanism of major earthquakes. J Physics of Earth 32:317–338
74. Irikura K (1986) Prediction of strong acceleration motions using empirical Green's function. Proc. of the 7th Japan Earthquake Engineering Symposium, pp 151–156
75. Irikura K, Kagawa T, Sekiguchi H (1997) Revision of the empirical Green's function method by Irikura, 1986. Programme and Abstracts. Seismol Soc Japan 2:B25
76. Irikura K, Kamae K (1994) Estimation of strong ground motion in broad-frequency band based on a seismic source scaling model and an empirical Green's function technique. Ann Geophys 37(6):1721–1743
77. Irikura K, Kurahashi S (2012) Strong ground motions during the 2011 pacific coast off Tohoku, Japan, earthquake. Proc. of the International Symposium on Engineering lessons learned from the 2011 Great East Japan earthquake, March 1-4, Tokyo, Japan

78. Irikura K, Muramatu I (1982) Synthesis of strong ground motions from large earthquakes using observed seismograms of small events. Proc. of the 3rd International Microzonation Conference, Seattle, pp 447–458
79. IS Code 1893: 2002
80. Iyengar RN, Iyengar KTSR (1969) A nonstationary random process model for earthquake accelerograms. Bull Seismol Soc Am 59:1163–1188
81. Jaiswal RK, Singh AP, Rastogi BK, Murty TS (2011) Aftershock sequences of two great Sumatran earthquakes of 2004 and 2005 and simulation of the minor tsunami generated on September 12, 2007 in the Indian Ocean and its effect. Nat Hazards 57:7–26
82. Joshi A (1997) Modeling of peak ground acceleration for Uttarkashi earthquake of 20th October, 1991. Bull Indian Soc Earthquake Tech 34:75–96
83. Joshi A (2000) Modeling of rupture planes for peak ground accelerations and its application to the isoseismal map of MMI scale in Indian region. J Seismol 4:143–160
84. Joshi A (2001) Strong motion envelope modeling of the source of the Chamoli earthquake of March 28, 1999 in the Garhwal Himalaya, India. J Seismol 5:499–518
85. Joshi A (2003) Predicting strong motion parameters for the Chamoli earthquake of 28th March, 1999, Garhwal Himalaya, India, from simplified finite fault model. J Seismol 7:1–17
86. Joshi A (2004) A simplified technique for simulating wide band strong ground motion for two recent Himalaya earthquakes. Pure Appl Geophys 161:1777–1805
87. Joshi A, Kumar A, Lomnitz C, Castanos H, Akhtar S (2012a) Applicability of attenuation relations for regional studies. Geof´ısica Internacional 51(4):349–363
88. Joshi A, Kumar B, Sinvhal A, Sinvhal H (1999) Generation of synthetic accelerograms by modeling of rupture plane. ISET J Earthquake Technol 36:43–60
89. Joshi A, Midorikawa S (2004) A simplified method for simulation of strong ground motion using rupture model of the earthquake source. J Seismol 8:467–484
90. Joshi A, Midorikawa S (2005) Attenuation characteristics of ground motion intensity from earthquakes with intermediate depth. J Seismol 9:23–37
91. Joshi A, Mohan K (2008) Simulation of accelerograms from simplified deterministic approach for the 23rd October 2004 Niigata-ken Chuetsu earthquake. J Seismol 12:35–51

92. Joshi A, Mohan K (2010) Expected peak ground acceleration in Uttarakhand Himalaya, India region from a deterministic hazard model. Nat Hazards 52:299–317
93. Joshi A, Mohanty M, Bansal AR, Dimri VP, Chadha RK (2010) Use of spectral acceleration data for determination of three-dimensional attenuation structure in the Pithoragarh region of Kumaon Himalaya. J Seismol 14:247–272
94. Joshi A, Patel RC (1997) Modeling of active lineaments for predicting a possible earthquake scenario around Dehradun, Garhwal Himalaya, India. Tectonophysics 283:289–310
95. Joshi A, Pushpa Kumari, Shushil Kumar, Sharma ML, Ghosh AK, Agarwal MK, Ravikiran A (2012b) Estimation of model parameter of Sumatra earthquake using empirical Green's function technique and generation of hypothetical earthquake scenario for Andaman Island, India. Nat Hazards 62:1081–1108
96. Joshi A, Singh S, Kavita G (2001) The Simulation of ground motions using envelope summations. Pure Appl Geophys 158:877–901
97. Joyner WB, Boore DM (1981) Peak horizontal acceleration and velocity from strong motion records including records from the 1979 Imperial Valley, California, earthquake. Bull Seismol Soc Am 71:2011–2038
98. Joyner WB, Boore DM (1988) Measurement, characterization, and prediction of strong ground motion. Proc. of Earthquake Eng Soil Dyn II, GT Div/ASCE, Park City, Utah, June 27–30, pp 43–102
99. Kamae K, Ikeda T, Miwa S (2005) Source model composed of asperities for the 2004 Mid Niigata Prefecture, Japan, earthquake (M_{JMA} = 6.8) by the forward modeling using the empirical Green's function method. Earth Planets Space 57:533–538
100. Kamae K, Irikura K (1998) Source model of the 1995 Hyogo-ken Nanbu earthquake and simulation of near-source ground motion. Bull Seismol Soc Am 88:400–412
101. Kamae K, Irikura K, Pitarka A (1998) A technique for simulating strong ground motion using hybrid Green's function. Bull Seismol Soc Am 88(2):357–367
102. Kameda H, Sugito M (1978) Prediction of strong earthquake motions by evolutionary process model. Proc. of the 6th Japan Earthquake Engineering Symposium, pp 41–48
103. Kanamori H (1977) The energy release in great earthquakes. J Geophys Res 82:2981–2987

104. Kanamori H (1979) A semi-empirical approach to prediction of long-period ground motions from great earthquakes. Bull Seismol Soc Am 69:1645–1670
105. Kanamori H, Anderson DL (1975) Theoretical basis of some empirical relations in Seismology. Bull Seismol Soc Am 65:1073–1095
106. Kayal JR (2001) Microearthquake activity in some parts of the Himalaya and the tectonic model. Tectonophysics 339:331–351
107. Keilis-Borok VI (1959) On estimation of the displacement in an earthquake source and of source dimensions. Ann Geofis (Rome) 12:205–214
108. Kiyono J (1992) Identification and synthesis of seismic ground motion in structural response analysis. Ph.D. thesis, Department of Civil Engineering Kyoto University
109. Koketsu K, Hikima K, Miyake H, Maruyama T, Wang Z (2008) Source process and ground motions of the 2008 Wenchuan, China, earthquake. EOS Transactions, AGU Fall Meeting Supplement Abstract AN: S31B-1914, 89(53), 1914
110. Kramer SL (1996) Geotechnical Earthquake Engineering. Prentice-Hall, New Jersey
111. Kumar D, Khattri KN, Teotia SS, Rai SS (1999) Modeling of accelerograms for two Himalayan earthquakes using a novel semi-empirical method and estimation of accelerogram for a hypothetical great earthquake in the Himalaya. Curr Sci 76:819–830
112. Kumar D, Teotia SS, Sriram V (2011) Modeling of strong ground motions from 1991 Uttarkashi, India, earthquake using a hybrid technique. Pure Appl Geophys 168:1621–1643
113. Lachet C, Bard PY (1994) Numerical and theoretical investigations on the possibilities and limitations of Nakamura's technique. J Phys Earth 42(4):377–397
114. Lai SP (1982) Statistical characterization of strong ground motions using power spectral density function. Bull Seismol Soc Am 72:259–274
115. Lay T, Kanamori H, Charles JA, Richard CA, Steven NM, Susan LB, Michael RB, Butler R, Heather RD, Ekstrom G, Satake K, Sipkin S (2005) The great Sumatra-Andaman earthquake of 26 December 2004. Science 308:1127–1133
116. Lay T, Wallace TC (1995) Modern Global Seismology. Academic Press, California, pp 521
117. Lermo J, Chavez-Garcia FJ (1994) Are microtremors useful in site response evaluation? Bull Seismol Soc Am 83:1350–1364

118. Mahajan AK, Vikram Gupta, Thakur VC (2012) Macroseismic field observations of 18 September 2011 Sikkim earthquake. Nat Hazards 63:589–603
119. McGuire RK (1977) Seismic design spectra and mapping procedures using hazard analysis based directly on oscillator response. Earthquake Engng Struct Dyn 5(3):211–234
120. McGuire RK (1978) Seismic ground motion parameter relations. J Geotech Eng-ASCE 104(GT4):481–490
121. McGuire RK, Becker AM, Donovan NC (1984) Spectral estimates of seismic shear waves. Bull Seismol Soc Am 74:2167–2185
122. Midorikawa S (1989) Synthesis of ground acceleration of large earthquakes using acceleration envelope waveform of small earthquake. J Struct Construct Eng 398:23–30
123. Midorikawa S (1993) Semi-empirical estimation of peak ground acceleration from large earthquakes. Tectonophysics 218:287–295
124. Mikumo T, Irikura K, Imagawa K (1981) Near field strong motion synthesis from foreshock and aftershock records and rupture process of the main shock fault (Abs). IASPEI 21st General Assembly, London
125. Motazedian D, Atkinson GM (2005) Stochastic finite-fault modeling based on a dynamic corner frequency. Bull Seismol Soc Am 95(3):995–1010
126. Mucciarelli M (1998) Reliability and applicability of Nakamura's technique using microtremors: an experimental approach. J Earthquake Eng 2:625–638
127. Munguia L, Brune JN (1984) Simulations of strong ground motion for earthquakes in the Mexicali-Imperial valley. Proc. of workshop on strong ground motion simulation and earthquake engineering applications, Pub. 85-02. Earthquake Engineering Research Institute, Los Altos, California 21-1−21-19
128. Nakamura Y (1989) A method for dynamic characteristics estimation of subsurface using microtremor on the ground surface. Quarterly Report of the Railway Technical Research Institute Japan 30:25–33
129. Nath SK, Thingbaijam KKS (2009) Seismic hazard assessment – a holistic microzonation approach. Nat Hazards Earth Syst Sci 9:1445–1459
130. Nath SK, Vyas M, Pal I, Sengupta P (2005) A Seismic hazard scenario in the Sikkim Himalaya from seismotectonics, spectral amplification, source parameterization and

spectral attenuation laws using strong motion seismometry. J Geophys Res 110:B01301. doi:10.1029/2004JB003199

131. Nau RF, Oliver RM, Prater KS (1982) Simulating and analyzing artificial nonstationary earthquake ground motions. Bull Seismol Soc Am 72:615–636
132. Newmark NM (1973) A study of vertical and horizontal earthquake spectra. Newmark NM Consulting Engineering Services, Directorate of Licensing, U.S. Atomic Energy Commission, Washington, D.C.
133. Ortiz M, Bilham R (2003) Source area and rupture parameters of the 31 December 1881 M_w = 7.9 Car Nicobar earthquake estimated from Tsunamis recorded in the Bay of Bengal. J Geophys Res 108(B4):2215. doi:10.1029/2002JB001941
134. Papageorgiou AS, Aki K (1983) A specific barrier model for the quantitative description of inhomogeneous faulting and the prediction of strong ground motion. Part I. Description of the model. Bull Seismol Soc Am 73(3):693–722
135. Parolai S, Bormann P, Milkereit C (2001) Assessment of the natural frequency of the sedimentary cover in the Cologne area (Germany) using noise measurements. J Earthquake Eng 5:541–564
136. Parolai S, Galiana-Merino JJ (2006) Effect of transient seismic noise on estimation of H/V spectral ratios. Bull Seismol Soc Am 96(1):228–236
137. Parvez IA, Vaccari F, Panza GF (2003) A deterministic seismic hazard map of India and adjacent areas. Geophys J Int 155:489–508
138. Pitarka A, Irikura K, Iwata T, Sekiguchi H (1998) Three-dimensional simulation of the near-fault ground motion for the 1995 Hyogo-ken Nanbu (Kobe), Japan, earthquake. Bull Seismol Soc Am 88:428–440
139. Rao NP, Chary AH (2005) What caused the great Sumatran earthquakes of 26 December 2004 and 28 March 2005? Curr Sci 89:449–452
140. Rosa-Cintas S, Galiana-Merino JJ, Molina-Palacios S, Rosa-Herranz J, Garcia-Fernandez M, Jimenez MJ (2011) Soil characterization in urban areas of the Bajo Segura Basin (Southeast Spain) using H/V, F–K and ESAC methods. J Appl Geophys 75:543–557
141. Ruiz JA, Baumont D, Bernard P, Berge-Thierry C (2011) Modeling directivity of strong ground motion with a fractal, k^{-2}, kinematic source model. Geophys J Int 186(1):226–244

142. Sato HP, Abe K, Ootaki O (2003) GPS-measured land subsidence in Ojiya City, Niigata Prefecture, Japan. Eng Geol 67:379–390
143. Seed HB, Murarka R, Lysmer J, Idriss IM (1976) Relationships of maximum acceleration, maximum velocity, distance from source and local site conditions for moderately strong earthquakes. Bull Seismol Soc Am 66(4):1323–1342
144. Sharma ML (1998) Attenuation relationship for estimation of peak ground horizontal acceleration using data from strong-motion arrays in India. Bull Seismol Soc Am 88:1063–1069
145. Sharma ML, Douglas J, Bungum H, Kotadia J (2009) Ground motion prediction equations based on data from the Himalayan and Zagros regions. J Earthquake Eng 13(8):1191–1210
146. Singh SK, Mohanty WK, Bansal BK, Roonwal GS (2002) Ground motion in Delhi from future large/great earthquakes in the Central seismic gap of the Himalayan arc. Bull Seismol Soc Am 92:555–569
147. Sinozuka M, Sato Y (1967) Simulation of nonstationary random process. Proc. ASCE 93:11–40
148. Sokolov VY, Loh CH, Wen KL (2001) Empirical models for site- and region- dependent ground-motion parameters in the Taipei area: A unified approach. Earthquake Spectra 17(2):313–331
149. Somerville PG, Sen MK, Cohee BP (1991) Simulation of strong ground motions recorded during the 1985 Michoacan, Mexico and Valparaiso Chile earthquakes. Bull Seismol Soc Am 81:1–27
150. Sorensen MB, Atakan K, Pulido N (2007) Simulated strong ground motions for the great *M* 9.3 Sumatra–Andaman earthquake of 26 December 2004. Bull Seismol Soc Am 97:S139–S151
151. Tapponnier P, Molnar P (1977) Active faulting and tectonics in China. J Geophys Res 82:2905–2930
152. Trifunac MD, Brady AG (1975) A study on the duration of strong earthquake ground motion. Bull Seismol Soc Am 65:581–626

153. Wells DL, Coppersmith KJ (1994) New empirical relationships among magnitude, rupture length, rupture width, rupture area, and surface displacement. Bull Seismol Soc Am 84:974–1002
154. Yagi Y (2005) Preliminary results of rupture process for 2004 off coast of northern Sumatra giant earthquake (ver. 1). http://iisee.kenken.go.jp/staff/yagi/eq/Sumatra2004/Sumatra2004.html
155. Yokoi T, Irikura K (1991) Empirical Green's function technique based on the scaling law of source spectra. ZISHIN series II, J Seismol Soc Japan 44:109–122 (in Japanese with English abstract)
156. Yu G (1994) Some aspects of earthquake seismology: slip partitioning along major convergent plate boundaries; composite source model for estimation of strong motion; and nonlinear soil response modeling. Ph.D. thesis, University of Nevada
157. Yu G, Khattri KN, Anderson JG, Brune JN, Zeng Y (1995) Strong ground motion from the Uttarkashi, Himalaya, India, earthquake: Comparison of observations with synthetics using the composite source model. Bull Seismol Soc Am 85:31–50
158. Zeng Y, Anderson JG, Yu G (1994) A composite source model for computing realistic synthetic strong ground motions. Geophys Res Lett 21(8):725–728

Websites used:

http://earthquake.usgs.gov
http://www.globalcmt.org
http://pesmos.in
http://www.kyoshin.bosai.go.jp